

DRAFT VERSION MARCH 2, 2022

Typeset using L^AT_EX **preprint** style in AASTeX62

Distant White Dwarfs in the US Naval Observatory Flagstaff Station Parallax Sample

S. K. LEGGETT,^{1,2} P. BERGERON,³ JOHN P. SUBASAVAGE,^{2,4} CONARD C. DAHN,² HUGH C. HARRIS,² JEFFREY A. MUNN,² HAROLD D. ABLES,² BLAISE J. CANZIAN,⁵ HARRY H. GUETTER,² ARNE H. HENDEN,⁶ STEPHEN E. LEVINE,⁷ CHRISTIAN B. LUGINBUHL,² ALICE B. MONET,² DAVID G. MONET,² JEFFREY R. PIER,² RONALD C. STONE,^{2,*} FREDERICK J. VRBA,² RICHARD L. WALKER,^{2,*} TRUDY M. TILLEMAN,² SIYI XU,¹ AND P. DUFOUR³

¹*Gemini Observatory, Northern Operations Center, 670 N. A'ohoku Place, Hilo, HI 96720, USA*

²*US Naval Observatory, Flagstaff Station, 10391 W. Naval Observatory Road, Flagstaff, AZ 86005–8521, USA*

³*Département de Physique, Université de Montréal, C.P. 6128, Succ. Centre-Ville, Montréal, Québec H3C 3J7, Canada*

⁴*The Aerospace Corporation, 2310 E. El Segundo Boulevard, El Segundo, CA 90245, USA*

⁵*L-3 Communications/Brashear, 615 Epsilon Dr., Pittsburgh, PA 15238–2807, USA*

⁶*AAVSO, Cambridge, MA 02138, USA*

⁷*Lowell Observatory, 1400 W. Mars Hill Road, Flagstaff, AZ 86001–4499, USA*

ABSTRACT

This paper presents new trigonometric parallaxes and proper motions for 214 stars. The measurements were made at the US Naval Observatory Flagstaff Station (NOFS) between 1989 and 2017, and the average uncertainty in the parallax values is 0.6 mas. We find good agreement with *Gaia* Data Release 2 measurements for the stars in common, although there may be a small systematic offset similar to what has been found by other investigators. The sample is matched to catalogs and the literature to create a photometric dataset which spans the ultraviolet to the mid-infrared. New mid-infrared photometry is obtained for nineteen stars from archived *Spitzer* mosaics. New optical spectroscopy is presented for seven systems and additional spectra were obtained from the literature. We identify a sub-sample of 179 white dwarfs (WDs) at distances of 25 – 200 pc. Their spectral energy distributions (SEDs) are analyzed using model atmospheres. The models reproduce the entire flux-calibrated SED very well and provide the atmospheric chemical composition, temperature, surface gravity, mass and cooling age of each WD. Twenty-six WDs are newly classified and twelve systems are presented as candidate unresolved binaries. We confirm one WD+red dwarf system and identify two WDs as candidate dust disk systems. Twelve old and high-velocity systems are identified as candidate thick disk or halo objects. The WDs in the sample generally have Galactic disk-like ages of < 8 Gyr and masses close to the canonical $0.6 M_{\odot}$.

sleggett@gemini.edu

* Deceased

1. INTRODUCTION

White dwarfs (WDs) are the remnants of the vast majority of stars. These Earth-sized objects have degenerate cores and typically a thin H or He atmosphere; nuclear fusion no longer occurs and they cool slowly. WDs as cold as 3000 K are known; these left the main-sequence ~ 10 Gyrs ago and hence are old disk or halo objects (e.g. Gianninas et al. 2015). WDs can provide insights into Galactic populations and the history of star formation (e.g. Kilic et al. 2017). Massive WDs and WDs in close binary systems constrain supernova models (e.g. Kilic et al. 2014) and the interiors of pulsating WDs shed light on details of stellar evolution (e.g. Giambicchele et al. 2018). Many WDs have atmospheres polluted by disrupted planetary systems (Barber et al. 2016; Jura & Young 2014; Zuckerman et al. 2007). Hence an improved understanding of WDs can contribute to all major areas of astrophysical research: planetary systems, the stars, the Galaxy and other galaxies.

Knowledge of a WD's mass, age and composition is key to extracting the important information contained in a WD. There are two common approaches to determining these parameters: the spectroscopic method which relies on absorption line profiles, and the photometric method which relies on the luminosity and spectral energy distribution (SED) of the WD (Bergeron et al. 1992, 2001, 2011; Giambicchele et al. 2012; Gianninas et al. 2011; Kilic et al. 2010; Limoges et al. 2015; Tremblay & Bergeron 2009). The photometric method is the only way to measure atmospheric parameters of WDs that do not show absorption lines in their spectra, for example WDs cooler than ~ 5000 K. In this paper we present new trigonometric parallaxes for more than 200 stars measured at the US Naval Observatory Flagstaff Station (NOFS). The majority of the sample are WDs, and about one-third of the WDs have an effective temperature (T_{eff}) $\lesssim 5000$ K. We use recent atmospheric models to analyse the WDs using the photometric method, for which the parallax must be well determined. For some of the warmer WDs we check the viability of the photometric analysis by comparing synthetic and observed optical spectra.

For 52 years the NOFS has been determining trigonometric parallaxes of faint high proper motion stars. NOFS parallaxes for 309 late-type dwarfs and subdwarfs were recently published (Dahn et al. 2017), and new NOFS parallaxes are included in a recent paper studying the sample of WDs that lie within 25 pc of the Sun (Subasavage et al. 2017). This paper presents new NOFS trigonometric parallaxes of WDs at distances of 25 pc to 1.2 kpc, as well as parallaxes measured for other objects of interest that are on the NOFS program and have not been previously published.

Section 2 presents new astrometric data for 214 stars and Section 3 presents optical and infrared photometry for the sample. New optical spectra for seven WDs are presented in Section 4. In Section 5 we describe the models and the fitting technique used to determine the composition, temperature and surface gravity of each WD's atmosphere, from which mass and cooling age are derived. Section 6 gives a broad overview of the entire sample and Section 7 described the observational properties of 179 WDs in the sample. Section 8 discusses the physical properties of the 179 WDs. Our conclusions are given in Section 9. Supporting material is given in the Appendix.

2. ASTROMETRY

2.1. *New Astrometry*

Table 1 lists 216 new NOFS astrometric measurements of 214 stars. Two targets — WD 0003+177 and WD 1042+593 — had two independent determinations carried out using different CCD cameras

to provide a consistency check. Note that in the rest of this paper we omit the letters “WD” in front of object names for clarity.

[Dahn et al. \(2017\)](#) give the history of the NOFS parallax program, including a description of the different filters and cameras used. Table 1 gives relative and absolute trigonometric parallaxes, proper motion, and the implied tangential velocity. The filters and cameras used for each measurement are also given. The methods used to determine parallax and proper motion are the same as described in previous NOFS publications ([Monet & Dahn 1983](#)). In brief, image centroids are determined and solutions for parallax are executed independently in right ascension and declination. The final value is a weighted average of the individual measurements. For this sample, the uncertainty in the parallax ranges from 0.2 mas to 1.6 mas, with an average of 0.6 mas.

The correction from relative to absolute parallax is carried out using the procedures described in detail by [Harris et al. \(2016\)](#). For six stars there is no correction to absolute parallax because these objects are in highly reddened regions where no reliable reference star distance estimates were available. The relative parallaxes will be lower limits; comparison to the *Gaia* Data Release 2 (DR2) parallax values ([Gaia Collaboration et al. 2018](#)) suggest a correction to absolute of $+0.4 \pm 0.3$ mas for these six stars.

The proper motion of the target star with respect to the mean proper motion of the reference stars is presented as the total relative proper motion in Table 1. As discussed in [Dahn et al. \(2017\)](#), we choose to present the relative total proper motions to 0.1 mas yr⁻¹ and the position angle of total motion to 0.1 degree. We do not attempt to convert these relative proper motions to absolute values because, as noted by Dahn et al., the corrections are 2 – 6 mas yr⁻¹ ([Harris et al. 2016](#)) and the vast majority of the targets have a large proper motion. On the other hand, the ten targets with measured relative proper motions $\lesssim 20$ mas yr⁻¹ (0015+004, 0939+071, 0956–017, 1053–092, 1126+185, 1219+130, 1711+335, 2006+481, 2157–079, PG2300+166) may have an absolute proper motion significantly different from the value given in Table 1. The tangential velocities in Table 1 are presented primarily to flag high-velocity stars.

2.2. Comparison to *Gaia* DR2 Parallaxes

Gaia DR2 occurred on 2018 April 25. The [DR2 overview](#) gives the number of sources with positions, parallaxes and proper motions as 1.3×10^9 and estimates that the survey is complete for stars with *Gaia G* magnitudes (a broad filter covering 330 – 1050 nm) between 12 and 17, although an estimated 20% of stars with proper motions $> 0''.6$ yr⁻¹ are missing. More information is given in the [Gaia DR2 documentation](#) and [Gaia Collaboration et al. \(2018\)](#); [Lindegren et al. \(2018\)](#).

Although the stars in our sample are near the faint limit of DR2 and predominantly have high proper motion, 90% have *Gaia* DR2 trigonometric parallaxes. Appendix Table 19 gives the DR2 location, parallax, proper motion and *G* magnitude for these 196 stars, as well as the values of the astrometric goodness of fit statistic (ASTROMETRIC_GOF_AL), the astrometric excess noise measurement (ASTROMETRIC_EXCESS_NOISE) and the significance of the noise measurement (ASTROMETRIC_EXCESS_NOISE_SIG). There are 36 stars (identified in Table 19) for which the NOFS and *Gaia* parallax values differ by more than twice the combined uncertainty, which is larger than would be expected for a Gaussian error distribution. Eighteen of these 36 are flagged in DR2 as having a poor astrometric fit and significant excess noise (Table 19). It is also possible that the *Gaia* and/or NOFS uncertainties are underestimated. [Lindegren et al. \(2018\)](#) describes the *Gaia* parallax uncertainties as underestimated by 8 – 12% for fainter sources such as those in Table 19, and the

discrepancy for three of the 18 discrepant (but apparently well-measured) sources becomes $< 2 \sigma$ if the NOFS uncertainties are also underestimated by 10 – 20%. Finally, nine of the remaining 18 are known, suspect or candidate binary systems (Sections 6 and 8); the *Gaia* data model does not include orbital binary motion, and unresolved systems are treated as point sources by both *Gaia* and NOFS, so the astrometry for these sources could be affected by unmodeled motions. A remainder of 9 sources with discrepant measurements in a (well-measured) sample of 178 is consistent with a Gaussian distribution.

Figure 1 shows the difference between the NOFS and *Gaia* DR2 parallax values for 115 stars in our sample which have absolute parallaxes determined both by NOFS and *Gaia*, and for which the *Gaia* astrometric solution is robust as indicated by `ASTROMETRIC_GOF_AL < 3` and `ASTROMETRIC_EXCESS_NOISE_SIG < 2` (see the [Gaia DR2 documentation](#)). For these 115 stars the average uncertainty in the parallax value is 0.63 mas for NOFS measurements and 0.15 mas for *Gaia* measurements. Systematic errors in the DR2 data are estimated to be below 0.1 mas and there is an average parallax offset of $\sim 30 \mu\text{as}$ in the sense that the *Gaia* DR2 parallaxes are too small ([Lindegren et al. 2018](#)). Other work however indicates that the negative offset is 50 – 110 μas ([Muraveva et al. 2018](#); [Stassun & Torres 2018](#)). In Figure 1 symbol types identify known and suspect binaries (Sections 6 and 8), and eleven notionally single stars for which the NOFS and *Gaia* parallax values differ by more than 2σ . Similar to the discussion above, an increase of 10% in the uncertainty of both measurements reduces the number of outliers to what would be expected for a Gaussian distribution. Using the 75 sources which are not known or suspect binaries, and which have parallax measurements

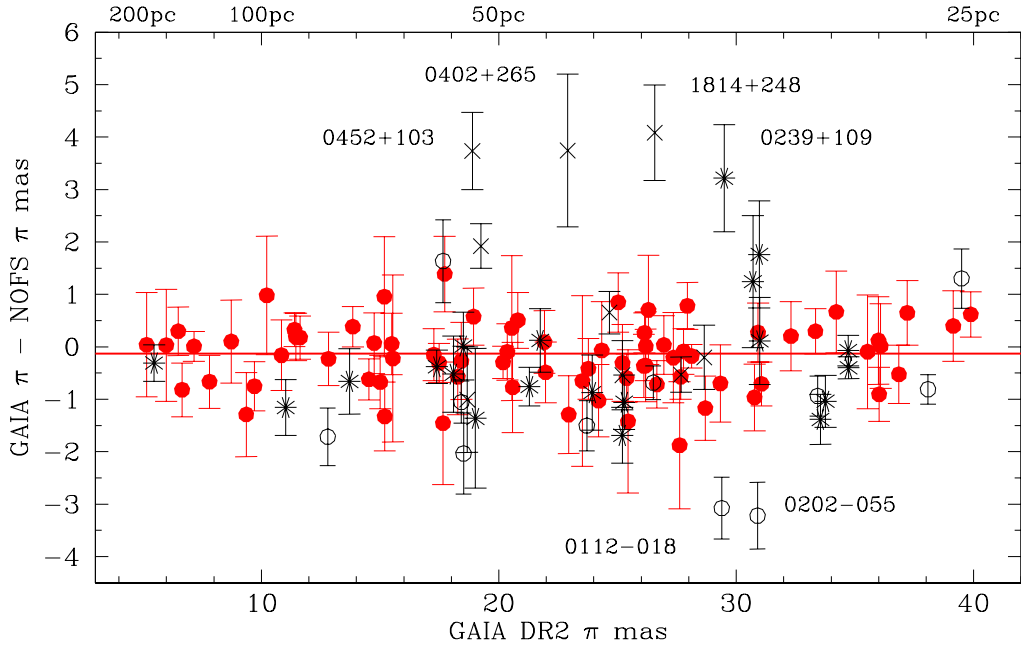


Figure 1. The difference between the absolute parallaxes from this work and *Gaia* Data Release 2 for 115 stars with *Gaia* `ASTROMETRIC_GOF_AL < 3` and `ASTROMETRIC_EXCESS_NOISE_SIG < 2`. Asterisks indicate known binary systems and crosses indicate suspected binary systems. Open circles are stars for which the two measurements differ by $> 2 \sigma$. The red line is a weighted fit to the remaining 75 stars (filled red circles); we find a small negative offset in the *Gaia* DR2 parallaxes of $-130 \pm 62 \mu\text{as}$.

that agree within 2σ (red symbols in Figure 1), we find that the difference between the NOFS and *Gaia* parallaxes is independent of distance and a weighted fit gives a mean offset of

$$\pi(\textit{Gaia} \text{ DR2}) - \pi(\text{NOFS}) = -130 \pm 62 \text{ } \mu\text{as}$$

with a spread around the mean of $260 \text{ } \mu\text{as}$. The size of the negative offset is consistent with that found by [Stassun & Torres \(2018\)](#).

The six most discrepant stars are identified in Figure 1. Four of these have *Gaia* parallaxes ~ 4 mas larger than the NOFS value; one is a known double degenerate (0239+109, [Bergeron et al. 1990a](#)), another a suspected double degenerate (1814+248, [Rolland & Bergeron 2015](#)), and we propose the other two are also double degenerate systems (0402+265, 0452+103; Sections 6 and 8).

A comparison of the relative proper motions measured by NOFS to the absolute proper motion measured by *Gaia* shows the known double degenerate 0239+109 as the extreme outlier in this comparison also, with the *Gaia* proper motion being larger than the NOFS relative value by 21 mas yr^{-1} . For this sample the average uncertainty in both the *Gaia* absolute motion and the NOFS relative motion is 0.3 mas yr^{-1} , with a correction to absolute for the NOFS values of $\pm 2 - 6 \text{ mas yr}^{-1}$ depending on position in the sky ([Harris et al. 2016](#)). Using the trimmed sample of 75 sources, we find an rms scatter in the difference between the NOFS relative motion and the *Gaia* absolute motion of 11 mas yr^{-1} , significantly smaller than the average motion of the sample which is 470 mas yr^{-1} .

3. PHOTOMETRY

The entire sample was matched to the optical photometric catalogs provided by the [Sloan Digital Sky Survey \(SDSS\) Data Release 14](#) and the [Pan-STARRS1 Data Release 1](#). The sample was also matched to the near-infrared photometric catalogs provided by the [Two Micron Sky Survey \(2MASS\)](#), the [tenth Data Release of the UKIRT Infrared Deep Sky Survey \(UKIDSS\)](#), the [UKIRT Hemisphere Survey \(UHS\) J–Band Data Release](#), and the [Visible and Infrared Survey Telescope for Astronomy \(VISTA\) public survey](#). The near-infrared sky survey photometry was supplemented by values for individual objects taken from the literature ([Bergeron & Leggett 2002](#); [Bergeron et al. 2005](#); [Farihi 2004](#); [Hall et al. 2008](#); [Harris et al. 1999](#); [Kilic et al. 2010](#); [Leggett et al. 1998](#)).

Table 2 lists *ugrizYJHK* for the sample. The *u* photometry is taken from the SDSS catalog, and *grizy* are from the Pan-STARRS1 Data Release 1. The *r* and *i* filters are very similar for the two surveys, but *g* and *z* differ ([Chambers et al. 2016](#)). The Appendix Table 20 lists the complete set of SDSS photometry where available. Pan-STARRS photometry is used as the default here because it is available for all stars in our sample, includes an additional filter in the red, agrees well with the SDSS values for stars in common, and has similar or smaller uncertainties. The *YJHK* photometry in Table 2 is all on the MKO photometric system, as defined by the UKIDSS filters. The 2MASS *JHK_s* magnitudes were converted to the UKIDSS system using transformations given in [Hodgkin et al. \(2009\)](#). The VISTA *ZYJHK_s* magnitudes were converted to the UKIDSS system using transformations given in [González-Fernández et al. \(2018\)](#). Some of the additional literature values were given in the CIT/LCO system, and these were converted to MKO using transformations given in [Leggett et al. \(2006\)](#). We adopted the near-infrared magnitudes with the smaller uncertainties, or in the case of multiple values with similar uncertainties we adopted the average value. The Appendix Tables 21, 22, 23 and 24 list the 2MASS, UKIDSS, UHS and VISTA magnitudes in each of those photometric systems.

Table 1. NOFS Astrometric Results

WD Number or Name	R.A. J2000.0	Decl. J2000.0	Filter	N_{tgt}	N_{frm}	Coverage	Years	N_{ref}	$\pi(\text{rel})$ (mas)	$\pi(\text{corr})$ (mas)	$\pi(\text{abs})$ (mas)	μ (mas yr $^{-1}$)	P.A. (deg)	V_{\tan} (km s $^{-1}$)	CCD
(1)	(2)	(3)	(4)	(5)	(6)	(7)	(8)	(9)	(10)	(11)	(12)	(13)	(14)	(15)	(16)
2359+636	00:02:23.80	+63:57:44.1	A2-1	89	143	2008.57–2012.95	4.37	29	37.49 ± 0.26	1.40 ± 0.07	38.89 ± 0.27	925.9 ± 0.1	83.2 ± 0.1	112.8	EEV24
0002+729	00:05:06.86	+73:13:09.4	A2-1	83	124	1998.57–2003.81	5.24	15	27.07 ± 0.48	1.28 ± 0.11	28.35 ± 0.49	227.2 ± 0.2	57.6 ± 0.1	38.0	Tek2K
0003–103	00:05:55.91	-10:02:13.5	A2-1	97	112	2007.72–2014.82	7.10	11	5.35 ± 0.41	0.85 ± 0.06	6.20 ± 0.41	82.9 ± 0.1	67.4 ± 0.1	63.4	Tek2K
0003+177	00:06:22.95	+18:00:13.4	ST-R	52	60	1990.78–1995.82	5.04	8	17.86 ± 1.16	0.54 ± 0.05	18.40 ± 1.16	427.2 ± 0.5	139.2 ± 0.1	110.0	T1800
0003+177	00:06:22.95	+18:00:13.4	A2-1	72	78	1992.57–1996.95	4.39	10	16.37 ± 0.53	0.83 ± 0.07	17.20 ± 0.53	419.4 ± 0.4	139.1 ± 0.1	115.5	Tek2K

Note—Table 1 is published in its entirety in the machine-readable format. A portion is shown here for guidance regarding its form and content.

Table 2. Optical and Near-Infrared Photometry

WD Number or Name	<i>u</i>	<i>g</i>	<i>r</i>	<i>i</i>	<i>z</i>	<i>y</i>	<i>Y</i>	<i>J</i>	<i>H</i>	<i>K</i>
SDSS										
	Pan-STARRS									
2359+636	... ± ...	17.654 ± 0.001	16.987 ± 0.002	16.725 ± 0.003	16.630 ± 0.002	16.595 ± 0.002	... ± ...	15.784 ± 0.067	15.561 ± 0.136	15.516 ± 0.216
0002+729	... ± ...	14.231 ± 0.002	14.445 ± 0.002	14.684 ± 0.003	14.872 ± 0.002	15.020 ± 0.005	... ± ...	14.614 ± 0.036	14.568 ± 0.055	14.757 ± 0.100
0003-103	17.346 ± 0.014	17.746 ± 0.005	18.199 ± 0.007	18.524 ± 0.013	18.796 ± 0.012	18.962 ± 0.025	... ± ± ± ± ...
0003+177	17.412 ± 0.029	17.053 ± 0.005	16.981 ± 0.001	17.046 ± 0.003	17.133 ± 0.004	17.192 ± 0.013	... ± ...	16.208 ± 0.126	... ± ± ...
0015+004	16.830 ± 0.012	16.970 ± 0.005	17.202 ± 0.002	17.450 ± 0.005	17.646 ± 0.006	17.792 ± 0.015	17.353 ± 0.015	17.346 ± 0.017	17.376 ± 0.066	17.554 ± 0.114

Note—*ugrizy* are AB magnitudes and *YJHK* are Vega magnitudes. Magnitudes are Pan-STARRS MeanPSFMag, and UKIDSS and VISTA apermag3. Table 2 is published in its entirety in the machine-readable format. A portion is shown here for guidance regarding its form and content.

Table 3. New *Spitzer* Photometry

WD Number or Name	AOR Number	Principal Investigator	3.6 μm	4.5 μm	5.8 μm	8.0 μm
			μJy			
0015+004	46975488	Luhman	30.30 \pm 0.15	21.12 \pm 0.13	... \pm \pm ...
0235+064 ^a	13106176	Zuckerman	207.52 \pm 6.35	122.76 \pm 5.34	70.88 \pm 4.73	21.84 \pm 2.73
PG 0235+064B	13106176	Zuckerman	16301.38 \pm 1.24	10827.47 \pm 1.01	9379.95 \pm 1.07	4648.51 \pm 3.22
0507+045A	10148352	Kuchner	... \pm ...	107.11 \pm 0.68	... \pm ...	61.43 \pm 1.37
0507+045A	39876352	Luhman	... \pm ...	101.86 \pm 0.66	... \pm \pm ...
0507+045B ^b	10148352	Kuchner	... \pm ...	218.84 \pm 1.07	... \pm ...	132.41 \pm 6.83
0507+045B	39876352	Luhman	... \pm ...	208.16 \pm 4.27	... \pm \pm ...
0919+296	17645568	Fazio	12.53 \pm 0.23	9.72 \pm 0.20	... \pm \pm ...
1042+593	5175040,7770880	Lonsdale	... \pm ...	38.43 \pm 1.07	... \pm \pm ...
1235+422	54331904	Trilling	... \pm ...	84.50 \pm 0.27	... \pm \pm ...
1314–153	58372096	Farihi	210.16 \pm 0.95	145.18 \pm 1.07	... \pm \pm ...
1439–195	61795584	Trilling	81.97 \pm 0.14	53.23 \pm 0.11	... \pm \pm ...
1540+236	40159744,58045952	Zuckerman	227.49 \pm 0.23	143.13 \pm 0.18	... \pm \pm ...
1552+177	47827456	Jura	54.08 \pm 0.20	37.21 \pm 0.17	... \pm \pm ...
1845+019 ^c	42671360	Whitney	7019.51 \pm 42.35	4910.5 \pm 4.27	... \pm \pm ...
1912+143	45942528	Whitney	89.70 \pm 2.71	50.87 \pm 2.24	... \pm \pm ...
2005+175	23614464	Howell	... \pm ...	1405.32 \pm 1.05	... \pm ...	1037.40 \pm 13.65
2028+390	27107072,27107840	Hora	543.35 \pm 1.48	388.46 \pm 1.29	150.02 \pm 9.45	... \pm ...
2148+539	37871360	Whitney	74.11 \pm 5.29	... \pm \pm \pm ...

NOTE—The absolute flux calibration uncertainty of 2% (Reach et al. 2005) is not included in the given errors.

^a[3.6], [4.5] and [5.8] fluxes determined here are brighter than published by Farihi et al. (2008).

^b[8.0] flux determined here is fainter than published by Mullally et al. (2007).

^c[3.6] and [4.5] fluxes determined here are fainter than published by Barber et al. (2016).

Mid-infrared photometry was also obtained for the sample from the Wide-field Infrared Survey Explorer (WISE) ALLWISE catalog. *Spitzer* Space Telescope Infrared Array Camera (IRAC) photometry was also included for some stars — this camera has smaller pixels and is more sensitive than the *WISE* imager. IRAC photometry was taken from the literature (Barber et al. 2012, 2014, 2016; Bergfors et al. 2014; Farihi et al. 2008, 2009, 2010, 2012; Jura et al. 2007; Kilic et al. 2009, 2010, 2012; Mullally et al. 2007; Xu & Jura 2012) and new photometry was also measured for this work using processed images taken from the *Spitzer* data archive. The *Spitzer* photometry was determined where the *WISE* data were missing or not consistent with the near-infrared photometry. Table 3 lists the *Spitzer* fluxes measured here. Stars are identified in Table 3 for which the fluxes measured here differ significantly from previously published values using the same images. The agreement with the modelled fluxes support the values determined here. The stars with discrepant photometry are in crowded fields and care has to be taken with target and sky aperture placement; possibly the more recent *Spitzer* pipeline produced cleaner images than were previously available. The Appendix Table 24 lists all *WISE* and *Spitzer* photometry available, as Vega magnitudes.

4. NEW OPTICAL SPECTROSCOPY

In this paper we explore the properties of the WDs primarily by comparing models to the SED as given by absolute photometric fluxes (Section 5). An optical spectrum can provide a check of the photometric fit or in some cases it can distinguish between equally likely photometric solutions. For these reasons we obtained spectra of seven WDs, as well as the red dwarf companion to one of the WDs. Targets were selected which were accessible in the sky, which had no or poor-quality spectra available and where the spectrum would significantly contribute to the model analysis. Spectra covering 490 – 820 nm were obtained at the Gemini North and South Observatories using the GMOS instruments (Hook et al. 2004; Gimeno et al. 2016). The data were obtained using Gemini’s Fast Turnaround program, via programs GN-2018A-FT-209 and GS-2018A-FT-206. The data were taken in thin cirrus with seeing that ranged from 0''.5 to 1''.0. The 1''.0 slit was used with the B600 grating, producing a resolution of 0.5 nm. Data were obtained for each star at wavelengths that differed by 10 nm so that chip gaps were covered. Flat fielding and wavelength calibration was done using calibration lamps mounted on the telescopes. The instrument sensitivity functions were determined using the calibration stars EG 131 at Gemini South and Feige 34 at Gemini North; final flux calibration was done using the Pan-STARRS *r* and *i* photometry for each target. Figure 2 shows the new spectra for the seven WDs. The observations are listed in Table 4, together with new spectral types for six of the seven targets.

5. MODEL ATMOSPHERES AND FITTING TECHNIQUE

The analyses presented here involve fitting the observed flux-calibrated WD SEDs with pure-H and pure-He atmospheric models using a least-squares method; models are also available for more unusual compositions. Holberg & Bergeron (2006) provide more information on the flux calibration process. The models for the hydrogen-atmosphere WDs are built from the code described in Bergeron et al. (1995) and references therein, with recent improvements discussed in Tremblay & Bergeron (2009). The helium-atmosphere models are described in Bergeron et al. (2011). Cooler models with mixed hydrogen-helium atmospheres are also available, as described in Gianninas et al. (2015). The analyses of DQ (carbon-rich) and DZ (metal-rich) white dwarfs rely on the LTE model atmosphere calculations developed by Dufour et al. (2005, 2007b,a, 2008).

Table 4. New Optical Spectroscopy

WD Number or Name	Coordinates 2018.3	Instrument	Date YYYYMMDD	Exposure minutes	Spectral Type Simbad	New
0637+335	06:40:33.59+33:27:34.6	GMOS-N	20180505, 20180506	18	High proper motion star	DC
0918–172 ^a	09:20:47.89–17:28:57.9	GMOS-S	20180419	18	DA	DA
LP 787–25 ^a	09:20:47.02–17:29:01.6	GMOS-S	20180419	18	High proper motion star	dM6 ^b
1401–149	14:03:42.57–15:14:21.8	GMOS-S	20180421	36	High proper motion star	DC
1524+566	15:25:42.75+56:29:05.8	GMOS-N	20180523	16	DC9	DA
1923+550	19:24:09.68+55:06:52.1	GMOS-N	20180521	16	dM7.5 ^c	DA
1944+467B	19:45:21.42+46:50:01.7	GMOS-N	20180526	18	High proper motion star	DA
1944+467A	19:45:21.44+46:50:10.4	GMOS-N	20180526	18	High proper motion star	DA

^a0918–172 and LP 787-25 form a binary system with separation 13''.0.

^bTyped by comparison to SDSS spectral templates (Bochanski et al. 2007).

^cSimbad gives the spectral type for the red dwarf companion determined by Kirkpatrick et al. (2010).

The fits are iterated allowing T_{eff} , the solid angle $\pi(R/D)^2$ (where R is stellar radius and D is distance) and surface gravity g to vary. The model flux is interpolated at T_{eff} and $\log g$ where $\log g$ is obtained from R and evolutionary models similar to those described in Fontaine et al. (2001) but with C/O cores, $q(\text{He}) \equiv \log M_{\text{He}}/M_{\star} = 10^{-2}$ and $q(\text{H}) = 10^{-4}$, which are representative of hydrogen-atmosphere white dwarfs, and $q(\text{He}) = 10^{-2}$ and $q(\text{H}) = 10^{-10}$, which are representative of helium-atmosphere white dwarfs. For the (few) WDs with mass $< 0.2 M_{\odot}$ the Althaus et al. (2013) mass-radius relationship was used. Iterations end when the value of R required for flux scaling the model is consistent with the value implied by g . The WD cooling age (the time since the star left the main-sequence) is determined once T_{eff} , mass and atmospheric composition are known. The method is described in detail by Bergeron et al. (1997).

The atmospheric parameters can be further checked by comparing synthetic spectra to any observed line profiles, the depth and width of which are sensitive to T_{eff} , g and atmospheric composition (e.g. Limoges et al. 2015). Spectra were obtained from the literature (Bergeron et al. 1992, 2001, 2011; Giannicchele et al. 2012; Gianninas et al. 2011; Greenstein 1986; Liebert et al. 2005; Limoges et al. 2015; Napiwotzki et al. 2003; Oppenheimer et al. 2001; Reid & Gizis 2005; Rolland et al. 2018;

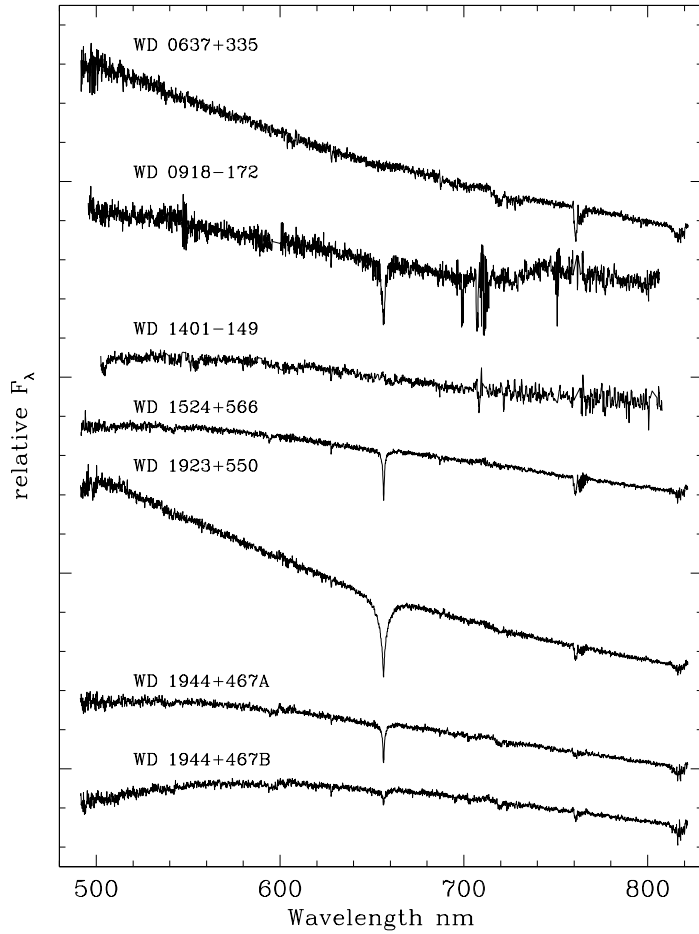


Figure 2. New Gemini WD spectra obtained for this work. The spectrum of the dM6 companion to WD 0918–172 is not shown. The features near 760 nm are telluric. For WD 0918–172 difficulty determining the instrument sensitivity function at longer wavelengths likely produces a spurious rise in flux at $\lambda > 720$ nm.

Subasavage et al. 2007, 2008, 2009) and from the SDSS spectroscopy archive. New spectra were also obtained for this work, as described in Section 4.

Figure 3 shows examples of fits to a warm DB and a warm DA WD, as well as a cool WD which is too cool to show H α but for which the photometric SED constrains the atmosphere to be pure hydrogen. This Figure shows that the u -band is a powerful composition diagnostic, however it is excluded in the fitting process because its inclusion distorts the helium-rich fit. Figure 4 shows examples of fits to a DQ and a DZ WD. The WDs in Figures 3 and 4 have photometry which covers a broad wavelength range. Usually very little flux emerges from the WD atmospheres at mid-infrared wavelengths, and those data are not used in the model fitting, however the Figures show that there is good agreement between the models and observations across the entire SED, including the mid-infrared.

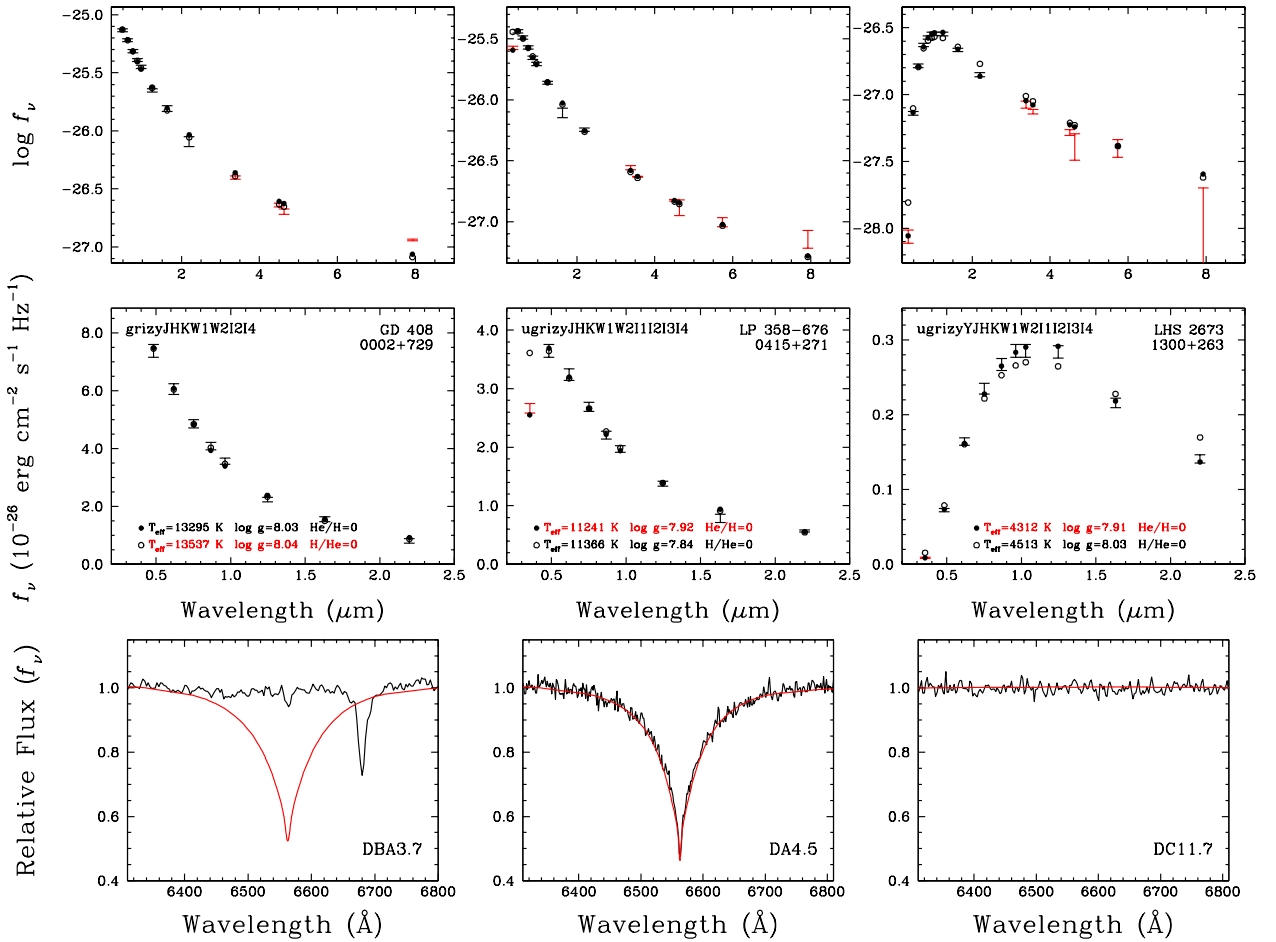


Figure 3. Examples of model fits to (left to right) a warm DB, a warm DA and a cool hydrogen-rich WD where the SED constrains the atmospheric composition. In the upper plots error bars represent the observed fluxes through various filters and circles are the fitted model datapoints. Red error bars indicate that the bandpass was omitted from the fit. In the bottom panel the observed spectrum is in black and the hydrogen-rich model spectrum in red. The adopted model parameters are given in red in the middle panels.

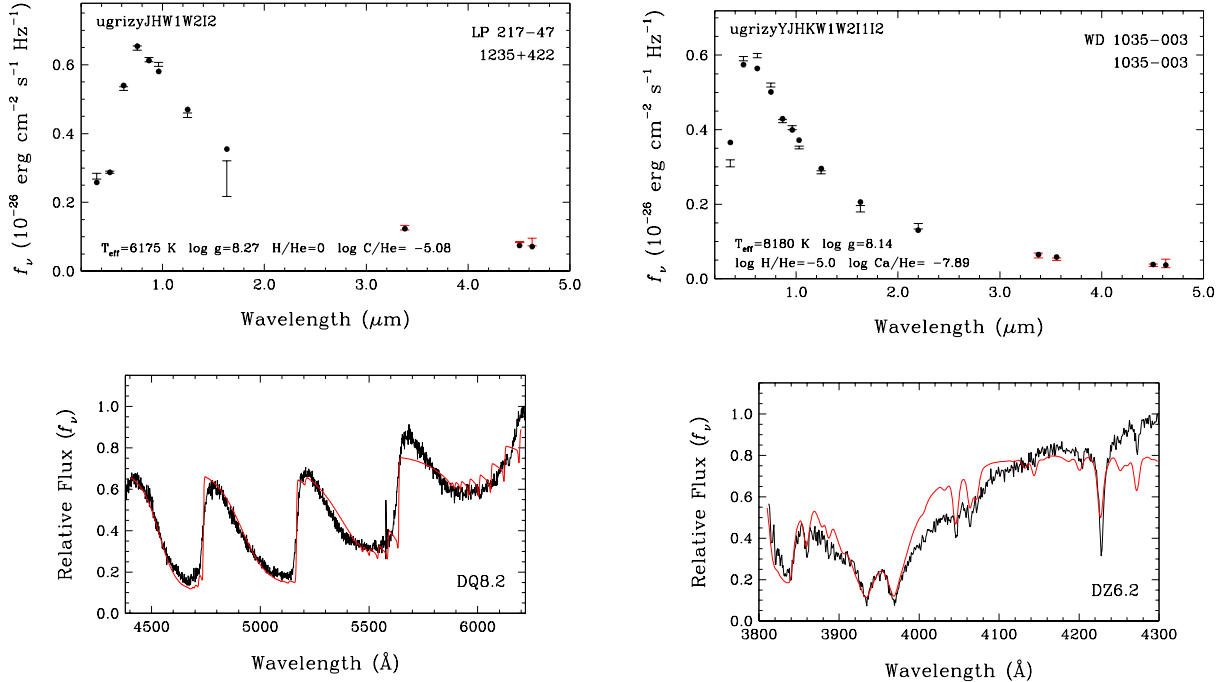


Figure 4. Model fits to a DQ and a DZ. Error bars represent the observed fluxes and circles are the model datapoints. Red error bars indicate that the bandpass was omitted from the fit. The observed spectrum is shown in black; the red spectrum is generated using the model parameters given in the top panels.

Table 5. Stars Not Analysed

WD Number	Name	Simbad Spectral Type	Note, Revised Classification
0104+509	GD 274	high PM star	subdwarf+K star (Ulla & Thejll 1998)
0136-005	LP 588-25	M6V eclipsing binary	D:+dM (Parsons et al. 2012)
	PG 0235+064B	Infra-Red source	dM3.5 from SDSS spectrum and classification (this work)
0330-090	V* LL Eri	DA+M2.5V	DA+M2.5V (Kawka et al. 2002)
	LP 787-25	high PM star	M dwarf (this work; Figures 5, 6)
	G117-B15B	M3.5V	M3.5V (Kirkpatrick et al. 2011)
	LHS 2140	sdM0.5	sdM0.5 (Gizis & Reid 1997)
0939+071	EGGR 431	DC7	dF (Gianninas et al. 2011)
1126+185	PG 1126+186	DC+G/K(e)	sdB+G/K (Farihi et al. 2005)
1135+036	V* T Leo	dwarf nova	ultrashort period red dwarf + WD (Shafter & Szkody 1984)
1148+544	LP 129-586	DA5	dM5 from SDSS spectrum and classification (this work)
1232+379	V* AM CVn	cataclysmic variable	interacting DB WDs (Ulla & Solheim 1990)
1303+182	V* GP Com	nova-like star	interacting DB WDs (Ulla & Solheim 1990)
1711+335	V* V795 Her	nova	SW Sex star — extreme mass transfer (Schmidtobreick 2017)
	V* AM Her	cataclysmic variable	interacting magnetic WD and M4V (Kawka & Vennes 2005)
2005+175	V* WZ Sge	dwarf nova	interacting WD and red or brown dwarf (Kato 2015)
2006+481		DB	sdOB (Bergeron et al. 2000)
2154+408		DA1.7	DA+dM3.5 (Hillwig et al. 2002)
	LP 400-21	high PM star	M dwarf (this work; Figures 5, 6)
2300+165	PG 2300+166	variable star	subdwarf or subdwarf binary (this work; Figures 5, 6)

6. OVERVIEW OF THE SAMPLE

6.1. Core Sample of 179 Notionally Single WDs

Figure 5 shows our entire parallax sample of 214 stars in a color-magnitude diagram which uses Pan-STARRS photometry. Sequences for $0.6 M_{\odot}$ WDs are shown, generated by the models described in Section 5. A 1 Gyr isochrone for solar-metallicity stars is also shown generated in Pan-STARRS colors using the PARSEC color-magnitude diagram web interface (Bressan et al. 2012; Marigo et al. 2013, 2017; Rosenfield et al. 2016). The majority of the sample — 179 stars, or 84% — are single WDs, or have not been confirmed to be multiple and can be fit with our models as single WDs. These 179 WDs form our core sample and the rest of this paper focusses on these stars.

6.2. Other Stars in the Sample

The remaining 35 stars are more complex. Twenty are either not WDs or are WDs in systems too complex for this study. These 20 stars are listed in Table 5 and identified in the left panel of Figure

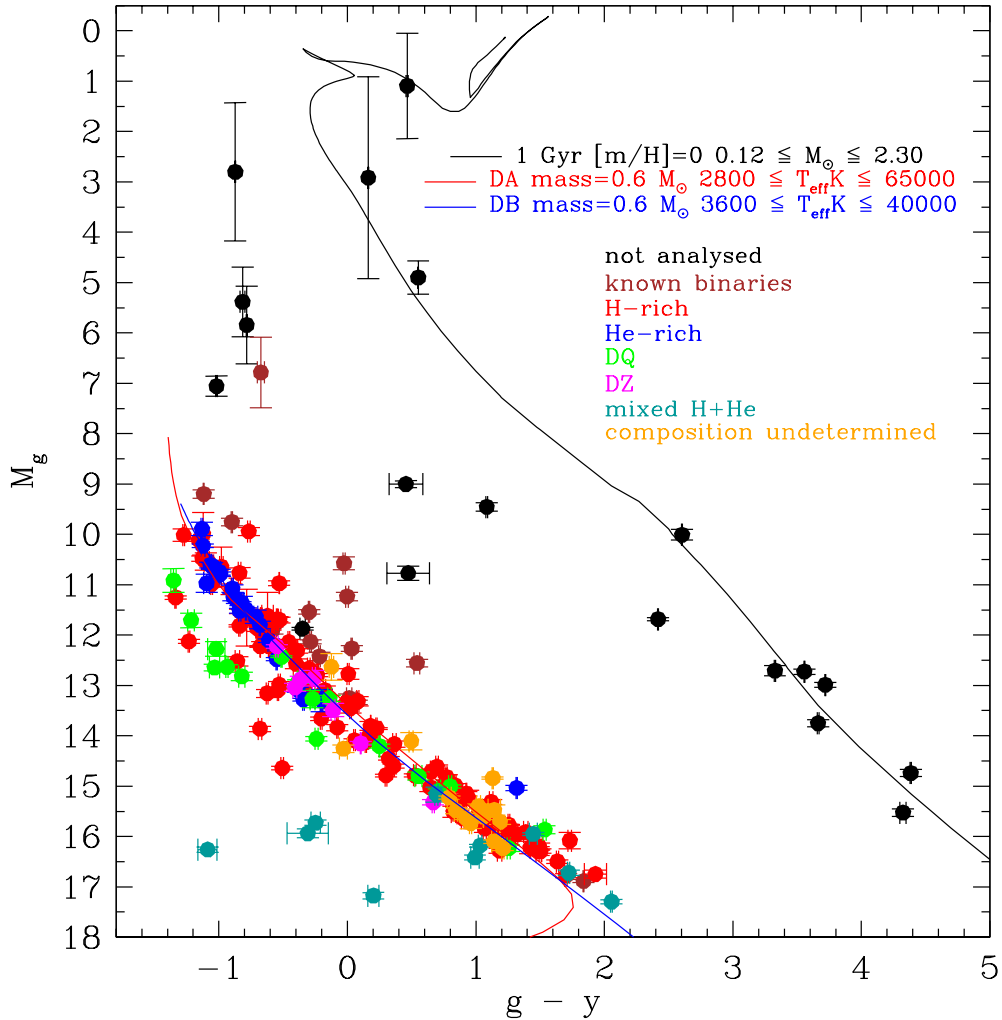


Figure 5. The $g - y : M_g$ color-magnitude diagram for the 214 stars in our sample.

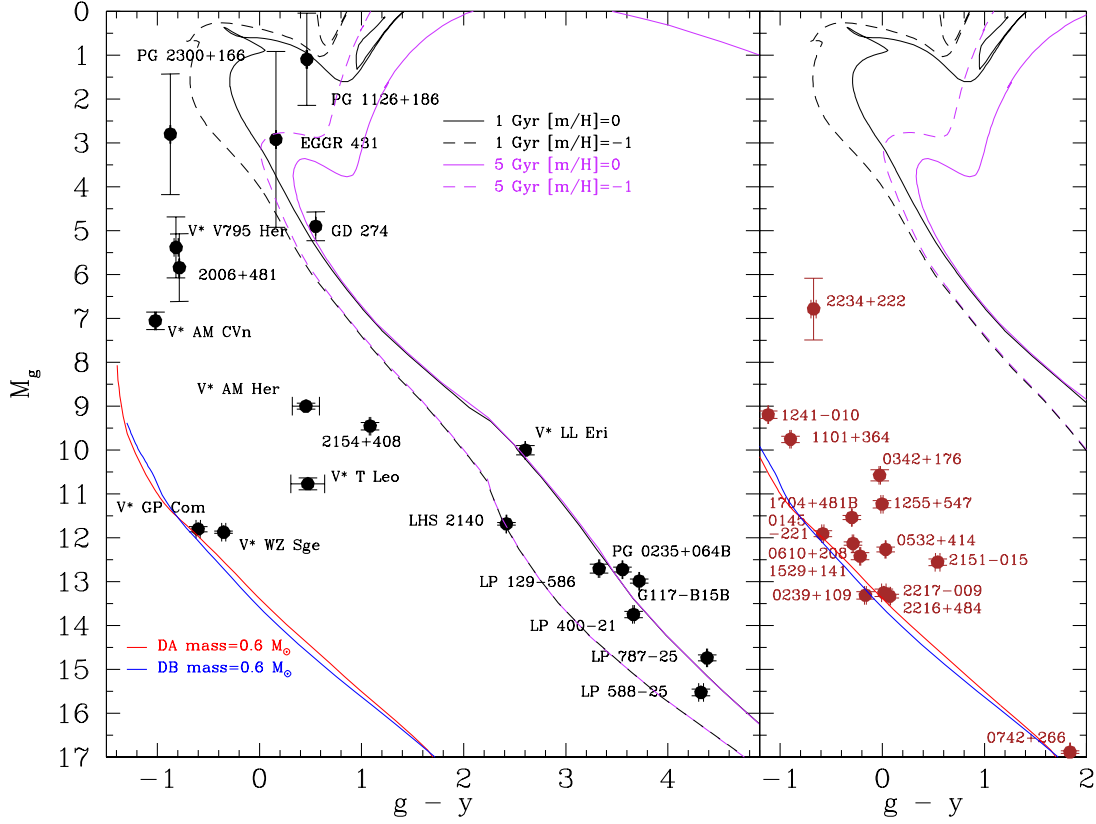


Figure 6. Same as Figure 5, for stars not analyzed (left panel) and unresolved binaries (right panel).

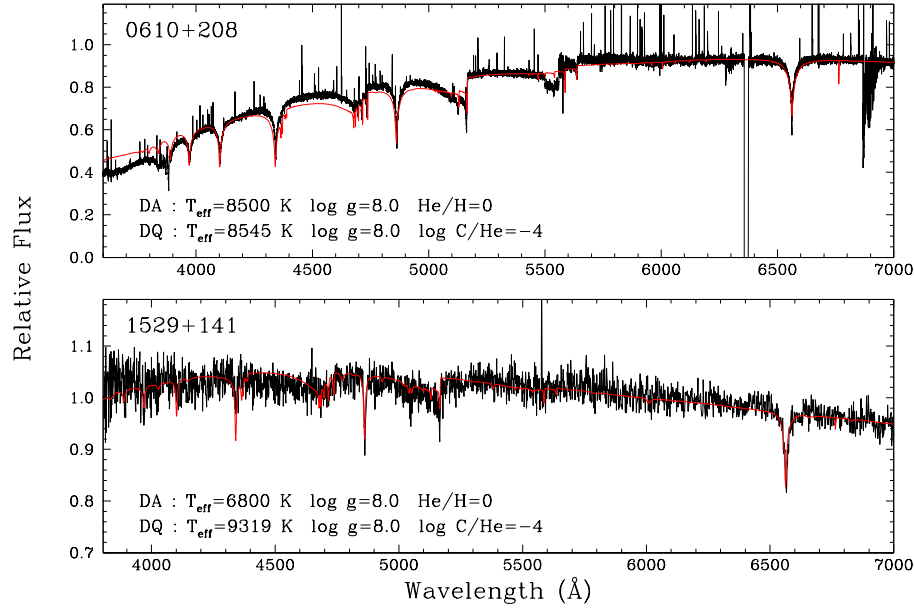


Figure 7. Preliminary fit to two DQ+DA binaries in the sample, see Table 6.

Table 6. White Dwarfs in Unresolved Binaries

WD Number	Name	Spectral Type	Binary Reference	Model Fit
0145–221	GD 1400	DA4.6+dL	Wachter et al. (2003)	dL optical flux contribution is negligible, DA fit: $T_{\text{eff}} = 10959$ K, $\log g = 8.04$
0239+109	G4-34	DA+DC	Bergeron et al. (1990a)	Gianninas et al. (2011) fit the spectrum and SED: $T_{\text{eff}} = 10060$ K DA and a $T_{\text{eff}} = 7620$ K DC
0342+176	LP 413-40	DA+DA	Kilic et al. (2010)	assuming the system is two identical DA WDs: $T_{\text{eff}} = 8314$ K, $\log g = 6.82$
0532+414	GD 69	D:+D:	Toonen et al. (2017)	assuming the system is a single DA: $T_{\text{eff}} = 7378$ K, $\log g = 7.14$
0610+208	GD 73	DQ+DA	Vennes & Kawka (2012)	Figure 7, the spectrum and SED can be fit as: $T_{\text{eff}} = 8500$ K DA and a $T_{\text{eff}} = 8545$ K DQ
0742+266	LSPM J0745+2627	D:+dM2	Parsons et al. (2013)	dM flux significant, if fit as single WD: $T_{\text{eff}} = 3933$ K, $\log g = 7.92$ DC
1101+364		D:+D:	Maxted & Marsh (1999)	assuming the system is a single DA: $T_{\text{eff}} = 13625$ K, $\log g = 6.92$
1241–010	PG 1241–010	DA+DA+dM	Farihi et al. (2005)	dM flux contribution small, fit as single DA: $T_{\text{eff}} = 22732$ K, $\log g = 7.24$
1255+547		DA+DA	Marsh et al. (2011)	assuming the system is two identical DA WDs: $T_{\text{eff}} = 7414$ K, $\log g = 7.09$
1529+141	GD 184	DQ+DA	Giambicheli et al. (2012)	Figure 7, the spectrum and SED can be fit as: $T_{\text{eff}} = 6800$ K DA and a $T_{\text{eff}} = 9319$ K DQ
1704+481B	EGGR 577	DA+DA	Maxted et al. (2000)	assuming the system is a single DA: $T_{\text{eff}} = 8767$ K, $\log g = 7.18$
2151–015	EGGR 151	DA5.6+dM8	Maxted & Marsh (1999)	dM optical flux contribution is negligible, DA fit: $T_{\text{eff}} = 8989$ K, $\log g = 7.98$
2216+484	GD 402	DC+DA	Bergeron et al. (1990a)	Bergeron et al. (1990a) fit the spectrum and SED: $T_{\text{eff}} = 6200$ K DA and a $T_{\text{eff}} = 7080$ K DC
2217–009	PHL 5038	DA6.8+dL8	Steele et al. (2009)	dL optical flux contribution is negligible, DA fit: $T_{\text{eff}} = 7466$ K, $\log g = 7.95$
2234+222	LP 400-22	DA+DA	Kilic et al. (2009)	assuming the system two identical DA WDs: $T_{\text{eff}} = 10716$ K, $\log g = 5.64$

6. Note that six stars with WD numbers are not in fact WDs: 0104+509, 0939+071, 1126+185, 1148+544, 2006+481, and 2300+165. Three stars in Table 5 are newly classified as red dwarfs: PG 0235+064B, 1148+544 (LP 129-586), and LP 400-21.

Table 6 and the right panel of Figure 6 identify fifteen known unresolved WD+WD or WD+dM/L binaries. In some cases we can produce model fits — Figure 7 shows a preliminary deconvolution of the spectra of two DA+DQ binaries for example. However these fits are not rigorous and detailed analyses are postponed to a future paper.

6.3. Interstellar Extinction and Reddening

The core sample of 179 WDs includes stars at large distances. We corrected for reddening the observed fluxes for the 13 WDs at > 100 pc (Table 7), before fitting the models. We use the approach described in Harris et al. (2006) except that we use extinction vectors from Green et al. (2018). Green et al. give vectors for Pan-STARRS and 2MASS filters, but not for MKO filters. We estimated the MKO $YJHK$ extinction by applying the λ^{-1} extinction dependence seen in the near-infrared (Cardelli et al. 1989) to Pan-STARRS y and 2MASS JHK_s values. The correction makes the WD brighter — T_{eff} increases and cooling age decreases. For the 11 WDs with $b > 10^\circ$,

Table 7. Reddening Correction for Distant White Dwarfs

WD Number	Spectral Type	Distance pc	Galactic Latitude deg.	T_{eff} K	Mass M_{\odot}	$\log g$ dex	Cooling Age Myr	Corrected – Uncorrected			
								$\delta(T_{\text{eff}})$	$\delta(\log g)$	$\delta(\text{mass})$	$\delta(\text{Age})$
0003–103	DQhot2.4	161	−69.8	20882	1.125	8.863	333	593	0.015	0.008	−19
0015+004	DBP3.5	132	−61.0	14532	0.621	8.054	240	172	0.011	0.007	−4
0112+104	DB1.8	116	−51.8	27942	0.518	7.818	13	582	0.014	0.007	−1
0500+573	D:6.0	108	9.7	8226	0.426	7.700	706	379	0.080	0.039	−29
0919+296	DQ6.2	116	44.3	8068	0.652	8.122	1277	19	0.002	0.001	−4
0954+342	DB1.9	207	52.3	27023	0.909	8.488	72	3760	0.057	0.039	−38
0956−017	DAZ3.7	196	39.3	13526	0.674	8.108	315	1080	0.028	0.019	−64
1002+430	DA2.5	124	53.1	19895	0.584	7.928	58	772	0.044	0.026	−4
1053−092	DA2.2	195	43.9	23298	0.498	7.736	22	1592	0.063	0.032	−7
1219+130	DAZ4.2	211	74.0	12018	0.573	7.943	345	603	0.026	0.016	−39
1327+594	DQAPhot2.7	134	57.3	18755	1.194	9.011	640	655	0.031	0.014	−30
1910+047	DA2.1	168	−2.4	24208	0.673	8.070	32	7540	0.300	0.179	−60
2157−079	DQhot1.9	236	−45.1	26142	1.009	8.649	120	3363	0.109	0.070	−28

T_{eff} increases by 4% and cooling age decreases by 10%, on average. The changes to $\log g$ and mass are small. The object with the largest correction is 1910+047; the nominal correction produces unphysical parameters and instead we applied 10% of the maximum extinction which gives a T_{eff} value consistent with that determined by Vennes (1990) from a fit to the observed Balmer lines and gives values for g and mass close to the canonical WD values.

7. OBSERVATIONAL PROPERTIES OF THE SAMPLE OF 179 WHITE DWARFS

7.1. Atmospheric Composition and Trends with Color

Table 8 lists the 179 WDs in this sample that are assumed to be single stars and which we have analyzed with the models described in Section 5. All the WDs in Table 8 have a numerical type based on our assigned T_{eff} . For each object the previous spectral classification as given in Simbad is listed, as well as the classification adopted here. Atmospheric composition is also given, based on our model analyses. Of these 179 stars, 17 were previously identified only as “High proper motion star” or “D:” in Simbad, and we reclassify one from “M7.5” to DA (Table 4). An additional eight WDs are reclassified from DC to DA either based on new spectra (Table 4) or reexamination of existing spectra. Table 9 lists these 26 WDs which have significantly revised types.

Table 8. White Dwarf Spectral Classification

WD Number	Name	Spectral Type		Composition
		Simbad	Adopted	
2359+636	LSR J0002+6357	DC	DC10.4	unconstrained
0002+729	GD 408	DB4	DBA3.7 ¹	He
0003-103	PHL 657	DQ	DQhot2.4 ²	$N(\text{He})/N(\text{C}) = 10^{-3.0}$
0003+177	G131-19	DQ6	DQ6.7	$N(\text{C})/N(\text{He}) = 10^{-5.62}$
0015+004	PB 5847	DBH	DBP3.5 ³	He
0042-064	PHL 6585	DC	DC10.1	$N(\text{He})/N(\text{H}) = 10^{-0.06}$
0102+210A	LHS 5023	DC9	DA9.5	H
0102+210B	LHS 5024	DC12	DC10.5	H
0112+104	EGGR 409	DB2.5	DB1.8	He
0112-018	LP 587-16	DC9	DA9.5	H
0114-049A	LP 647-33	DC9	DC:10.3	H
0114-049B	LP 647-34	DC9	DC:9.8	He
0145-174	EGGR 467	DA6.9	DA6.8	H
0202-055		DC	DC12.2	H
0203+207	G35-26	DAQ3	DQA3.1	$N(\text{He})/N(\text{C}) = 10^{-3.0}$
0203+183	LHS 1341	DC:	DC11.6	H
0228+269	LP 354-381	DC9	DC:10.4	H
0235+064	PG 0235+064	DA3.5	DA3.8	H
0236+745	LP 30-203	DA5.5	DA5.7	H
0239+167	LP 410-80	DQ	DQ7.7 ⁴	
0246+326		DA4.2	DA4.6	H
0246+734	LP 30-265	DZ6	DZ6.5 ⁵	$N(\text{Ca})/N(\text{He}) = 10^{-10.0}$
0300-013	GD 40	DBZ4	DBZ3.6	He
0302+621	GD 426	DA4.5	DA4.8	H
0306+663	LSR J0310+6634	DC	DC10.7	unconstrained
0339+523	EGGR 567	DA3.8	DA3.8	H
0343+247		D:	DC14.4	$N(\text{He})/N(\text{H}) = 10^{-0.39}$
0346-011	GD 50	DA1.2	DA1.2	H
0349+495	LHS 1611	DA6.8	DA6.7	H
0357+513	LSR J0401+5131	DC8	DC10.0	unconstrained
0402+265	LHS 1625a	High PM star	DC12.7	H
0407+197	LHS 1636	DC9	DC:9.6	H
0409+237	EGGR 480	DC7	DC:6.7	unconstrained
0415+271	LP 358-676	DA4.3	DA4.5	H
0437+093	LHS 1693	DA8.1	DA8.0	H
0452+103	G83-43	DA6.5	DA6.8	H
0500+573	LP 85-9	High PM star	D:6.0	unconstrained
0506-154	LP 777-3	DA	DA9.7	H
0507+045B	HS 0507+0434A	DA2.3	DA2.6	H
0507+045A	HS 0507+0434B	DA4.1	DA4.6	H
0527+185	LP 517-35	High PM star	D:9.3	H
0530+054	LP 538-4	High PM star	D:9.7	H
0531+572	LP 85-33	High PM star	DC:10.2	unconstrained

Table 8 continued on next page

Table 8 (*continued*)

WD Number	Name	Spectral Type		Composition
		Simbad	Adopted	
0541+260	LSR J0544+2603	DC	DC10.0	He
0541+750	LP 33-221	High PM star	D:8.4	unconstrained
0546+234	LSR J0549+2329	High PM star	D:10.6	He
0557+237	G104-10	DA6.0	DA6.0	H
0559+158	G105-4	DA7.0	DA7.2	H
0600+735	EGGR 421	Dawk	DA7.8	H
0625+100	G105-B2B	DZ6	DZ5.9 ⁵	N(Ca)/N(He)= 10 ^{-10.33}
0632+409	G107-9	DA6.3	DA6.4	H
0637+335	LP 254-13	High PM star	DC5.7	He
0637+477	GD 77	DAP3.4	DAP3.7 ³	H
0651-020	GD 80	DA1.5	DA1.7	H
0650+397	GD 79	High PM star	D:4.8	He
0654+027	G108-42	DC5	DC5.4	He
0701+517	LP 122-34	High PM star	D:9.8	unconstrained
0708+462	LHS 1905	DC	DC:10.5	unconstrained
0714+458	GD 84	DBAZ?6	DQ5.0	He ⁶
0749+426	LP 207-50	DC	DC10.9	H
0826+455	GD 91	DA4.8	DA5.0	H
0855+416		DAH	DAH6.8	H
0913+103	PG 0913+104	DCQ5	DQ5.9	N(C)/N(He)= 10 ^{-4.66}
0918-172	LP 787-26	DA	DA8.1	H
0919+296	LP 313-49	DQ	DQ6.2	N(C)/N(He)= 10 ^{-4.52}
0921+354	G117-B15A	DA4.1	DA4.3	H
0922+053	LSPM J0925+0509	DA	DA4.7	H
0922+005	LHS 2139	High PM star	D:12.2	N(H)/N(He)= 10 ^{-6.39}
0937+654	SDSS J0941+6511	DC:	DC11.3	H
0944+452B		DC	DC16.7	N(H)/N(He)=10 ^{-2.92}
0944+452A		DA	DA10.3	H
0955+247	EGGR 69	DA5.8	DA5.9	H
0954+342		DB	DB1.9	He
0956-017	EQ J0959-0200	DAZ	DAZ3.7	H
1002+430	GD 111	DA2.4	DA2.5	H
1012+083B	LP 549-32	DC	DC:10.8	H
1012+083A	LP 549-33	DA7.5	DA7.6	H
1015+014	PG 1015+014	DAH	DAH4.7	H
1022+009	LP 610-10	DC	DA9.3	H
1034+077	LHS 2288	DC	DC11.7	H
1035-003		DZ	DZ6.2 ⁵	N(Ca)/N(He)= 10 ^{-7.89}
1042+593	LP 93-21	DQ8	DQ5.2	N(C)/N(He)= 10 ^{-2.73}
1046-017	GD 124	DBZ5	DBZ3.6	He
1053-092	PG 1053-092	DA2.1	DA2.2	H
1056+345	LSPM J1059+3414	DB5	DBA4.2 ¹	He
1059+415	SDSS J1102+4113	DC	DC14.9	N(He)/N(H)= 10 ^{-1.85}
1100+211	SDSS J1102+2054	Dox	DS5.7 ⁷	H
1104+491	LSR J1107+4855	DC	DC10.8	H
1108+207	LP 374-4	DC?9	DC10.6	H

Table 8 continued on next page

Table 8 (*continued*)

WD Number	Name	Spectral Type		Composition
		Simbad	Adopted	
1111+020	LSPM J1113+0146	DQH	DQP9.9 ³	N(C)/N(He)= 10 ^{-7.0}
1124+595	GD 309	DA4.7	DA4.9	H
1129+373	PG 1129+373	DB4	DBA4.0 ¹	He
1148+544	EGGR 435	DA	DA5.1	H
1150-153		DA4.0	DA4.4	H
1153+135	LP 493-78	DC9	DC10.3	H
1200+651		DQ	DQA4.2	N(C)/N(He)= 10 ^{-2.31}
1208+076	LSPM J1211+0724	DA8.5	DA9.5	H
1212-022	LP 614-59	DZP	DZP10.9 ⁵	N(Ca)/N(He)= 10 ^{-10.60}
1218+095		DC	DC14.3	N(H)/N(He)= 10 ^{-1.22}
1219+130	SDSS J1221+1245	DAZ	DAZ4.2	H
1224+354	LP 266-55	DC9	DA9.8	H
1235+422	LP 217-47	DQ	DQ8.2	N(C)/N(He)= 10 ^{-5.08}
1236+457	LP 171-40	DA	DA7.9	H
1238+183	LP 435-447	DA	DA9.3	H
1239+302	LP 321-98	DA	DA10.1	H
1252+471		DC	DC10.6	unconstrained
1300+263	LHS 2673	DC9	DC11.7	H
1302+597	GD 323	DAB2	DAB2.4	H
1309+296	LSR J1311+2923	DQpec	DQ9.4	N(C)/N(He)= 10 ^{-4.85}
1310+583	PG 1310+583	DA4.7	DA5.0	H
1310+027	LP 557-24	DC	DC11.7	H
1314-153	LP 737-47	DA3.2	DA3.4	H
1327+594		DQAP	DQAPhot2.7 ³	N(C)/N(He)= 10 ^{-3.00}
1328+307	G165-7	DZ7	DZ8.8 ⁵	N(Ca)/N(He)= 10 ^{-9.03}
1335+002		DC	DC18.2	N(H)/N(He)= 10 ^{-3.23}
1338+023	LHS 2781	DC	DA9.0	H
1350+656	V* DUDra	DA4.1	DA4.4	H
1401+457	LSPM J1403+4533	DC	DC17.4	N(H)/N(He)= 10 ^{-3.43}
1401-149	LP 739-19	High PM star	DC11.1	N(H)/N(He)= 10 ^{-3.13}
1408+029	LSPM J1410+0245	DAZ	DAZ9.0	H
1409+157	EGGR 105	DC	DA10.1	H
1434+437	SDSS J1436+4332	DC	DC10.7	H
1439-195	LP 800-31	DC	DC9.5	unconstrained
1444-096	PG 1444-096	DB3	DB3.3	He
1459+821	G 256-18	DB4	DB3.4	He
1458+362	[MFL2000] J1500+3600	DC	DC10.3	H
1521+320	LSPM J1523+3152	High PM star	D10.7	H
1524+566	LP 135-438	DC9	DA9.2	H
1541+650	V* KXDra	DA4.2	DA4.5	H
1540+236	LP 384-38	DA	DA8.5	H
1542+182	GD 190	DB2	DB2.4	He
1552+177		DZ	DZ7.7 ⁵	N(Ca)/N(He)= 10 ^{-9.13}
1602+011	EGGR 492	DC9	DA?10.3	H
1611+176	LP 444-33	DQpec	DQ9.3	N(C)/N(He)= 10 ^{-7.0}
1630+245	EGGR 542	DC	DC10.8	N(H)/N(He)= 10 ^{-0.48}

Table 8 continued on next page

Table 8 (*continued*)

WD Number	Name	Spectral Type		Composition
		Simbad	Adopted	
1632+177	PG 1632+177	DA4.9	DA5.2	H
1636+057	LHS 3230	DA5.9	DA6.0	H
1645+325	GD 358	DB2	DB2.3	He
1659+662	GD 518	DA4.2	DA4.5	H
1658+440	PG 1658+441	DAP1.6	DAP1.8 ³	H
1704+481A	EGGR 576	DA3.6	DA3.7 ⁸	H
1709+230	GD 205	DBAZ	DBAZ2.5 ¹	He
1717-014	EGGR 495	DC9	DC:10.9	H
1727+560	GD 524	DBQ4	DQAB3.6	$N(C)/N(He) = 10^{-1.54}$
1729+371	GD 362	DAZB	DAZB4.9	$N(H)/N(He) = 10^{-1.69}$
1736+052	EGGR 371	DA5.6	DA5.7	H
1747+450	GD 366	DC6	DC5.8	He
1814+248	G183-35	DAP8	DAP7.3	H
1827-106	EGGR 177	DA3.6	DA4.2	H
1845+019		DA1.7	DA2.4	H
1855+338	EGGR 127	DA4.1	DA4.4	H
1857+119	EGGR 128	DA5.0	DA5.2	H
1858+393	G205-52	DA5.3	DA5.4	H
1910+047		DA	DA2.1	H
1912+143	G142-20	DA	DA7.3	H
1923+550	LP 141-35	DM7.5	DA5.3	H
1946+837	LSR J1940+8348	High PM star	DC10.5	unconstrained
1944+467B	LSR J1945+4650B	High PM star	DA10.3	H
1944+467A	LSR J1945+4650A	High PM star	DA9.4	H
1950+250	V* PT Vul	DA4.2	DA4.5	H
2028+390	GD 391	DA2.0	DA2.0	H
2043-073		DAH	DAH5.8	H
2058+342A	GD 392A	DB5	DBA4.6 ¹	He
2058+342B	GD 392B	DC	DC15.5	H
2130-047	GD 233	DB4	DBA2.9 ¹	He
2139+132B	LP 518-35	DC:	DC:9.3	unconstrained
2139+132A	G126-25	DA6.6	DA6.6	H
2148+539	G232-38	DA4.2	DA4.9	H
2157-079	PB 7043	DQ	DQhot1.9	$N(He)/N(C) = 10^{-3}$
2220+121	LSR J2222+1221	DC	DC12.5	H
2229-080	LP 700-32	DQ	DQ8.1	$N(C)/N(He) = 10^{-5.53}$
2245+146		DAH	DAP3.2 ³	H
2253-062	GD 243	DBA4	DBA3.0 ¹	He
2254+076	G28-27	DAH	DAH4.2	H
2303+242	PG 2303+243	DA4.3	DA4.5	H
2316-064	LHS 542	DC9	DC11.2	H
2328+510	GD 406	DB	DBA3.6 ¹	He
2347+128	EGGR 405	DA4.4	DA4.6	H
2349-031	LHS 4033	DA4.7	DA4.8	H

Table 8 continued on next page

Table 8 (*continued*)

WD Number	Name	Spectral Type		Composition		
		Simbad	Adopted			
¹ Hydrogen is a trace element in these WDs (Rolland et al. 2018).						
² See Dufour (2011) for a description of the different types of DQ stars.						
³ These WDs are polarized, i.e. magnetic which would otherwise be indicated by the letter “H”.						
⁴ 0239+167: classified DQ by Kawka & Vennes (2012), no spectrum available, will be analyzed in future paper.						
⁵ The DZ model atmospheres include trace H as well as Ca, and in all cases N(H)/N(He)= 10 ^{-5.0} .						
⁶ 0714+458: Classified as a DQ by Weidemann & Koester (1995), the SED is well reproduced by a pure-He atmosphere although C will be a trace element.						
⁷ Proposed oxygen-rich classification is DS, K. Williams private communication 2018.						
⁸ 1704+481A,B: A triple system made up of a close pair of WDs and a distant WD; the unresolved pair are both low-mass WDs (Andrews et al. 2015, Maxted et al. 2000).						

Table 9. Reclassified White Dwarfs

WD Number	Name	Spectral Type	
		Simbad	Adopted
0102+210A	LHS 5023	DC9	DA9.5
0112-018	LP 587-16	DC9	DA9.5
0343+247		D:	DC14.4
0402+265	LHS 1625a	High PM star	DC12.7
0500+573	LP 85-9	High PM star	D:6.0
0527+185	LP 517-35	High PM star	D:9.3
0530+054	LP 538-4	High PM star	D:9.7
0531+572	LP 85-33	High PM star	DC:10.2
0541+750	LP 33-221	High PM star	D:8.4
0546+234	LSR J0549+2329	High PM star	D:10.6
0637+335	LP 254-13	High PM star	DC5.7
0650+397	GD 79	High PM star	D:4.8
0701+517	LP 122-34	High PM star	D:9.8
0922+005	LHS 2139	High PM star	D:12.2
1022+009	LP 610-10	DC	DA9.3
1224+354	LP 266-55	DC9	DA9.8
1338+023	LHS 2781	DC	DA9.0
1401-149	LP 739-19	High PM star	DC11.1
1409+157	EGGR 105	DC	DA10.1
1521+320	LSPM J1523+3152	High PM star	D:10.7
1524+566	LP 135-438	DC9	DA9.2
1602+011	EGGR 492	DC9	DA?10.3
1923+550	LP 141-35	M7.5	DA5.3
1946+837	LSR J1940+8348	High PM star	DC10.5
1944+467B	LSR J1945+4650B	High PM star	DA10.3
1944+467A	LSR J1945+4650A	High PM star	DA9.4

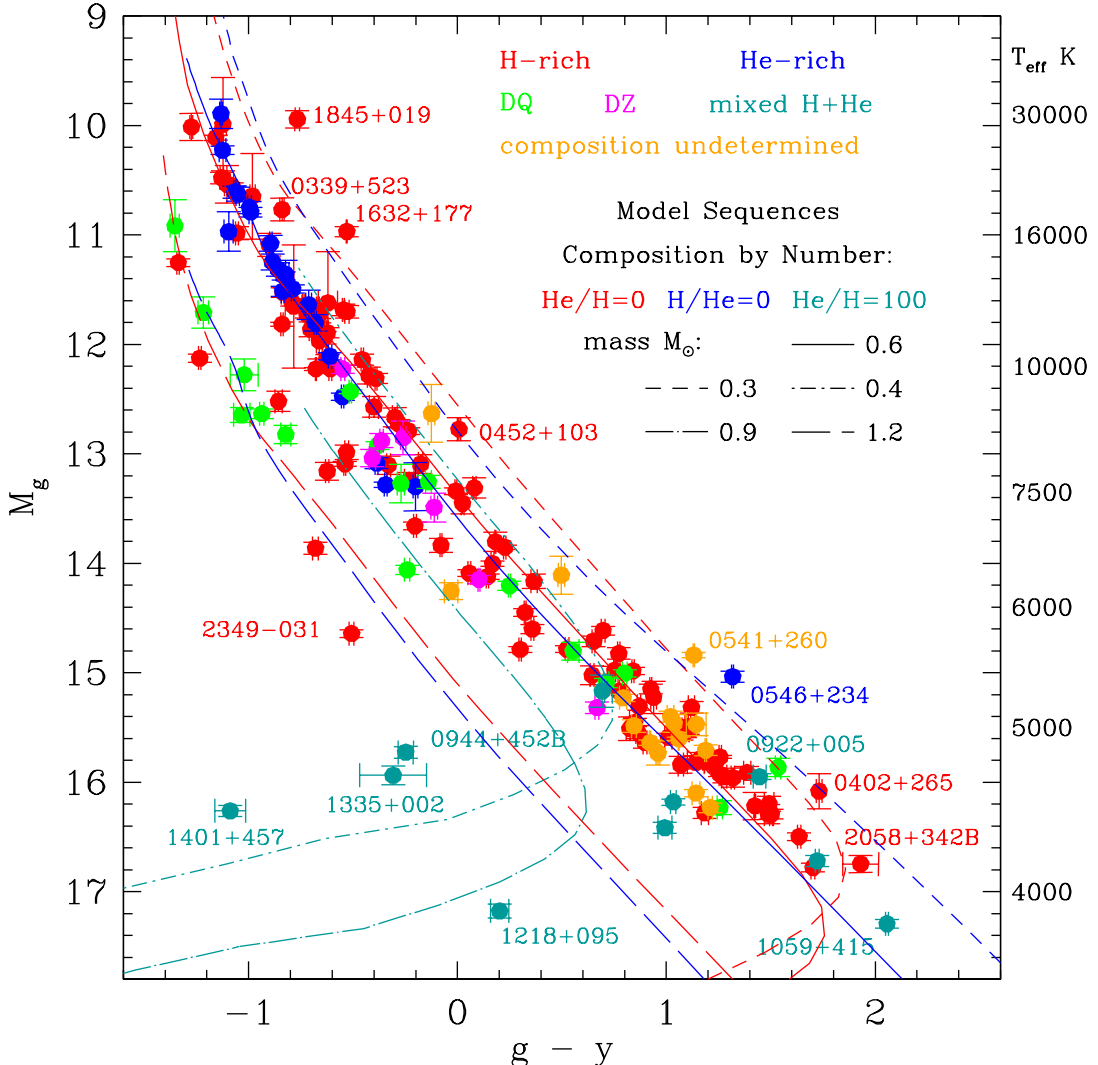


Figure 8. Symbols represent the core sample of 179 WDs with NOFS parallaxes. Lines are iso-mass model sequences. The five line types indicate mass, and the line color indicates atmospheric composition, as shown in the legend. Values of T_{eff} for the mass- $0.6 M_{\odot}$ models are indicated on the right axis. Outliers and candidate binary systems (Section 8.2) are identified.

Figure 8 shows the 179 stars in the $g - y : M_g$ color-magnitude diagram, with outliers identified. Figure 9 shows $u - g : M_g$ and $g - i : M_g$ and Figure 10 shows $J - K : M_J$ and $J - W2$ or [4.5] against M_J . Some stars have both W2 and [4.5] measurements and are plotted twice in Figure 10. Model sequences are also shown in the Figures. In Figure 10 the model sequence is for W2 only; the models show a difference of $\lesssim 5\%$ between W2 and [4.5] for our sample.

Stars that appear over-luminous are either low-gravity and low-mass WDs, binaries (e.g. Figure 6), or are unusually red. In Section 8.2 we discuss the mass distribution of the sample and identify new candidate unresolved binary systems. Stars that appear sub-luminous are either high-gravity

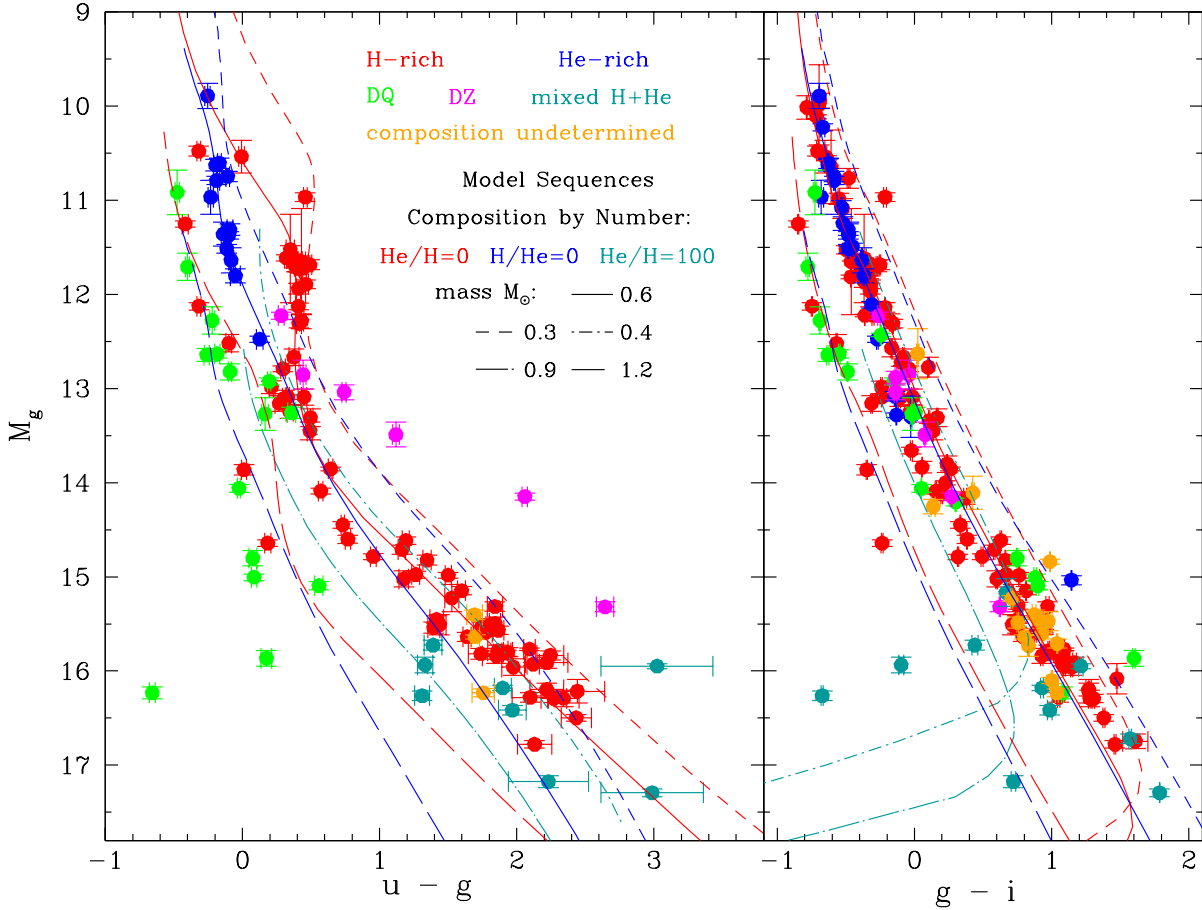


Figure 9. Optical color-magnitude diagrams. Symbol colors and line types are as given in the legend.

and high-mass WDs or are unusually blue. One hydrogen-rich WD that stands out in Figure 8 is 2349–031; this WD is the most massive in our sample with a mass $1.326 \pm 0.012 M_{\odot}$ (Section 8).

Figures 8 and 9 show that the cool mixed hydrogen plus helium atmosphere WDs can be extremely blue in $g - y$ and $g - i$. These objects generally show strong pressure-induced H₂ absorption in the far-red and near-infrared, leading to blue $g - y$, $g - i$ and $J - K$, as well as faint M_J values (Jørgensen et al. 2000, Figures 8–10). Figure 10 demonstrates that $J - K$ diverges for hydrogen plus helium atmospheres cooler than $T_{\text{eff}} \approx 4500$ K, due to the strong pressure-induced H₂ absorption at $\lambda \sim 2 \mu\text{m}$ in cool pure-hydrogen atmospheres (Bergeron et al. 1995).

Figure 9 shows that the $u - g$ color is a particularly useful indicator of atmospheric composition. DQ stars have carbon absorption bands at $\lambda \sim 450$ nm (Wesemael et al. 1993; Gentile Fusillo et al. 2018, Figure 7), and hence have blue $u - g$ colors. DZ stars generally show calcium absorption at $\lambda \sim 390$ nm (Wesemael et al. 1993) and so are red in $u - g$. The $u - g$ color also separates DA from DB stars for $10000 \lesssim T_{\text{eff}} \text{ K} \lesssim 16000$, where DAs have strong hydrogen absorption in the u -band.

Figure 11 shows blue to red and green to mid-infrared color-color plots. The $g - y : u - g$ plot shows some of the features already highlighted: the significant separation in $u - g$ for DAs and DBs

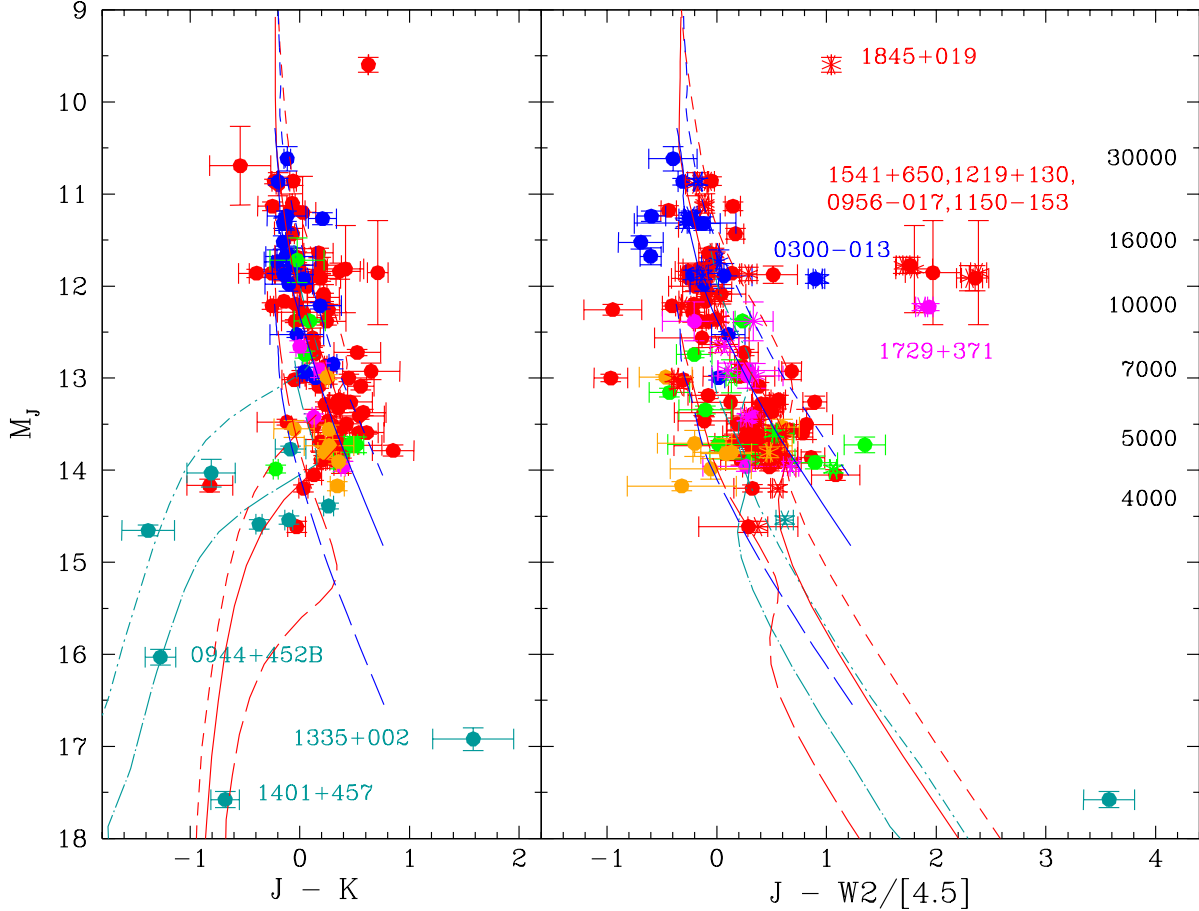


Figure 10. Infrared and mid-infrared color-magnitude diagrams for our core sample. Symbol colors and line types are as in Figures 8 and 9. T_{eff} for mass = $0.6 M_{\odot}$ are indicated on the right axis.

with $10000 \lesssim T_{\text{eff}} \text{ K} \lesssim 16000$, the bluer and redder $u - g$ colors of DQ and DZ stars respectively, and the blue $g - y$ colors of cool mixed H and He WDs. The $g - y : y - \text{W2}/[4.5]$ plot in Figure 11 and the $J - \text{W2}/[4.5] : M_J$ plot in Figure 10 shows that there are WDs in the sample with mid-infrared flux excesses; we discuss these further in the next sub-section.

White dwarfs cooler than ~ 5000 K are generally featureless, apart from the broad pressure-induced H_2 features in hydrogen-rich atmospheres. In some cases the SED allows us to determine the composition of the atmospheres (Figure 3) but in others the data coverage or precision, or the particular combination of parameters, leaves the composition unconstrained. Kowalski & Saumon (2006) compared their models to observed color-color diagrams and concluded that most cool DC stars are hydrogen-rich. The trends we see in Figures 9 and 11 support that conclusion.

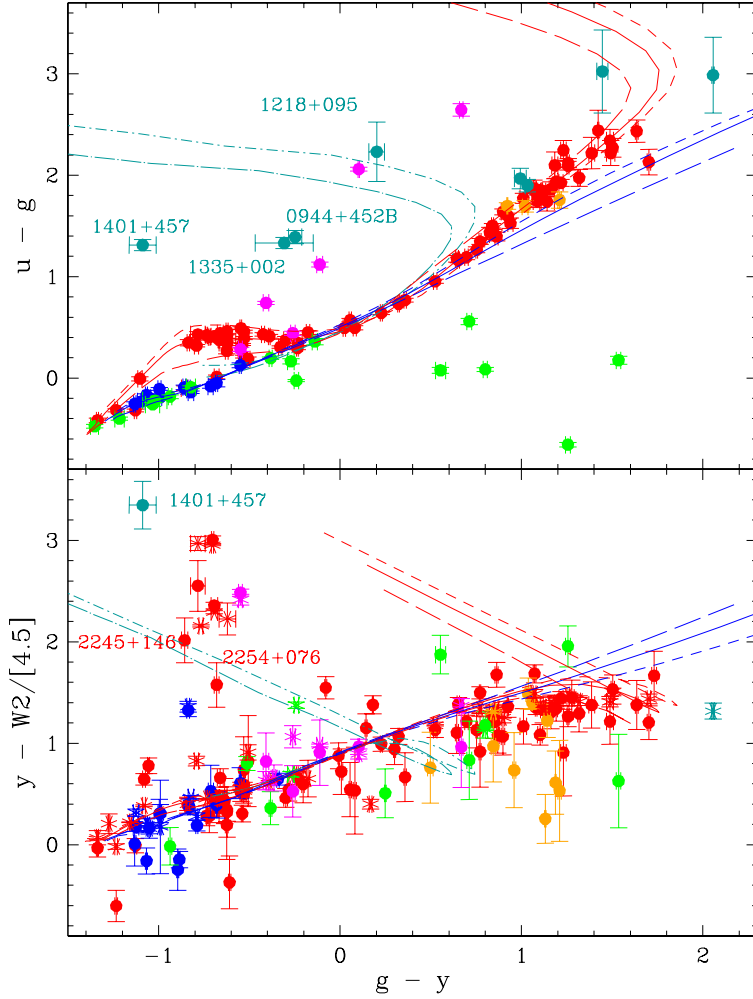


Figure 11. Blue to red, and green to mid-infrared, color-color plots for our core sample. Symbol colors and line types are as in Figures 8 and 9.

7.2. White Dwarfs with Mid-Infrared Excess Flux

Table 10. White Dwarfs with Mid-Infrared Excess Flux

WD Number	Name	Sp. Type	Reference	Notes
0300–013	GD 40	DBZ3.6	Jura et al. (2007)	Known disk
0956–017	EQ J0959–0200	DAZ4.0	Girven et al. (2011)	Known disk
1150–153		DA4.0	Kilic & Redfield (2007)	Known disk
1219+130	SDSS J1221+1245	DAZ4.2	Girven et al. (2011)	Known disk
1541+650	V* KX Dra	DA4.5	Kilic et al. (2012)	Known disk
1729+371	GD 362	DAZB4.9	Becklin et al. (2005); Kilic et al. (2005)	Known disk
1845+019		DA2.4	candidate DA+dM Hoard et al. (2007)	SED supports red dwarf companion
2245+146		DAP3.2	this work	SED suggests circumstellar disk
2254+076	G28-27	DAH4.2	candidate DA+M0 Debes et al. (2011)	SED supports disk, not companion

Seven WDs are identified in the $M_J : J - W2/[4.5]$ plot (Figure 10) that are very red in $J - W2/[4.5]$. An additional two WDs are identified in Figure 11 that are red in $y - W2/[4.5]$. Table 10 lists these nine WDs which have significant mid-infrared excess. Six of them are WDs with previously known circumstellar dust disks. Two have been flagged in the literature as possibly having red companions and the last has not previously been recognized to have an infrared excess to our knowledge. We compared the SEDs of these three WDs to those with similar type known to have red companions or disks in Figure 12. The WDs with red dwarf companions show excess flux in the near-infrared as well as the mid-infrared, while WDs with lower temperature dust disks have a mid-infrared flux excess only. We find that the SED of 1845+019 matches the SED of a WD with an M or L dwarf companion, as previously suggested by Hoard et al. (2007) (note that 1845+019 appears red in $g - y$ in Figure 8). However the SED of 2254+076 does not look like a WD with a red companion, as previously suggested by Debes et al. (2011), instead it looks like a WD with a dust disk. 2245+146 also appears to have a dust disk although near-infrared photometry would help to secure this.

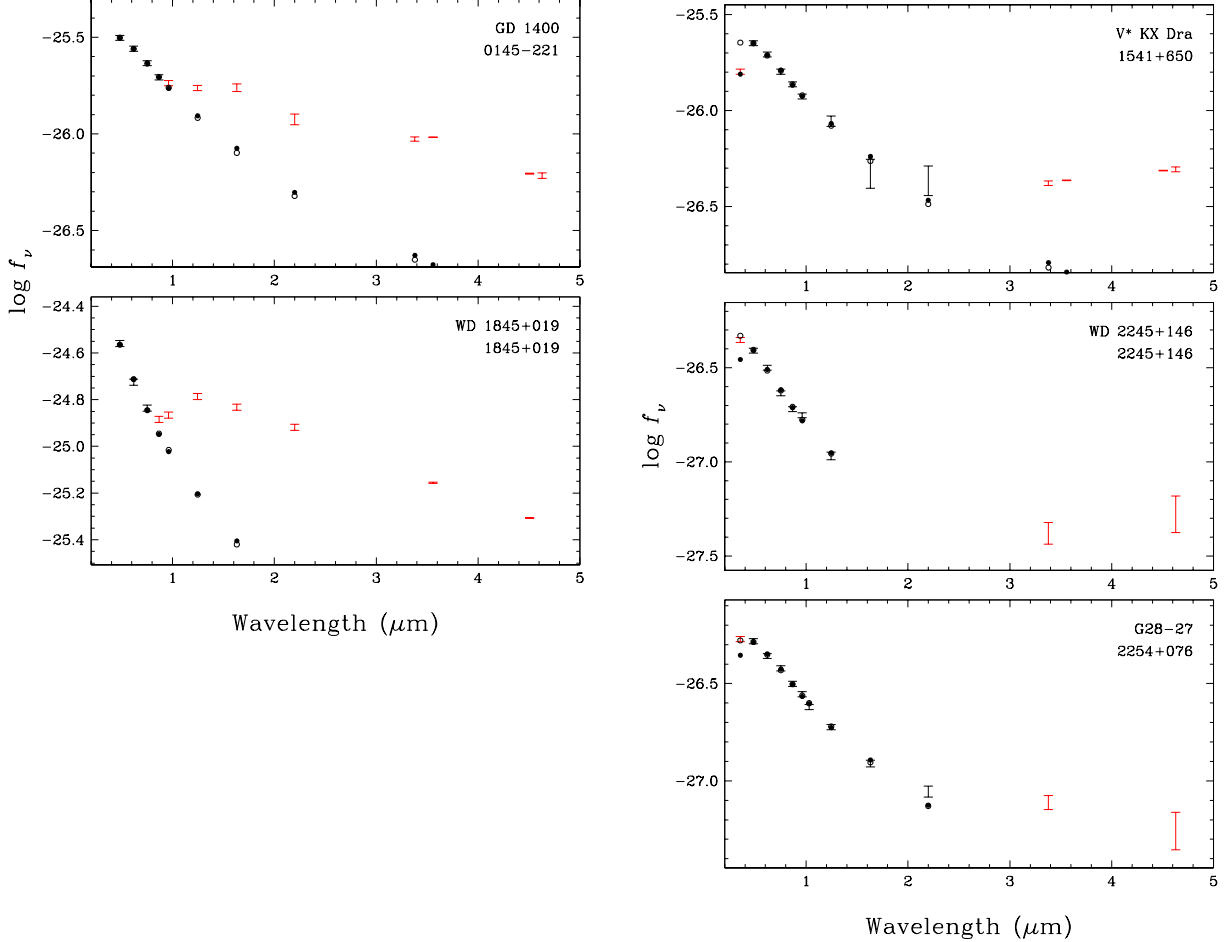


Figure 12. The left panel compares the SED of 0145–221, a DA4.6 with an L dwarf companion (Table 6), to that of 1845+019, confirming that the latter has a red dwarf companion. The right panel compares the SED of 1541+650, a DA4.5 with a dust disk (Table 10) to those of 2245+146 and 2254+076, which we suggest also have disks.

8. PHYSICAL PROPERTIES OF THE SAMPLE OF 179 WHITE DWARFS

8.1. *Properties by Atmospheric Composition*

Tables 11 – 15 list the derived parameters and their uncertainties for each WD, grouped by atmospheric compositions: pure hydrogen, pure helium, the metal-rich DQ and DZ, the cool mixed hydrogen-helium and the unconstrained atmospheres. The T_{eff} , $\log g$, mass and cooling age are determined by the model fits as described in Section 5. For the WDs with unknown composition we adopted the average of the pure-hydrogen and pure-helium parameters, and included the range of solutions in the uncertainties. Uncertainties in the photometry are propagated through the model derived parameters.

Our sample of DA and DB WDs overlaps with those of Gianninas et al. (2011) and Rolland et al. (2018). Those authors used the same models used in this study to determine WD atmospheric properties spectroscopically, while we used the photometric technique together with updated parallaxes. Most of our WDs have pure-hydrogen atmospheres, and so we compared the properties determined for 49 DA stars in common with Gianninas et al. (2011). The T_{eff} values agree for WDs with $T_{\text{eff}} < 10000$ K, but for the warmer stars the spectroscopic temperatures are higher by ~ 700 K. Similarly, the gravity and mass determinations agree within 2σ ($\delta(\log g) \approx 0.1$ and $\delta(\text{mass}) \approx 0.05 M_{\odot}$) for 60% of the sample but for 35% of the sample the spectroscopic values are higher, with $\delta(\log g) \approx 0.3$ and $\delta(\text{mass}) \approx 0.2 M_{\odot}$. The high values found for these parameters by the spectroscopic method has been noted previously (e.g. Bergeron et al. 1990b; Eisenstein et al. 2006; Genest-Beaulieu & Bergeron 2014; Kepler et al. 2007; Limoges et al. 2015; Tremblay et al. 2015) and has been attributed to shortcomings in the modelled line broadening. Recently, three-dimensional pure-hydrogen model atmospheres have been calculated (Tremblay et al. 2013) which provide a correction to the one-dimensional model-derived parameters. Figure 4 of Tremblay et al. shows that for DAs with $T_{\text{eff}} > 10000$ K the correction to T_{eff} is ~ -500 K, and for DAs with $7000 \lesssim T_{\text{eff}} \lesssim 12000$ the correction to $\log g$ is ~ -0.2 dex. Application of these corrections bring the T_{eff} values for all but one WD within 2σ , and excluding four very discrepant stars, all $\log g$ values then agree within 2.5σ . One of the $\log g$ discrepant stars is a magnetic WD where the spectroscopic fit is poor (1658+440, Gianninas et al. 2011). Two of the three other very $\log g$ discrepant WDs are identified as candidate binary systems in Section 8.3 (0452+103, 1632+177) and it is possible that the third object, 1310+583, is an unresolved binary also. Hence the comparison to the spectroscopic analysis of DAs by Gianninas et al. (2011) indicates that our results are valid.

The total age of each WD was estimated for the WDs more massive than $0.5 M_{\odot}$. Less massive WDs cannot have formed as a normal single WD (Bergeron et al. 1992). These systems may be unresolved multiple systems in which case an analysis assuming a single WD will produce too large a radius and too small a mass. The systems may also be very close binaries which have evolved through a common-envelope stage which can produce low mass WDs (Iben & Livio 1993).

The initial mass M_i was estimated from the WD final mass M_f using the initial-final mass relations from Kalirai et al. (2009) and Cummings et al. (2016) for WDs with masses $0.5 - 0.7 M_{\odot}$ and $> 0.7 M_{\odot}$, respectively:

$$M_f = (0.109 \pm 0.007) \times M_i + (0.428 \pm 0.025)$$

for $0.5 \leq M_f \leq 0.7$ and

$$M_f = (0.143 \pm 0.005) \times M_i + (0.294 \pm 0.020)$$

for $M_f > 0.7$. The time spent on the main sequence as a function of M_i was determined from the PARSEC stellar evolutionary code (Bressan et al. 2012). Using solar metallicity tracks, a fit to the main sequence lifetime MS_t as a function of initial stellar mass M_i gives

$$MS_t = (9.377 \pm 0.022)10^9 \times M_i^{(-2.715 \pm 0.042)}$$

This time was added to the cooling age to give the total age in Tables 11 – 15. Uncertainties were propagated through the mass and age calculations.

8.2. Mass

Figure 13 shows that the sample has the typical peak in mass around $0.6 M_\odot$ (Giambicchele et al. 2012; Limoges et al. 2015). Kilic et al. (2018) uses a large volume-limited sample of WDs with *Gaia* parallaxes to show that there are a significant number of WDs with mass $\sim 0.8 M_\odot$ which likely formed through mergers. Our smaller and more inhomogeneous sample does not show evidence of this bump in the mass distribution.

In our sample of 179 notionally single WDs, twelve have masses below $0.45 M_\odot$ (allowing for the uncertainty in mass). These are possibly unresolved binary systems, and are listed in Table 16 for future followup such as radial velocity or variability studies. The twelve WDs are also identified in the color-magnitude diagram of Figure 8.

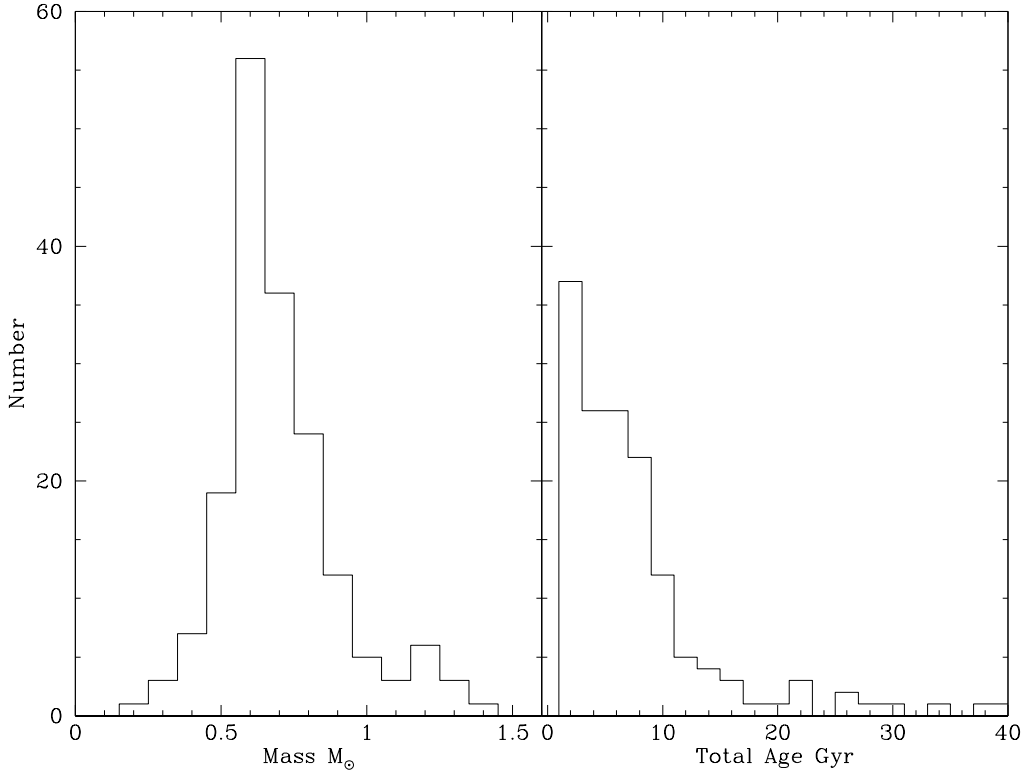


Figure 13. Histograms of WD mass as determined by our model fits (left) and total age (right) which is the sum of the WD cooling age and the progenitor’s time on the main sequence. The typical uncertainty in mass is $0.04 M_\odot$. The uncertainty in age can be as large as 1000 Gyr, but the typical uncertainty is 2 Gyr.

Table 11. Properties of WDs with Hydrogen-Rich Atmospheres

WD Number	Spectral Type	Parallax mas	T_{eff} K	Mass M_{\odot}	$\log g$ dex	Cooling Age	Total Age Myr	V_{\tan} km s $^{-1}$
0102+210A	DA9.5	29.31 ± 0.79	5278 ± 89	0.777 ± 0.039	8.301 ± 0.042	7101 + 461 - 494	7445 + 345 - 300	78.5
0102+210B	DC10.5	29.31 ± 0.79	4818 ± 78	0.620 ± 0.041	8.067 ± 0.046	7158 + 488 - 533	9174 + 4783 - 781	79.8
0112-018	DA9.5	8.60 ± 0.53	5311 ± 73	0.752 ± 0.028	8.265 ± 0.030	6712 + 384 - 418	7110 + 262 - 230	91.7
0114-049A	DC:10.3	24.55 ± 0.55	4885 ± 75	0.550 ± 0.036	7.951 ± 0.043	5650 + 594 - 609	12556 + 43857 - 4394	73.0
0145-174	DA6.8	13.12 ± 0.56	7403 ± 169	0.552 ± 0.048	7.929 ± 0.059	1192 + 128 - 119	7799 + 76090 - 4909	400.9
0202-055	DC12.2	34.12 ± 0.60	4124 ± 52	0.596 ± 0.032	8.031 ± 0.036	8956 + 305 - 333	11853 + 7084 - 1498	144.1
0203+183	DC11.6	27.56 ± 0.84	4329 ± 83	0.493 ± 0.046	7.857 ± 0.057	6640 + 678 - 687	44801 + ⋯ - 33273	135.7
0228+269	DC:10.4	35.63 ± 1.08	4855 ± 77	0.513 ± 0.042	7.888 ± 0.052	5068 + 683 - 681	23489 + ⋯ - 14619	56.8
0235+064	DA3.8	17.11 ± 0.26	13283 ± 682	0.680 ± 0.027	8.119 ± 0.032	336 + 54 - 46	1300 + 1098 - 492	22.5
0236+745	DA5.7	21.36 ± 0.86	8792 ± 286	0.596 ± 0.054	7.998 ± 0.065	839 + 115 - 97	3736 + 15131 - 1951	73.0
0246+326	DA4.6	15.15 ± 0.39	11018 ± 401	0.643 ± 0.039	8.067 ± 0.045	512 + 64 - 55	1995 + 2884 - 815	24.8
0302+621	DA4.8	28.11 ± 0.49	10568 ± 357	0.708 ± 0.038	8.174 ± 0.043	673 + 80 - 71	1196 + 1076 - 112	21.2
0339+523	DA3.8	10.59 ± 0.51	13093 ± 613	0.371 ± 0.033	7.506 ± 0.062	160 + 28 - 23	⋯ + ⋯ - ⋯	54.5
0346-011	DA1.2	30.51 ± 0.48	40814 ± 12333	1.244 ± 0.053	9.089 ± 0.137	60 + 140 - 49	115 + 125 - 29	27.5
0349+495	DA6.7	16.33 ± 0.71	7540 ± 153	0.648 ± 0.047	8.090 ± 0.054	1416 + 143 - 121	2809 + 3238 - 711	140.6
0402+265	DC12.7	19.16 ± 1.42	3970 ± 49	0.242 ± 0.053	7.286 ± 0.117	3171 + 391 - 281	⋯ + ⋯ - ⋯	131.4
0407+197	DC:9.6	33.55 ± 0.76	5235 ± 79	0.792 ± 0.034	8.324 ± 0.036	7423 + 386 - 413	7740 + 288 - 255	80.0
0415+271	DA4.5	21.65 ± 0.47	11241 ± 359	0.556 ± 0.029	7.917 ± 0.037	400 + 40 - 37	6461 + 24541 - 4103	20.4
0437+093	DA8.0	31.74 ± 0.63	6287 ± 114	0.801 ± 0.030	8.331 ± 0.032	4010 + 252 - 255	4312 + 162 - 120	110.3
0452+103	DA6.8	15.15 ± 0.73	7418 ± 151	0.369 ± 0.039	7.560 ± 0.066	789 + 59 - 55	⋯ + ⋯ - ⋯	132.6
0506-154	DA9.7	27.38 ± 0.44	5219 ± 101	0.647 ± 0.041	8.105 ± 0.046	5794 + 681 - 752	7204 + 2106 - 164	107.4
0507+045A	DA4.6	19.59 ± 0.22	10884 ± 418	0.582 ± 0.036	7.964 ± 0.044	461 + 57 - 49	4130 + 12408 - 2389	23.9
0507+045B	DA2.6	19.59 ± 0.22	19285 ± 1872	0.567 ± 0.054	7.899 ± 0.072	62 + 38 - 23	4908 + 40317 - 3672	23.3
0527+185	D:9.3	21.83 ± 1.07	5396 ± 93	0.820 ± 0.053	8.365 ± 0.059	6942 + 503 - 593	7215 + 405 - 414	46.8
0530+054	D:9.7	24.17 ± 1.62	5183 ± 103	0.600 ± 0.076	8.031 ± 0.088	5148 + 1079 - 1286	7866 + 31551 - 991	42.3
0557+237	DA6.0	16.52 ± 0.65	8368 ± 170	0.685 ± 0.043	8.145 ± 0.048	1188 + 113 - 105	2101 + 1473 - 429	67.5
0559+158	DA7.2	27.19 ± 0.31	7001 ± 131	0.808 ± 0.023	8.338 ± 0.026	3073 + 224 - 230	3364 + 145 - 116	55.2
0600+735	DA7.8	31.77 ± 0.41	6434 ± 170	0.927 ± 0.035	8.519 ± 0.040	4584 + 282 - 270	4749 + 236 - 203	106.0
0632+409	DA6.4	25.52 ± 0.73	7874 ± 223	0.890 ± 0.040	8.460 ± 0.046	2730 + 293 - 301	2925 + 235 - 212	42.9
0637+477	DAP3.7	26.07 ± 0.23	13664 ± 890	0.787 ± 0.032	8.288 ± 0.036	403 + 84 - 68	729 + 87 - 17	30.3
0651-020	DA1.7	12.02 ± 0.69	29524 ± 2710	0.719 ± 0.077	8.131 ± 0.097	12 + 11 - 5	500 + 1829 - 230	47.3

Table 11 continued on next page

Table 11 (*continued*)

WD Number	Spectral Type	Parallax mas	T_{eff} K	Mass M_{\odot}	log g dex	Cooling Age Myr	Total Age Myr	V_{\tan} km s $^{-1}$
0749+426	DC10.9	36.28 ± 0.22	4642 ± 74	0.497 ± 0.031	7.863 ± 0.039	5641 + 527 - 534	38090 + ⋯ - 26639	52.8
0826+455	DA5.0	21.13 ± 0.50	10044 ± 280	0.430 ± 0.030	7.677 ± 0.046	408 + 38 - 34	⋯ + ⋯ - ⋯	32.5
0855+416	DAH6.8	25.87 ± 0.37	7361 ± 198	0.878 ± 0.033	8.442 ± 0.037	3174 + 272 - 270	3380 + 214 - 183	69.1
0918-172	DA8.1	19.15 ± 1.51	6237 ± 127	0.597 ± 0.040	8.013 ± 0.047	2081 + 256 - 198	4932 + 9241 - 1611	46.1
0921+354	DA4.3	17.50 ± 0.37	11614 ± 480	0.618 ± 0.032	8.022 ± 0.039	419 + 54 - 47	2493 + 4217 - 1180	39.3
0922+053	DA4.7	24.01 ± 0.40	10836 ± 277	0.697 ± 0.026	8.155 ± 0.030	611 + 53 - 48	1418 + 815 - 373	32.2
0937+654	DC11.3	21.83 ± 0.56	4446 ± 85	0.443 ± 0.043	7.764 ± 0.058	5171 + 756 - 676	⋯ + ⋯ - ⋯	255.2
0944+452A	DA10.3	18.54 ± 0.42	4877 ± 83	0.667 ± 0.040	8.139 ± 0.043	7586 + 426 - 468	8699 + 1490 - 266	22.5
0955+247	DA5.9	34.40 ± 0.49	8516 ± 223	0.590 ± 0.034	7.989 ± 0.041	899 + 85 - 75	4096 + 9340 - 1977	55.6
0956-017	DAZ3.8	5.09 ± 1.29	13526 ± 1029	0.674 ± 0.220	8.108 ± 0.276	315 + 156 - 130	1343 + ⋯ - 701	22.3
1002+430	DA2.5	8.07 ± 0.64	19895 ± 2020	0.584 ± 0.083	7.928 ± 0.112	58 + 40 - 25	3601 + 75075 - 2829	86.6
1012+083A	DA7.6	34.88 ± 0.29	6650 ± 117	0.593 ± 0.022	8.004 ± 0.027	1739 + 114 - 103	4781 + 5604 - 1658	44.6
1012+083B	DC10.8	34.88 ± 0.29	4676 ± 70	0.586 ± 0.030	8.013 ± 0.034	7116 + 400 - 405	10538 + 8786 - 1752	44.7
1015+014	DAH4.7	21.37 ± 0.65	10617 ± 254	0.992 ± 0.029	8.613 ± 0.036	1564 + 160 - 163	1691 + 129 - 120	13.6
1022+009	DA9.3	19.44 ± 0.47	5442 ± 80	0.547 ± 0.033	7.937 ± 0.040	2904 + 406 - 329	10293 + 43654 - 4883	270.0
1034+077	DC11.7	19.11 ± 1.10	4324 ± 88	0.498 ± 0.067	7.866 ± 0.084	6761 + 916 - 989	37967 + ⋯ - 27664	169.9
1053-092	DA2.2	5.13 ± 0.99	23298 ± 2401	0.498 ± 0.130	7.736 ± 0.215	22 + 14 - 7	31227 + ⋯ - 30252	14.6
1100+211	DS5.7	14.68 ± 0.57	9250 ± 274	0.846 ± 0.047	8.390 ± 0.053	1416 + 245 - 208	1656 + 165 - 74	51.0
1104+491	DC11.0	20.30 ± 0.44	4685 ± 75	0.554 ± 0.038	7.960 ± 0.045	6561 + 524 - 547	12888 + 40255 - 4070	170.5
1108+207	DC10.6	35.87 ± 0.81	4733 ± 76	0.572 ± 0.039	7.990 ± 0.045	6693 + 521 - 543	11096 + 19101 - 2544	108.5
1124+595	DA4.9	39.30 ± 0.41	10323 ± 316	0.998 ± 0.027	8.624 ± 0.035	1731 + 184 - 179	1855 + 155 - 139	19.4
1148+544	DA5.1	13.38 ± 0.63	9793 ± 282	0.609 ± 0.046	8.016 ± 0.055	651 + 74 - 66	3017 + 8137 - 1496	99.1
1150-153	DA4.4	15.02 ± 0.46	11380 ± 530	0.654 ± 0.047	8.083 ± 0.055	481 + 76 - 65	1776 + 2836 - 785	19.3
1153+35	DC10.3	28.29 ± 0.66	4889 ± 69	0.447 ± 0.032	7.766 ± 0.043	3700 + 456 - 421	⋯ + ⋯ - ⋯	107.7
1208+076	DA9.5	38.19 ± 0.56	5283 ± 71	0.531 ± 0.025	7.912 ± 0.031	3266 + 427 - 374	14201 + 67334 - 7389	28.3
1219+130	DAZ4.2	4.75 ± 1.01	12018 ± 686	0.573 ± 0.178	7.943 ± 0.238	345 + 129 - 110	4666 + ⋯ - 3861	13.0
1224+354	DA9.8	29.87 ± 0.60	5142 ± 84	0.528 ± 0.036	7.911 ± 0.044	3851 + 678 - 572	15700 + 145471 - 8500	105.5
1236+457	DA7.9	36.56 ± 0.61	6402 ± 145	0.775 ± 0.034	8.291 ± 0.038	3595 + 329 - 325	3943 + 216 - 148	107.9
1238+183	DA9.3	25.98 ± 0.44	5433 ± 95	0.612 ± 0.035	8.046 ± 0.040	3871 + 705 - 568	6134 + 4824 - 689	108.4
1239+302	DA10.1	20.55 ± 0.74	4969 ± 75	0.736 ± 0.044	8.243 ± 0.047	7996 + 366 - 422	8434 + 457 - ⋯	136.9
1300+263	DC11.7	25.60 ± 1.02	4312 ± 60	0.525 ± 0.048	7.913 ± 0.058	7302 + 606 - 659	20170 + ⋯ - 9922	156.0
1302+597	DAB2.4	17.01 ± 0.41	21409 ± 2141	0.623 ± 0.059	7.993 ± 0.076	49 + 33 - 21	1982 + 7423 - 1318	29.5
1310+027	DC11.7	32.10 ± 0.63	4317 ± 58	0.515 ± 0.032	7.896 ± 0.039	7108 + 456 - 466	24401 + ⋯ - 13229	110.1
1310+583	DA5.0	33.62 ± 0.90	10131 ± 260	0.445 ± 0.030	7.709 ± 0.045	412 + 36 - 33	⋯ + ⋯ - ⋯	30.2

Table 11 continued on next page

Table 11 (*continued*)

WD Number	Spectral Type	Parallax mas	T_{eff} K	Mass M_{\odot}	$\log g$ dex	Cooling Age Myr	Total Age Myr	V_{\tan} km s $^{-1}$
1314–153	DA3.4	17.89 ± 0.48	14893 ± 847	0.536 ± 0.036	7.861 ± 0.048	162 + 37 – 30	9776 + 87671 – 7235	185.4
1338+023	DA9.0	24.75 ± 0.97	5628 ± 81	0.728 ± 0.043	8.225 ± 0.047	4798 + 488 – 497	5258 + 471 – ...	101.4
1350+056	DA4.4	17.13 ± 0.43	11485 ± 527	0.579 ± 0.040	7.956 ± 0.050	396 + 59 – 50	4267 + 15931 – 2619	79.0
1408+029	DAZ9.0	36.07 ± 0.80	5612 ± 81	0.583 ± 0.030	7.996 ± 0.035	2828 + 322 – 266	6433 + 9785 – 1963	31.7
1409+157	DA10.1	26.45 ± 0.48	5008 ± 81	0.647 ± 0.036	8.107 ± 0.040	6820 + 469 – 524	8230 + 2049 – 343	117.0
1434+437	DC10.7	37.38 ± 0.55	4690 ± 75	0.550 ± 0.035	7.954 ± 0.041	6478 + 499 – 516	13384 + 39707 – 4489	75.3
1458+362	DC10.3	14.51 ± 0.49	4878 ± 82	0.535 ± 0.047	7.927 ± 0.056	5402 + 746 – 754	15263 + ... – 7108	296.8
1521+320	D:10.7	20.46 ± 0.47	4732 ± 82	0.789 ± 0.039	8.323 ± 0.042	9046 + 228 – 250	9368 + 121 – 76	149.7
1524+566	DA9.2	30.65 ± 0.56	5485 ± 96	0.483 ± 0.033	7.822 ± 0.043	2222 + 229 – 183	... + ... – ...	25.6
1540+236	DA8.5	36.93 ± 0.51	5915 ± 117	0.744 ± 0.033	8.247 ± 0.036	4189 + 356 – 345	4606 + 217 – 123	51.9
1541+650	DA4.5	16.99 ± 0.48	11175 ± 472	0.556 ± 0.041	7.917 ± 0.052	406 + 56 – 49	6468 + 41019 – 4414	18.8
1602+011	DA710.3	32.01 ± 0.65	4876 ± 88	0.559 ± 0.042	7.968 ± 0.049	5885 + 674 – 697	11577 + 36962 – 3511	93.1
1632+177	DA5.2	37.06 ± 0.78	9711 ± 188	0.235 ± 0.009	7.088 ± 0.031	272 + 17 – 17	... + ... – ...	11.3
1636+057	DA6.0	27.87 ± 0.43	8356 ± 247	0.916 ± 0.034	8.499 ± 0.039	2485 + 256 – 258	2658 + 208 – 189	88.9
1658+440	DAP1.8	31.64 ± 0.50	28475 ± 1396	1.275 ± 0.015	9.197 ± 0.044	244 + 48 – 40	294 + 39 – 29	15.7
1659+662	DA4.5	15.43 ± 0.58	11298 ± 542	1.106 ± 0.037	8.811 ± 0.056	1788 + 220 – 213	1872 + 199 – 185	60.0
1704+481A	DA3.7	26.21 ± 0.53	13452 ± 804	0.660 ± 0.036	8.086 ± 0.042	309 + 60 – 50	1515 + 1912 – 616	13.5
1717–014	DC10.9	26.54 ± 0.64	4605 ± 75	0.565 ± 0.040	7.980 ± 0.046	7041 + 505 – 532	12082 + 26204 – 3088	66.4
1736+052	DA5.7	22.74 ± 0.40	8803 ± 247	0.621 ± 0.037	8.040 ± 0.044	889 + 92 – 82	2877 + 4532 – 1124	58.6
1814+248	DAP7.3	22.48 ± 0.91	6868 ± 170	0.633 ± 0.050	8.069 ± 0.058	1772 + 236 – 197	3460 + 4856 – 853	75.8
1827–106	DA4.2	14.96 ± 0.72 ^a	12016 ± 634	0.425 ± 0.039	7.649 ± 0.062	239 + 45 – 38	... + ... – ...	93.0
1845+019	DA2.4	26.84 ± 0.99 ^a	21260 ± 4531	0.447 ± 0.107	7.631 ± 0.180	31 + 43 – 16	... + ... – ...	14.5
1855+338	DA4.4	33.49 ± 0.23	11438 ± 430	0.805 ± 0.029	8.321 ± 0.033	687 + 82 – 73	982 + 56 – 6	50.8
1857+119	DA5.2	20.33 ± 0.48 ^a	96447 ± 197	0.540 ± 0.028	7.897 ± 0.036	581 + 41 – 38	9291 + 47406 – 6170	55.4
1858+393	DA5.4	21.45 ± 0.44	9380 ± 255	0.557 ± 0.036	7.928 ± 0.045	648 + 61 – 55	6583 + 30961 – 4166	52.1
1910+047	DA2.2	5.96 ± 1.06	24208 ± 2235	0.673 ± 0.151	8.070 ± 0.196	32 + 33 – 18	1072 + 38919 – 785	91.5
1912+143	DA7.3	25.87 ± 0.28 ^a	6916 ± 126	0.732 ± 0.024	8.224 ± 0.026	2399 + 243 – 217	2848 + 108 – 13	73.2
1923+550	DA5.3	12.18 ± 0.53	9566 ± 281	0.692 ± 0.053	8.152 ± 0.059	844 + 103 – 94	1693 + 1621 – 412	77.6
1944+467A	DA9.4	35.02 ± 0.16	5389 ± 93	0.674 ± 0.031	8.146 ± 0.034	5226 + 657 – 658	6255 + 735 – ...	81.2
1944+467B	DA10.3	35.02 ± 0.16	4906 ± 78	0.559 ± 0.031	7.967 ± 0.036	5736 + 557 – 572	11428 + 23293 – 3353	81.2
1950+250	DA4.5	20.97 ± 0.22 ^a	11090 ± 317	0.563 ± 0.022	7.930 ± 0.028	421 + 37 – 33	5667 + 13973 – 3291	34.6
2028+390	DA2.0	23.83 ± 0.24 ^a	25702 ± 1747	0.622 ± 0.042	7.974 ± 0.055	18 + 8 – 5	1978 + 4775 – 1243	34.4
2043–073	DAH5.8	11.45 ± 0.38	8670 ± 280	0.802 ± 0.049	8.325 ± 0.054	1451 + 285 – 192	1751 + 177 – 8	29.3
2058+342B	DC15.5	19.56 ± 0.31	3249 ± 75	0.177 ± 0.028	7.068 ± 0.078	3492 + 444 – 420	... + ... – ...	41.6

Table 11 continued on next page

Table 11 (*continued*)

WD Number	Spectral Type	Parallax mas	T_{eff} K	Mass M_{\odot}	$\log g$ dex	Cooling Age Myr	Total Age Myr	V_{\tan} km s $^{-1}$
2139+132A	DA6.6	21.93 ± 0.31	7623 ± 204	0.627 ± 0.036	8.056 ± 0.042	1314 + 123	- 110	3143 + 3688 - 975 72.8
2148+539	DA4.9	10.65 ± 0.80	10320 ± 261	0.582 ± 0.070	7.967 ± 0.087	532 + 73	- 65	4201 + 55042 - 2765 189.0
2220+121	DC12.5	27.38 ± 0.43	4032 ± 98	0.453 ± 0.043	7.785 ± 0.056	6889 + 655	- 642	... + ... - ... 127.2
2245+146	DAP3.2	10.46 ± 0.44	15662 ± 1145	1.116 ± 0.035	8.824 ± 0.056	741 + 241	- 190	822 + 221 - 163 33.8
2254+076	DAH4.2	22.46 ± 0.56	12074 ± 471	1.281 ± 0.012	9.230 ± 0.036	1737 + 101	- 95	1786 + 93 - 85 49.1
2303+242	DA4.5	19.20 ± 0.35	11124 ± 409	0.570 ± 0.033	7.941 ± 0.041	423 + 49	- 44	4996 + 17195 - 3017 21.0
2316-064	DC11.2	29.49 ± 1.18	4515 ± 73	0.514 ± 0.050	7.893 ± 0.061	6444 + 686	- 774	24289 + ... - 14488 270.8
2347+128	DA4.6	14.93 ± 0.32	11002 ± 299	0.622 ± 0.028	8.032 ± 0.033	490 + 44	- 39	2450 + 3415 - 1067 91.5
2349-031	DA4.8	34.04 ± 0.55	10555 ± 321	1.326 ± 0.012	9.382 ± 0.033	1842 + 73	- 70	1886 + 66 - 62 97.6

a Relative parallax; absolute parallax will be larger.

Table 12. Properties of WDs with Helium-Rich Atmospheres

WD Number	Spectral Type	Parallax mas	T_{eff} K	Mass M_{\odot}	$\log g$ dex	Cooling Age	Total Age Myr	V_{\tan} km s $^{-1}$
0002+729	DBA3.7	28.35 ± 0.49	13537 ± 733	0.610 ± 0.046	8.040 ± 0.055	290 + 48 - 58	2621 + 7451 - 1503	38.0
0015+004	DBP3.5	7.55 ± 0.44	14532 ± 580	0.621 ± 0.063	8.054 ± 0.075	240 + 45 - 39	2228 + 9950 - 1344	17.1
0112+104	DB1.8	8.60 ± 0.53	27861 ± 1507	0.517 ± 0.047	7.816 ± 0.072	13 + 2 - 3	16271 + ... - 13630	27.3
0114-049B	DC:9.8	24.55 ± 0.55	4979 ± 54	0.535 ± 0.029	7.945 ± 0.035	5250 + 293 - 324	15111 + 64567 - 6897	76.1
0300-013	DBZ3.6	16.61 ± 0.35	13921 ± 428	0.651 ± 0.032	8.106 ± 0.037	299 + 31 - 34	1641 + 2057 - 710	27.6
0541+260	DC10.0	28.21 ± 0.32	5050 ± 51	0.306 ± 0.017	7.475 ± 0.030	2225 + 85 - 79	... + ... - ...	286.4
0546+234	D:10.6	17.33 ± 0.39	4746 ± 40	0.236 ± 0.018	7.274 ± 0.041	2160 + 79 - 81	... + ... - ...	375.6
0637+335	DC5.7	15.76 ± 1.59	8336 ± 276	0.739 ± 0.103	8.255 ± 0.114	1501 + 442 - 328	1931 + 2174 - ...	55.5
0650+397	D:4.8	20.48 ± 0.30	10574 ± 447	0.739 ± 0.042	8.251 ± 0.046	783 + 104 - 90	1213 + 698 - 54	43.7
0654+027	DC5.4	24.18 ± 0.56	9269 ± 249	0.815 ± 0.034	8.368 ± 0.036	1333 + 140 - 182	1613 + 96 - 9	41.3
0954+342	DB1.9	4.83 ± 0.40	27023 ± 2979	0.909 ± 0.074	8.488 ± 0.089	72 + 43 - 32	251 + 102 - 24	43.7
1046-017	DBZ3.6	13.47 ± 0.38	13988 ± 450	0.576 ± 0.037	7.980 ± 0.045	239 + 27 - 31	4326 + 15737 - 2753	40.7
1056+345	DBA4.2	18.38 ± 0.63	12021 ± 376	0.601 ± 0.042	8.028 ± 0.051	397 + 48 - 43	3072 + 8958 - 1719	72.8
1129+373	DBA4.0	11.01 ± 0.67	12685 ± 405	0.592 ± 0.062	8.011 ± 0.075	333 + 52 - 45	3426 + 24406 - 2228	40.8
1444-096	DB3.3	17.58 ± 0.58	15234 ± 797	0.570 ± 0.049	7.964 ± 0.061	178 + 32 - 39	4751 + 32345 - 3342	45.3
1459+821	DB3.4	20.08 ± 0.67	14697 ± 1090	0.603 ± 0.068	8.023 ± 0.083	220 + 52 - 68	2813 + 17832 - 1878	86.1
1542+182	DB2.4	16.52 ± 0.48	20618 ± 1584	0.661 ± 0.049	8.105 ± 0.059	79 + 32 - 25	1271 + 2634 - 752	33.7
1645+325	DB2.3	22.69 ± 0.37	21926 ± 3668	0.544 ± 0.044	7.894 ± 0.059	36 + 45 - 18	7955 + 84185 - 6091	32.8
1709+230	DBAZ2.5	15.24 ± 0.39	20287 ± 1552	0.646 ± 0.049	8.082 ± 0.059	79 + 33 - 25	1507 + 3476 - 871	51.4
1747+450	DC5.8	34.37 ± 0.38	8634 ± 293	0.804 ± 0.040	8.352 ± 0.044	1646 + 282 - 238	1943 + 183 - 80	23.4
2058+342A	DBA4.6	19.56 ± 0.31	11064 ± 490	0.642 ± 0.042	8.098 ± 0.048	552 + 84 - 71	2054 + 3179 - 831	41.6
2130-047	DBA2.9	18.99 ± 0.38	17271 ± 1104	0.577 ± 0.052	7.972 ± 0.065	117 + 28 - 35	4130 + 24485 - 2947	60.0
2253-062	DBA3.0	14.66 ± 0.37	16839 ± 973	0.547 ± 0.049	7.919 ± 0.064	116 + 25 - 32	7505 + 89902 - 5787	24.4
2328+510	DBA3.6	18.98 ± 0.33	14101 ± 553	0.608 ± 0.038	8.034 ± 0.045	254 + 38 - 33	2657 + 6314 - 1486	44.0

Table 13. Properties of WDs with Metal-Rich Atmospheres

WD Number	Spectral Type	Parallax mas	T_{eff} K	Mass M_{\odot}	$\log g$ dex	Cooling Age Myr	Total Age Myr	V_{tan} km s $^{-1}$
0003–103	DQhot2.4	6.20 ± 0.41	20882 ± 1103	1.125 ± 0.046	8.863 ± 0.075	333 + 72 – 53	412 + 52 – 23	63.4
0003+177	DQ6.7	18.40 ± 1.16	7468 ± 66	0.535 ± 0.029	7.932 ± 0.035	1213 + 60 – 59	11074 + 64832 – 7085	115.5
0203+207	DQA3.1	11.93 ± 0.38	16150 ± 612	1.205 ± 0.021	9.038 ± 0.044	966 + 91 – 88	1027 + 79 – 73	130.3
0239+167 ^a	DQ7.7	25.21 ± 0.47	... ± ± ± + ... – + ... – ...	133.2
0246+734	DZ6.5	13.14 ± 0.93	7709 ± 106	0.444 ± 0.063	7.762 ± 0.088	902 + 105 – 93	... + ... – ...	86.0
0625+100	DZ5.9	18.36 ± 0.54	8519 ± 96	0.603 ± 0.031	8.042 ± 0.036	1002 + 57 – 55	3595 + 6101 – 1505	37.4
0714+458	DQ5.0	28.30 ± 0.22	10007 ± 393	0.652 ± 0.040	8.117 ± 0.045	742 + 98 – 86	2068 + 2438 – 679	35.0
0913+103	DQ5.9	26.72 ± 0.45	8534 ± 62	0.612 ± 0.017	8.058 ± 0.020	1018 + 34 – 33	3281 + 3119 – 1148	33.7
0919+296	DQ6.2	8.63 ± 0.69	8068 ± 66	0.652 ± 0.077	8.122 ± 0.088	1277 + 196 – 146	2604 + 7276 – 756	148.0
1035–003	DZ6.2	16.35 ± 0.59	8180 ± 73	0.664 ± 0.036	8.142 ± 0.040	1271 + 90 – 78	2422 + 1841 – ...	26.7
1042+593	DQ5.2	17.79 ± 0.35	9730 ± 49	1.139 ± 0.011	8.899 ± 0.018	2366 + 20 – 20	2441 + 7 – 4	468.3
1111+020	DQP9.9	24.24 ± 0.70	5091 ± 12	0.858 ± 0.026	8.439 ± 0.029	7013 + 19 – 16	7239 + 72 – 40	77.5
1200+651	DQA4.2	11.27 ± 0.44	11930 ± 275	1.019 ± 0.033	8.680 ± 0.043	1264 + 128 – 139	1378 + 100 – 98	61.6
1212–022	DZP10.9	26.18 ± 0.64	4618 ± 16	0.494 ± 0.025	7.873 ± 0.031	5385 + 275 – 298	41996 + ... – 29566	99.9
1235+422	DQ8.2	28.23 ± 0.42	6174 ± 19	0.734 ± 0.016	8.253 ± 0.017	4037 + 106 – 117	4480 + 53 – 10	83.5
1309+296	DQ9.4	18.69 ± 0.71	5309 ± 34	0.653 ± 0.039	8.133 ± 0.042	5590 + 270 – 313	6901 + 2227 – 481	126.8
1327+594	DQAPhot2.7	7.48 ± 0.50	18755 ± 2164	1.194 ± 0.055	9.011 ± 0.110	640 + 268 – 227	703 + 251 – 202	55.9
1328+307	DZ8.8	38.75 ± 0.67	5726 ± 20	0.533 ± 0.018	7.937 ± 0.021	2807 + 150 – 142	13186 + 38667 – 6816	58.8
1552+177	DZ7.7	15.23 ± 0.92	6550 ± 27	0.484 ± 0.055	7.844 ± 0.073	1518 + 124 – 141	... + ... – ...	45.5
1611+176	DQ9.3	19.48 ± 0.38	5426 ± 19	0.584 ± 0.021	8.023 ± 0.023	4384 + 212 – 222	7929 + 7067 – 1844	63.8
1727+560	DQAB3.6	20.71 ± 0.42	13825 ± 320	1.112 ± 0.018	8.843 ± 0.027	1117 + 80 – 79	1199 + 64 – 58	57.7
1729+371	DAZB4.9	17.49 ± 0.29	10057 ± 374	0.551 ± 0.042	7.950 ± 0.051	574 + 73 – 64	7328 + 51959 – 4997	58.4
2157–079	DQhot2.0	4.23 ± 0.46	26142 ± 2412	1.009 ± 0.094	8.649 ± 0.124	120 + 54 – 43	238 + 53 – ...	27.9
2229–080	DQ8.1	18.84 ± 0.70	6197 ± 21	0.717 ± 0.037	8.228 ± 0.040	3817 + 250 – 316	4311 + 706 – ...	73.1

^a Analysis postponed to future work

Table 14. Properties of Cool WDs with Mixed Hydrogen and Helium Atmospheres

WD Number	Spectral Type	Parallax mas	T_{eff} K	Mass M_{\odot}	$\log g$ dex	Cooling Age Myr	Total Age Myr	V_{\tan} km s $^{-1}$
0042–064	DC10.1	33.04 ± 0.40	4983 ± 80	0.890 ± 0.029	8.486 ± 0.032	7120 + 106 – 100	7315 + 55 – 25	98.2
0343+247	DC14.4	25.75 ± 0.59	3506 ± 39	0.320 ± 0.027	7.519 ± 0.046	5418 + 419 – 387	… + … – …	233.2
0922+005	D:12.2	15.67 ± 0.16	4127 ± 65	0.338 ± 0.024	7.559 ± 0.040	4018 + 343 – 303	… + … – …	175.6
0944+452B	DC16.7	18.54 ± 0.42	3009 ± 27	0.125 ± 0.024	6.864 ± 0.089	3072 + 308 – 254	… + … – …	22.5
1059+415	DC14.9	28.85 ± 0.54	3371 ± 36	0.354 ± 0.025	7.598 ± 0.040	6640 + 355 – 360	… + … – …	286.9
1218+095	DC14.3	24.94 ± 0.72	3531 ± 37	0.893 ± 0.033	8.492 ± 0.037	8535 + 166 – 140	8727 + 113 – 61	96.4
1335+002	DC18.2	19.68 ± 0.76	2772 ± 32	0.311 ± 0.021	7.301 ± 0.051	1866 + 108 – 83	… + … – …	41.5
1401–149	DC11.1	20.19 ± 1.37	4554 ± 90	0.404 ± 0.069	7.701 ± 0.100	4022 + 849 – 695	… + … – …	91.4
1401+457	DC17.4	30.03 ± 0.70	2895 ± 28	0.481 ± 0.036	7.852 ± 0.045	9200 + 152 – 156	… + … – …	43.4
1630+245	DC10.8	24.19 ± 0.53	4684 ± 37	0.900 ± 0.025	8.502 ± 0.029	7442 + 81 – 69	7628 + 34 – 3	65.5

Table 15. Properties of WDs with Unconstrained Composition Atmospheres

WD Number	Spectral Type	Parallax mas	T_{eff} K	Mass M_{\odot}	$\log g$ dex	Cooling Age	Total Age Myr	V_{\tan} km s $^{-1}$
0306+663	DC10.7	26.48 ± 0.59	4707 ± 78	0.506 ± 0.041	7.886 ± 0.051	5503 + 570 - 599	30649 + ⋯ - 20907	145.1
0357+513	DC10.0	39.26 ± 0.42	5139 ± 65	0.741 ± 0.023	8.256 ± 0.026	7023 + 251 - 269	7634 + 274 - 39	106.2
0409+237	DC:6.7	13.06 ± 0.45	7378 ± 229	0.935 ± 0.045	8.542 ± 0.053	3474 + 270 - 267	3637 + 220 - 189	160.9
0500+573	D:6.2	9.25 ± 1.12	8226 ± 262	0.426 ± 0.101	7.700 ± 0.154	706 + 138 - 106	⋯ + ⋯ - ⋯	148.7
0531+572	DC:10.2	24.41 ± 0.92	4903 ± 72	0.523 ± 0.047	7.916 ± 0.057	5166 + 651 - 694	24146 + ⋯ - 15587	53.8
0541+750	D:8.4	14.22 ± 1.14	5892 ± 140	0.440 ± 0.078	7.747 ± 0.110	1765 + 287 - 257	⋯ + ⋯ - ⋯	85.4
0701+517	D:9.8	26.86 ± 1.35	5064 ± 79	0.742 ± 0.057	8.264 ± 0.061	7315 + 326 - 424	7748 + 620 - 145	83.2
0708+462	DC:10.5	13.82 ± 0.63	4803 ± 76	0.463 ± 0.054	7.806 ± 0.070	4348 + 779 - 714	⋯ + ⋯ - ⋯	184.7
1253+471	DC10.6	26.92 ± 0.53	4707 ± 68	0.748 ± 0.034	8.269 ± 0.037	8208 + 174 - 194	8624 + 340 - 59	191.8
1439-195	DC:9.5	25.23 ± 0.67	5212 ± 77	0.718 ± 0.037	8.223 ± 0.040	6596 + 350 - 390	7307 + 548 - 28	112.7
1946+837	DC10.5	27.16 ± 0.42	4748 ± 84	0.717 ± 0.040	8.224 ± 0.043	7953 + 251 - 283	8595 + 509 - 75	162.3
2139+132B	DC:9.3	21.93 ± 0.31	5301 ± 87	0.651 ± 0.033	8.120 ± 0.037	5495 + 497 - 525	7155 + 2919 - 497	74.6
2359+636	DC10.4	38.89 ± 0.27	4896 ± 80	0.581 ± 0.035	8.011 ± 0.040	6130 + 426 - 462	10374 + 17097 - 2449	112.8

Table 16. Candidate Unresolved White Dwarf Binaries

WD Number	Name	Spectral Type	Mass M_{\odot} ^a
0339+523	EGGR 567	DA3.8	0.37 ± 0.03
0343+247		DC14.4	0.32 ± 0.03
0402+265	LHS 1625a	DC12.7	0.24 ± 0.05
0452+103	G83-43	DA6.8	0.37 ± 0.04
0541+260	LSR J0544+2603	DC10.0	0.31 ± 0.02
0546+234	LSR J0549+2329	D:10.6	0.24 ± 0.02
0922+005	LHS 2139	D:12.2	0.34 ± 0.02
0944+452B		DC16.7	0.13 ± 0.02
1059+415	SDSS J1102+4113	DC14.9	0.35 ± 0.03
1335+002		DC18.2	0.31 ± 0.02
1632+177	PG 1632+177	DA5.2	0.24 ± 0.01
2058+342B	GD 392B	DC15.5	0.18 ± 0.03

^aIf a single white dwarf.

8.3. Age and Kinematics

Figure 13 shows that most of the stars in the sample are younger than 10 Gyr as would be expected for a relatively local disk sample. Gagné et al. (2018) has shown that one object in our sample, 0346–011, is a member of the AB Doradus moving group. Gagné et al. used the *Gaia* DR2 parallax and proper motion, MESA Isochrones and Stellar Tracks (MIST) isochrones (Choi et al. 2016), and the same atmosphere models and initial-final mass relation used here, to demonstrate that this massive DA1.2 star is a member of the young AB Dor group. Our analysis using the NOFS parallax and proper motion and PARSEC isochrones supports this conclusion — we find a total age for 0346–011 of 115^{+125}_{-29} Myr, consistent with the AB Dor age given by Gagné et al. of 133^{+15}_{-20} Myr.

Figure 14 is a plot of the tangential velocity (V_{\tan}) of the sample as a function of total age. Using the Besançon Galaxy model (Robin et al. 2003), Dupuy & Liu (2012) calculate probabilities of population membership as a function of V_{\tan} . They find a 90% probability of thick disk membership for $150 \lesssim V_{\tan} \text{ km s}^{-1} \lesssim 210$ and a $\gtrsim 50\%$ probability of halo membership for $V_{\tan} > 250 \text{ km s}^{-1}$. Kilic et al. (2017) examine the faint end of the luminosity functions of samples of WDs and derive ages of 7.5 ± 1.2 Gyr for the thin disk, and 9.3 ± 0.6 Gyr for the thick disk. The halo age is less constrained but Kilic et al. estimate it to lie in the range 9 – 14 Gyr.

Table 17 lists the twelve WDs in our core sample of 179 for which $V_{\tan} > 140 \text{ km s}^{-1}$ and the total age range encompasses values > 9.5 Gyr. One of these WDs (0202–055) is a normal-mass cool WD with a cooling age of 9 Gyr. Seven of them (0306+663, 1022+009, 1034+077, 1104+491, 1300+263, 1458+362, 2316–064) are cool low-mass WDs which have cooling ages of a few Gyr and low-mass progenitors that spent several Gyr on the main sequence. Four others (0145–174, 0919+296, 1314–153, 2148+539) are not particularly cool but the possible fits include masses low enough that the progenitor time on the main sequence is high. Based on the Galaxy model described above, the

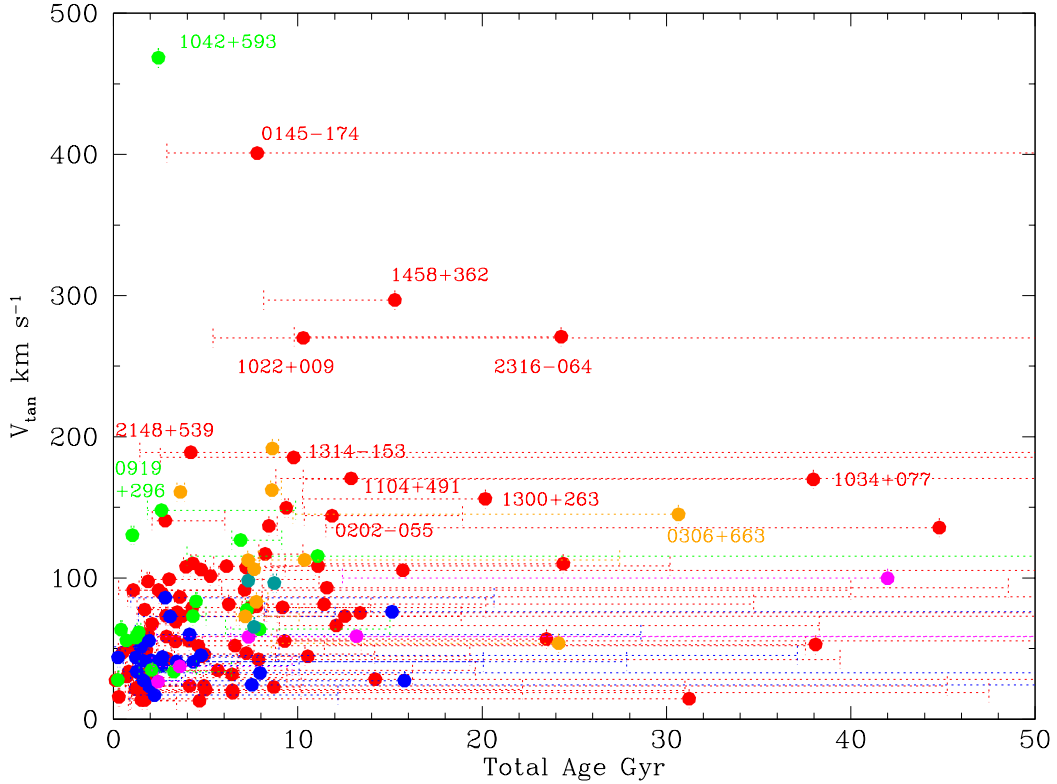


Figure 14. The tangential velocity as a function of total age. Symbol colors are as in Figure 9. Uncertainties in age are shown as dotted lines.

Table 17. Candidate Halo White dwarfs

WD Number	Name	Spectral Type	Mass M_{\odot}	Lower Age Limit Gyr	V_{\tan} km s $^{-1}$
0145-174	EGGR 467	DA6.8	0.55	2.9	401
0202-055		DC12.2	0.60	10.4	144
0306+663	LSR J0310+6634	DC10.7	0.51	9.7	145
0919+296	LP 313-49	DQ6.2	0.65	1.8	148
1022+009	LP 610-10	DA9.3	0.55	5.4	270
1034+077	LHS 2288	DC11.7	0.50	10.3	170
1104+491	LSR J1107+4855	DC10.8	0.55	8.8	171
1300+263	LHS 2673	DC11.7	0.53	10.2	156
1314-153	LP 737-47	DA3.4	0.54	2.5	185
1458+362	[MFL2000]J1500+3600	DC10.3	0.54	8.2	297
2148+539	G232-38	DA4.9	0.58	1.4	189
2316-064	LHS 542	DC11.2	0.51	9.8	271

four WDs with $V_{\tan} > 250 \text{ km s}^{-1}$ (0145–174, 1022+009, 1458+362, and 2316–064) have a high probability of halo membership while the remaining eight are likely to be members of the thick disk.

Total age was only determined for WDs with mass $\geq 0.5 M_{\odot}$ because of the likelihood that lower mass WDs are the product of binary evolution. There is one very low-temperature WD with a mass $0.48 M_{\odot}$ which has the largest cooling age in the sample. The DC17.4 1401+457 has a cooling age of 9.2 Gyr. The V_{\tan} is low at 43 km s^{-1} , however if indeed this is a single low mass WD then the main sequence lifetime would be significant, making this star very old.

The DQ5.2 1042+593 has the highest velocity in our core sample ($> 450 \text{ km s}^{-1}$, Figure 14), but a well-constrained young-disk-like age of 2.4 Gyr. The astrometric measurements are robust as this WD was observed independently with two different NOFS cameras (Table 1). This WD appears to be a less extreme version of the binary system WD 2234+222 (LP 400-22) for which $V_{\tan} = 1190 \text{ km s}^{-1}$ (Table 1, Table 5). Kilic et al. (2013) suggest that a dynamical interaction with other binary stars or a central black hole in a dense cluster could explain the origin of WD 2234+222. Hansen (2003) has suggested that high velocity white dwarfs may be the result of disruption of a close binary orbit by a Type Ia supernova explosion. In the case of the massive DQ 1042+593 it does appear that a dynamical kick of some kind is required to explain its high velocity.

8.4. Ages of Resolved Double Degenerate Binaries

Table 18. Ages of Resolved Double Degenerate Binaries

WD	Composition	T_{eff}	Mass	Initial	Cooling	Total	V_{\tan}
Number		K	M_{\odot}	Mass M_{\odot}	Age Gyr	Age Gyr	km s^{-1}
0102+210A	H	5278 ± 89	0.78 ± 0.04	3.4 ± 0.5	7.10 ± 0.48	$7.4^{+0.3}_{-0.3}$	78.7
0102+210B	H	4818 ± 78	0.62 ± 0.04	1.8 ± 0.7	7.16 ± 0.51	$9.2^{+4.8}_{-0.8}$	79.3
0114–049A	H	4885 ± 75	0.55 ± 0.04	1.1 ± 0.7	5.65 ± 0.60	$12.6^{+42}_{-4.2}$	73.8
0114–049B	He	4979 ± 54	0.54 ± 0.03	1.0 ± 0.5	5.25 ± 0.31	$15.1^{+65}_{-6.9}$	74.7
0507+045A	H	10884 ± 418	0.58 ± 0.04	1.4 ± 0.6	0.46 ± 0.05	$4.1^{+12.4}_{-2.4}$	23.9
0507+045B	H	19285 ± 1872	0.57 ± 0.05	1.3 ± 0.8	0.06 ± 0.03	$4.9^{+40}_{-3.7}$	23.2
0944+452A	H	4877 ± 83	0.67 ± 0.04	2.2 ± 0.8	7.59 ± 0.45	$8.7^{+1.5}_{-0.27}$	22.5
0944+452B	N(H)/N(He)= $10^{-2.92}$	3009 ± 27	0.13 ± 0.02	...	3.07 ± 0.33	...	22.8
1012+083A	H	6650 ± 117	0.59 ± 0.02	1.5 ± 0.5	1.74 ± 0.10	$4.8^{+5.6}_{-1.6}$	44.7
1012+083B	H	4676 ± 70	0.59 ± 0.03	1.5 ± 0.5	7.12 ± 0.40	$10.5^{+8.8}_{-2.7}$	45.0
1944+467A	H	5389 ± 93	0.67 ± 0.03	2.3 ± 0.7	5.23 ± 0.66	$6.3^{+0.7}_{-0.7}$	81.7
1944+467B	H	4906 ± 78	0.56 ± 0.03	1.2 ± 0.6	5.74 ± 0.61	$11.4^{+23}_{-3.4}$	81.6
2058+342A	He	11064 ± 490	0.64 ± 0.04	2.0 ± 0.7	0.55 ± 0.08	$2.1^{+3.2}_{-0.8}$	41.6
2058+342B	H	3249 ± 75	0.18 ± 0.03	...	3.49 ± 0.43	...	39.9
2139+132A	H	7623 ± 204	0.63 ± 0.04	1.8 ± 0.6	1.31 ± 0.11	$3.1^{+3.7}_{-1.0}$	73.4
2139+132B	unconstrained	5301 ± 87	0.65 ± 0.03	2.0 ± 0.7	5.49 ± 0.52	$7.2^{+2.9}_{-0.5}$	73.7

Table 18 lists the parameters for the eight resolved WD binaries in the sample. Such binaries would be expected to have the same total age, within the uncertainties. The ages can therefore be used to test the robustness of our analysis. Six systems consist of normal-mass WD pairs; four of these have component ages which agree within 1.0σ and the other two agree to $1.5 - 2.1\sigma$, validating the results presented here.

Two systems in Table 18 contain an unusually low-mass WD, and for these the primaries may provide insight into the true nature of these objects. Both low-mass components have colors suggesting they are cool. If they are in fact normal-mass unresolved binaries then the cooling time is around 10 Gyr. This could work for the 0944+452 system where the primary is also cool, but is unlikely to be true for the 2058+342 system where the primary is warm and the total age is < 5.3 Gyr. Further exploration is postponed to future work.

The binaries may also provide constraints on the chemical evolution of WDs. For example, the 0114–049 system apparently consists of a nearly identical pair of objects, but the chemical composition of their atmospheres is different. Again, further work is postponed to subsequent papers.

9. CONCLUSION

Trigonometric parallaxes have been measured at the Naval Observatory Flagstaff Station (NOFS) telescopes for more than fifty years. In the last thirty years, refereed papers that have used NOFS parallaxes to study dwarf stars have been cited more than 5000 times. The Northern hemisphere observations for the US Naval Observatory CCD Astrograph Catalog (UCAC) were obtained at the Flagstaff Station. The UCAC in turn provided the fundamental reference frame for the Sloan Digital Sky Survey (Pier et al. 2003; Zacharias et al. 2004). The Flagstaff Station is also where photographic plates were scanned to produce the USNO-B catalog (Monet et al. 2003). The work done by the small group of staff at the NOFS has been of the highest quality, and has been of fundamental importance to astronomy. The parallax work at the NOFS is now winding down and this paper will be one of the last presenting NOFS parallaxes. In the next five years the *Gaia* satellite (Gaia Collaboration et al. 2018) will become the primary source of stellar parallaxes and proper motions, with a final release planned in 2022.

In this paper we have presented new NOFS trigonometric parallaxes for 214 stars (or unresolved systems) at distances between 25 pc and 1.2 kpc. The observations of each star took place over periods of 3 – 10 years, and the uncertainty in the parallax ranges from 0.2 mas to 1.6 mas with an average of 0.6 mas. Ninety percent of our sample also has a *Gaia* parallax, although 40% of those objects are flagged in the *Gaia* Data Release 2 as having a poor astrometric fit or excess noise. We find generally good agreement between the NOFS and *Gaia* measurements with an indication of an offset in the *Gaia* values of -0.13 mas, similar to that found by Stassun & Torres (2018). Eighteen stars with good quality NOFS and *Gaia* measurements have parallaxes that differ significantly, and these differences can be explained by binarity and/or by small $\sim 10\%$ underestimates in the uncertainties for both sets of measurements.

More than 80% of the stars with new NOFS parallaxes presented here are WDs and we analyse these objects in detail. We combine the parallaxes with photometry to determine flux-calibrated SEDs for each star. In many cases the photometry spans a wide wavelength range from the ultra-violet to the mid-infrared, and precise fluxes are provided by the sky surveys Pan-STARRS, SDSS,

UHS, UKIDSS, VISTA and WISE. We compare the SEDs, and spectroscopy where available, to flux distributions generated by model atmospheres. In the last few years white dwarf models have improved significantly. Treatments of the non-ideal equation of state and of line broadening have advanced, and opacities are more complete (Bergeron et al. 2011; Dufour et al. 2005, 2007b; Kowalski & Saumon 2006; Tremblay & Bergeron 2009). We show here that the models do an excellent job of reproducing the entire SED for this inhomogeneous sample of WDs.

The sample contains hot and cool WDs with high and low gravities and a range of chemical composition. More than 60% of the sample have pure-hydrogen atmospheres but pure-helium, mixed hydrogen-helium and metal-rich atmospheres are also present and are generally modelled successfully (Appendix Figure 15). The highest mass object in the sample is 2349–031 with a mass of $1.33 M_{\odot}$, close to the Chandrasekhar limit. Twelve WDs have extremely low masses of $< 0.4 M_{\odot}$ — these may be the single product of binary evolution or may themselves be unresolved binaries; we identify these candidate binary systems. Thirty objects in the sample have a total age of 10 Gyr or more; we identify candidate thick disk and halo WDs based on total age and tangential velocity. The youngest object in the sample for which an age can be determined is 0346–011, with an age of 115 Myr, and which Gagné et al. (2018) has shown to be a member of the AB Dor moving group. The young 0346–011 is also the warmest star in the sample with $T_{\text{eff}} \approx 41000$ K. The five coldest stars have $2800 \lesssim T_{\text{eff}} \text{ K} \lesssim 3400$. For two of these the model fits give extremely low masses of $0.13 - 0.18 M_{\odot}$. The other three cold WDs are low-mass to a lesser extent: the model fits give masses of $0.3 - 0.5 M_{\odot}$.

The future holds the promise of exquisitely detailed studies of the end points of stellar evolution, the WDs. New WDs will be identified in photometric or astrometric studies; accurate distances will be available as well as precise photometry. The models will reproduce observations across a wide wavelength range, allowing the confident exploration of the physics and chemistry of these high pressure atmospheres, illuminating the evolution of these intriguing objects.

This research has made use of the SIMBAD database, operated at CDS, Strasbourg, France.

This publication makes use of data from the Pan-STARRS1 Surveys (PS1). PS1 and the PS1 public science archive have been made possible through contributions by the Institute for Astronomy, the University of Hawaii, the Pan-STARRS Project Office, the Max-Planck Society and its participating institutes, the Max Planck Institute for Astronomy, Heidelberg and the Max Planck Institute for Extraterrestrial Physics, Garching, The Johns Hopkins University, Durham University, the University of Edinburgh, the Queen’s University Belfast, the Harvard-Smithsonian Center for Astrophysics, the Las Cumbres Observatory Global Telescope Network Incorporated, the National Central University of Taiwan, the Space Telescope Science Institute, the National Aeronautics and Space Administration under Grant No. NNX08AR22G issued through the Planetary Science Division of the NASA Science Mission Directorate, the National Science Foundation Grant No. AST-1238877, the University of Maryland, Eotvos Lorand University (ELTE), the Los Alamos National Laboratory, and the Gordon and Betty Moore Foundation.

This publication makes use of data from the Sloan Digital Sky Survey (SDSS). Funding for the SDSS has been provided by the Alfred P. Sloan Foundation, the U.S. Department of Energy Office of Science, and the Participating Institutions. SDSS-IV acknowledges support and resources from the Center for High-Performance Computing at the University of Utah. The SDSS web site is www.sdss.org. SDSS-IV is managed by the Astrophysical Research Consortium for the Participating

Institutions of the SDSS Collaboration including the Brazilian Participation Group, the Carnegie Institution for Science, Carnegie Mellon University, the Chilean Participation Group, the French Participation Group, Harvard-Smithsonian Center for Astrophysics, Instituto de Astrofísica de Canarias, The Johns Hopkins University, Kavli Institute for the Physics and Mathematics of the Universe (IPMU) / University of Tokyo, the Korean Participation Group, Lawrence Berkeley National Laboratory, Leibniz Institut für Astrophysik Potsdam (AIP), Max-Planck-Institut für Astronomie (MPIA Heidelberg), Max-Planck-Institut für Astrophysik (MPA Garching), Max-Planck-Institut für Extraterrestrische Physik (MPE), National Astronomical Observatories of China, New Mexico State University, New York University, University of Notre Dame, Observatório Nacional / MCTI, The Ohio State University, Pennsylvania State University, Shanghai Astronomical Observatory, United Kingdom Participation Group, Universidad Nacional Autónoma de México, University of Arizona, University of Colorado Boulder, University of Oxford, University of Portsmouth, University of Utah, University of Virginia, University of Washington, University of Wisconsin, Vanderbilt University, and Yale University.

This work is based in part on observations obtained for the VISTA Hemisphere Survey, ESO Program, 179.A-2010 (PI: McMahon).

This work is based in part on data obtained as part of the UKIRT Infrared Deep Sky Survey and the UKIRT Hemisphere Survey (UHS). The UHS is a partnership between the UK STFC, The University of Hawaii, The University of Arizona, Lockheed Martin and NASA.

This publication makes use of data products from the Two Micron All Sky Survey, a joint project of the University of Massachusetts and the Infrared Processing and Analysis Center/California Institute of Technology, funded by the National Aeronautics and Space Administration and the National Science Foundation.

This publication makes use of data from the Wide-field Infrared Survey Explorer, a joint project of the University of California, Los Angeles, and the Jet Propulsion Laboratory/California Institute of Technology, funded by the National Aeronautics and Space Administration.

This work is based in part on archival data obtained with the Spitzer Space Telescope, operated by the Jet Propulsion Laboratory, California Institute of Technology under a contract with NASA.

This work is based in part on observations obtained at the Gemini Observatory and processed using the Gemini IRAF package. Gemini is operated by the Association of Universities for Research in Astronomy, Inc., under a cooperative agreement with the NSF on behalf of the Gemini partnership: the National Science Foundation (United States), the National Research Council (Canada), CONICYT (Chile), Ministerio de Ciencia, Tecnología e Innovación Productiva (Argentina), and Ministério da Ciência, Tecnologia e Inovação (Brazil).

This work was supported in part by the NSERC Canada and by the Fund FQRNT (Québec).

REFERENCES

- Althaus, L. G., Miller Bertolami, M. M., & Córscico, A. H. 2013, A&A, 557, A19, doi: [10.1051/0004-6361/201321868](https://doi.org/10.1051/0004-6361/201321868)
- Barber, S. D., Belardi, C., Kilic, M., & Gianninas, A. 2016, MNRAS, 459, 1415, doi: [10.1093/mnras/stw683](https://doi.org/10.1093/mnras/stw683)
- Barber, S. D., Kilic, M., Brown, W. R., & Gianninas, A. 2014, ApJ, 786, 77, doi: [10.1088/0004-637X/786/2/77](https://doi.org/10.1088/0004-637X/786/2/77)
- Barber, S. D., Patterson, A. J., Kilic, M., et al. 2012, ApJ, 760, 26, doi: [10.1088/0004-637X/760/1/26](https://doi.org/10.1088/0004-637X/760/1/26)

- Becklin, E. E., Farihi, J., Jura, M., et al. 2005, ApJL, 632, L119, doi: [10.1086/497826](https://doi.org/10.1086/497826)
- Bergeron, P., Greenstein, J. L., & Liebert, J. 1990a, ApJ, 361, 190, doi: [10.1086/169182](https://doi.org/10.1086/169182)
- Bergeron, P., & Leggett, S. K. 2002, ApJ, 580, 1070, doi: [10.1086/343795](https://doi.org/10.1086/343795)
- Bergeron, P., Leggett, S. K., & Ruiz, M. T. 2001, ApJS, 133, 413, doi: [10.1086/320356](https://doi.org/10.1086/320356)
- Bergeron, P., Ruiz, M. T., Hamuy, M., et al. 2005, ApJ, 625, 838, doi: [10.1086/429715](https://doi.org/10.1086/429715)
- Bergeron, P., Ruiz, M. T., & Leggett, S. K. 1997, ApJS, 108, 339, doi: [10.1086/312955](https://doi.org/10.1086/312955)
- Bergeron, P., Saffer, R. A., & Liebert, J. 1992, ApJ, 394, 228, doi: [10.1086/171575](https://doi.org/10.1086/171575)
- Bergeron, P., Wesemael, F., & Dufour, P., et al. 2011, ApJ, 737, 28, doi: [10.1088/0004-637X/737/1/28](https://doi.org/10.1088/0004-637X/737/1/28)
- Bergeron, P., Wesemael, F., Fontaine, G., & Liebert, J. 1990b, ApJL, 351, L21, doi: [10.1086/185670](https://doi.org/10.1086/185670)
- Bergeron, P., Wesemael, F., Lamontagne, R., et al. 1995, ApJ, 449, 258, doi: [10.1086/176053](https://doi.org/10.1086/176053)
- Bergeron, P., Wesemael, F., & Saffer, R. A. 2000, PASP, 112, 837, doi: [10.1086/316582](https://doi.org/10.1086/316582)
- Bergfors, C., Farihi, J., Dufour, P., & Rocchetto, M. 2014, MNRAS, 444, 2147, doi: [10.1093/mnras/stu1565](https://doi.org/10.1093/mnras/stu1565)
- Bochanski, J. J., West, A. A., Hawley, S. L., & Covey, K. R. 2007, AJ, 133, 531, doi: [10.1086/510240](https://doi.org/10.1086/510240)
- Bressan, A., Marigo, P., Girardi, L., et al. 2012, MNRAS, 427, 127, doi: [10.1111/j.1365-2966.2012.21948.x](https://doi.org/10.1111/j.1365-2966.2012.21948.x)
- Cardelli, J. A., Clayton, G. C., & Mathis, J. S. 1989, ApJ, 345, 245, doi: [10.1086/167900](https://doi.org/10.1086/167900)
- Chambers, K. C., Magnier, E. A., Metcalfe, N., et al. 2016, ArXiv e-prints. <https://arxiv.org/abs/1612.05560>
- Choi, J., Dotter, A., Conroy, C., et al. 2016, ApJ, 823, 102, doi: [10.3847/0004-637X/823/2/102](https://doi.org/10.3847/0004-637X/823/2/102)
- Cummings, J. D., Kalirai, J. S., Tremblay, P.-E., & Ramirez-Ruiz, E. 2016, ApJ, 818, 84, doi: [10.3847/0004-637X/818/1/84](https://doi.org/10.3847/0004-637X/818/1/84)
- Dahn, C. C., Harris, H. C., Subasavage, J. P., et al. 2017, AJ, 154, 147, doi: [10.3847/1538-3881/aa880b](https://doi.org/10.3847/1538-3881/aa880b)
- Debes, J. H., Hoard, D. W., Wachter, S., Leisawitz, D. T., & Cohen, M. 2011, ApJS, 197, 38, doi: [10.1088/0067-0049/197/2/38](https://doi.org/10.1088/0067-0049/197/2/38)
- Dufour, P., Bergeron, P., & Fontaine, G. 2005, ApJ, 627, 404, doi: [10.1086/430373](https://doi.org/10.1086/430373)
- Dufour, P., Fontaine, G., Liebert, J., Schmidt, G. D., & Behara, N. 2008, ApJ, 683, 978, doi: [10.1086/589855](https://doi.org/10.1086/589855)
- Dufour, P., Liebert, J., Fontaine, G., & Behara, N. 2007a, Nature, 450, 522, doi: [10.1038/nature06318](https://doi.org/10.1038/nature06318)
- Dufour, P., Bergeron, P., Liebert, J., et al. 2007b, ApJ, 663, 1291, doi: [10.1086/518468](https://doi.org/10.1086/518468)
- Dupuy, T. J., & Liu, M. C. 2012, ApJS, 201, 19, doi: [10.1088/0067-0049/201/2/19](https://doi.org/10.1088/0067-0049/201/2/19)
- Eisenstein, D. J., Liebert, J., Harris, H. C., et al. 2006, ApJS, 167, 40, doi: [10.1086/507110](https://doi.org/10.1086/507110)
- Farihi, J. 2004, ApJ, 610, 1013, doi: [10.1086/382682](https://doi.org/10.1086/382682)
- Farihi, J., Gänsicke, B. T., Steele, P. R., et al. 2012, MNRAS, 421, 1635, doi: [10.1111/j.1365-2966.2012.20421.x](https://doi.org/10.1111/j.1365-2966.2012.20421.x)
- Farihi, J., Jura, M., Lee, J., & Zuckerman, B. 2010, ApJ, 714, 1386, doi: [10.1088/0004-637X/714/2/1386](https://doi.org/10.1088/0004-637X/714/2/1386)
- Farihi, J., Jura, M., & Zuckerman, B. 2009, ApJ, 694, 805, doi: [10.1088/0004-637X/694/2/805](https://doi.org/10.1088/0004-637X/694/2/805)
- Farihi, J., Zuckerman, B., & Becklin, E. E. 2005, AJ, 130, 2237, doi: [10.1086/491707](https://doi.org/10.1086/491707)
- . 2008, ApJ, 674, 431, doi: [10.1086/521715](https://doi.org/10.1086/521715)
- Fontaine, G., Brassard, P., & Bergeron, P. 2001, PASP, 113, 409, doi: [10.1086/319535](https://doi.org/10.1086/319535)
- Gagné, J., Fontaine, G., Simon, A., & Faherty, J. K. 2018, ApJL, 861, L13, doi: [10.3847/2041-8213/aacdff](https://doi.org/10.3847/2041-8213/aacdff)
- Gaia Collaboration, Brown, A. G. A., Vallenari, A., et al. 2018, A&A, 616, A1, doi: [10.1051/0004-6361/201833051](https://doi.org/10.1051/0004-6361/201833051)
- Genest-Beaulieu, C., & Bergeron, P. 2014, ApJ, 796, 128, doi: [10.1088/0004-637X/796/2/128](https://doi.org/10.1088/0004-637X/796/2/128)
- Gentile Fusillo, N. P., Tremblay, P.-E., Gänsicke, B. T., et al. 2018, ArXiv e-prints. <https://arxiv.org/abs/1807.03315>
- Giannicola, N., Bergeron, P., & Dufour, P. 2012, ApJS, 199, 29, doi: [10.1088/0067-0049/199/2/29](https://doi.org/10.1088/0067-0049/199/2/29)
- Giannicola, N., Charpinet, S., Fontaine, G., et al. 2018, Nature, 554, 73, doi: [10.1038/nature25136](https://doi.org/10.1038/nature25136)
- Gianninas, A., Bergeron, P., & Ruiz, M. T. 2011, ApJ, 743, 138, doi: [10.1088/0004-637X/743/2/138](https://doi.org/10.1088/0004-637X/743/2/138)

- Gianninas, A., Curd, B., Thorstensen, J. R., et al. 2015, MNRAS, 449, 3966, doi: [10.1093/mnras/stv545](https://doi.org/10.1093/mnras/stv545)
- Gimeno, G., Roth, K., Chiboucas, K., et al. 2016, in Proc. SPIE, Vol. 9908, Ground-based and Airborne Instrumentation for Astronomy VI, 99082S
- Girven, J., Gänsicke, B. T., Steeghs, D., & Koester, D. 2011, MNRAS, 417, 1210, doi: [10.1111/j.1365-2966.2011.19337.x](https://doi.org/10.1111/j.1365-2966.2011.19337.x)
- Gizis, J. E., & Reid, I. N. 1997, PASP, 109, 849, doi: [10.1086/133955](https://doi.org/10.1086/133955)
- González-Fernández, C., Hodgkin, S. T., Irwin, M. J., et al. 2018, MNRAS, 474, 5459, doi: [10.1093/mnras/stx3073](https://doi.org/10.1093/mnras/stx3073)
- Green, G. M., Schlafly, E. F., Finkbeiner, D., et al. 2018, MNRAS, 478, 651, doi: [10.1093/mnras/sty1008](https://doi.org/10.1093/mnras/sty1008)
- Greenstein, J. L. 1986, ApJ, 304, 334, doi: [10.1086/164168](https://doi.org/10.1086/164168)
- Hall, P. B., Kowalski, P. M., Harris, H. C., et al. 2008, AJ, 136, 76, doi: [10.1088/0004-6256/136/1/76](https://doi.org/10.1088/0004-6256/136/1/76)
- Hansen, B. M. S. 2003, ApJ, 582, 915, doi: [10.1086/344782](https://doi.org/10.1086/344782)
- Harris, H. C., Dahn, C. C., Vrba, F. J., et al. 1999, ApJ, 524, 1000, doi: [10.1086/307856](https://doi.org/10.1086/307856)
- Harris, H. C., Munn, J. A., Kilic, M., et al. 2006, AJ, 131, 571, doi: [10.1086/497966](https://doi.org/10.1086/497966)
- Harris, H. C., Dahn, C. C., Zacharias, N., et al. 2016, AJ, 152, 118, doi: [10.3847/0004-6256/152/5/118](https://doi.org/10.3847/0004-6256/152/5/118)
- Hillwig, T. C., Gale, A. A., Honeycutt, R. K., & Rengstorff, A. W. 2002, PASP, 114, 756, doi: [10.1086/341700](https://doi.org/10.1086/341700)
- Hoard, D. W., Wachter, S., Sturch, L. K., & et al. 2007, AJ, 134, 26, doi: [10.1086/517878](https://doi.org/10.1086/517878)
- Hodgkin, S. T., Irwin, M. J., Hewett, P. C., & Warren, S. J. 2009, MNRAS, 394, 675, doi: [10.1111/j.1365-2966.2008.14387.x](https://doi.org/10.1111/j.1365-2966.2008.14387.x)
- Holberg, J. B., & Bergeron, P. 2006, AJ, 132, 1221, doi: [10.1086/505938](https://doi.org/10.1086/505938)
- Hook, I. M., Jørgensen, I., Allington-Smith, J. R., et al. 2004, PASP, 116, 425, doi: [10.1086/383624](https://doi.org/10.1086/383624)
- Iben, Jr., I., & Livio, M. 1993, ApJL, 406, L15, doi: [10.1086/186775](https://doi.org/10.1086/186775)
- Jørgensen, U. G., Hammer, D., Borysow, A., & Falkesgaard, J. 2000, A&A, 361, 283
- Jura, M., Farihi, J., & Zuckerman, B. 2007, ApJ, 663, 1285, doi: [10.1086/518767](https://doi.org/10.1086/518767)
- Jura, M., & Young, E. D. 2014, Annual Review of Earth and Planetary Sciences, 42, 45, doi: [10.1146/annurev-earth-060313-054740](https://doi.org/10.1146/annurev-earth-060313-054740)
- Kalirai, J. S., Saul Davis, D., Richer, H. B., et al. 2009, ApJ, 705, 408, doi: [10.1088/0004-637X/705/1/408](https://doi.org/10.1088/0004-637X/705/1/408)
- Kato, T. 2015, PASJ, 67, 108, doi: [10.1093/pasj/psv077](https://doi.org/10.1093/pasj/psv077)
- Kawka, A., & Vennes, S. 2005, Ap&SS, 296, 481, doi: [10.1007/s10509-005-4898-9](https://doi.org/10.1007/s10509-005-4898-9)
- Kawka, A., Vennes, S., Koch, R., & Williams, A. 2002, AJ, 124, 2853, doi: [10.1086/343836](https://doi.org/10.1086/343836)
- Kepler, S. O., Kleinman, S. J., Nitta, A., et al. 2007, MNRAS, 375, 1315, doi: [10.1111/j.1365-2966.2006.11388.x](https://doi.org/10.1111/j.1365-2966.2006.11388.x)
- Kilic, M., Hambly, N. C., Bergeron, P., Genest-Beaulieu, C., & Rowell, N. 2018, MNRAS, doi: [10.1093/mnrasl/sly110](https://doi.org/10.1093/mnrasl/sly110)
- Kilic, M., Kowalski, P. M., Reach, W. T., & von Hippel, T. 2009, ApJ, 696, 2094, doi: [10.1088/0004-637X/696/2/2094](https://doi.org/10.1088/0004-637X/696/2/2094)
- Kilic, M., Munn, J. A., Harris, H. C., et al. 2017, ApJ, 837, 162, doi: [10.3847/1538-4357/aa62a5](https://doi.org/10.3847/1538-4357/aa62a5)
- Kilic, M., Patterson, A. J., Barber, S., Leggett, S. K., & Dufour, P. 2012, MNRAS, 419, L59, doi: [10.1111/j.1745-3933.2011.01177.x](https://doi.org/10.1111/j.1745-3933.2011.01177.x)
- Kilic, M., & Redfield, S. 2007, ApJ, 660, 641, doi: [10.1086/513008](https://doi.org/10.1086/513008)
- Kilic, M., von Hippel, T., Leggett, S. K., & Winget, D. E. 2005, ApJL, 632, L115, doi: [10.1086/497825](https://doi.org/10.1086/497825)
- Kilic, M., Leggett, S. K., Tremblay, P.-E., et al. 2010, ApJS, 190, 77, doi: [10.1088/0067-0049/190/1/77](https://doi.org/10.1088/0067-0049/190/1/77)
- Kilic, M., Gianninas, A., Brown, W. R., et al. 2013, MNRAS, 434, 3582, doi: [10.1093/mnras/stt1282](https://doi.org/10.1093/mnras/stt1282)
- Kilic, M., Hermes, J. J., Gianninas, A., et al. 2014, MNRAS, 438, L26, doi: [10.1093/mnrasl/slt151](https://doi.org/10.1093/mnrasl/slt151)
- Kirkpatrick, J. D.,Looper, D. L.,Burgasser, A. J., et al. 2010, ApJS, 190, 100, doi: [10.1088/0067-0049/190/1/100](https://doi.org/10.1088/0067-0049/190/1/100)
- Kirkpatrick, J. D., Cushing, M. C., Gelino, C. R., et al. 2011, ApJS, 197, 19, doi: [10.1088/0067-0049/197/2/19](https://doi.org/10.1088/0067-0049/197/2/19)
- Kowalski, P. M., & Saumon, D. 2006, ApJL, 651, L137, doi: [10.1086/509723](https://doi.org/10.1086/509723)
- Leggett, S. K., Ruiz, M. T., & Bergeron, P. 1998, ApJ, 497, 294, doi: [10.1086/305463](https://doi.org/10.1086/305463)

- Leggett, S. K., Currie, M. J., Varricatt, W. P., et al. 2006, MNRAS, 373, 781, doi: [10.1111/j.1365-2966.2006.11069.x](https://doi.org/10.1111/j.1365-2966.2006.11069.x)
- Liebert, J., Bergeron, P., & Holberg, J. B. 2005, ApJS, 156, 47, doi: [10.1086/425738](https://doi.org/10.1086/425738)
- Limoges, M.-M., Bergeron, P., & Lépine, S. 2015, ApJS, 219, 19, doi: [10.1088/0067-0049/219/2/19](https://doi.org/10.1088/0067-0049/219/2/19)
- Lindegren, L., Hernández, J., Bombrun, A., et al. 2018, A&A, 616, A2, doi: [10.1051/0004-6361/201832727](https://doi.org/10.1051/0004-6361/201832727)
- Marigo, P., Bressan, A., Nanni, A., Girardi, L., & Pumo, M. L. 2013, MNRAS, 434, 488, doi: [10.1093/mnras/stt1034](https://doi.org/10.1093/mnras/stt1034)
- Marigo, P., Girardi, L., Bressan, A., et al. 2017, ApJ, 835, 77, doi: [10.3847/1538-4357/835/1/77](https://doi.org/10.3847/1538-4357/835/1/77)
- Marsh, T. R., Gänsicke, B. T., Steeghs, D., et al. 2011, ApJ, 736, 95, doi: [10.1088/0004-637X/736/2/95](https://doi.org/10.1088/0004-637X/736/2/95)
- Maxted, P. F. L., & Marsh, T. R. 1999, MNRAS, 307, 122, doi: [10.1046/j.1365-8711.1999.02635.x](https://doi.org/10.1046/j.1365-8711.1999.02635.x)
- Maxted, P. F. L., Marsh, T. R., Moran, C. K. J., & Han, Z. 2000, MNRAS, 314, 334, doi: [10.1046/j.1365-8711.2000.03343.x](https://doi.org/10.1046/j.1365-8711.2000.03343.x)
- Monet, D. G., & Dahn, C. C. 1983, AJ, 88, 1489, doi: [10.1086/113438](https://doi.org/10.1086/113438)
- Monet, D. G., Levine, S. E., Canzian, B., et al. 2003, AJ, 125, 984, doi: [10.1086/345888](https://doi.org/10.1086/345888)
- Mullally, F., Kilic, M., Reach, W. T., et al. 2007, ApJS, 171, 206, doi: [10.1086/511858](https://doi.org/10.1086/511858)
- Muraveva, T., Delgado, H. E., Clementini, G., Sarro, L. M., & Garofalo, A. 2018, MNRAS, 481, 1195, doi: [10.1093/mnras/sty2241](https://doi.org/10.1093/mnras/sty2241)
- Napiwotzki, R., Christlieb, N., Drechsel, H., et al. 2003, The Messenger, 112, 25
- Oppenheimer, B. R., Saumon, D., Hodgkin, S. T., et al. 2001, ApJ, 550, 448, doi: [10.1086/319718](https://doi.org/10.1086/319718)
- Parsons, S. G., Gänsicke, B. T., Marsh, T. R., et al. 2012, MNRAS, 426, 1950, doi: [10.1111/j.1365-2966.2012.21773.x](https://doi.org/10.1111/j.1365-2966.2012.21773.x)
- . 2013, MNRAS, 429, 256, doi: [10.1093/mnras/sts332](https://doi.org/10.1093/mnras/sts332)
- Pier, J. R., Munn, J. A., Hindsley, R. B., et al. 2003, The Astronomical Journal, 125, 1559
- Reach, W. T., Megeath, S. T., Cohen, M., et al. 2005, PASP, 117, 978, doi: [10.1086/432670](https://doi.org/10.1086/432670)
- Reid, I. N., & Gizis, J. E. 2005, PASP, 117, 676, doi: [10.1086/430462](https://doi.org/10.1086/430462)
- Robin, A. C., Reylé, C., Derrière, S., & Picaud, S. 2003, A&A, 409, 523, doi: [10.1051/0004-6361:20031117](https://doi.org/10.1051/0004-6361:20031117)
- Rolland, B., & Bergeron, P. 2015, in Astronomical Society of the Pacific Conference Series, Vol. 493, 19th European Workshop on White Dwarfs, ed. P. Dufour, P. Bergeron, & G. Fontaine, 53
- Rolland, B., Bergeron, P., & Fontaine, G. 2018, ApJ, 857, 56, doi: [10.3847/1538-4357/aab713](https://doi.org/10.3847/1538-4357/aab713)
- Rosenfield, P., Marigo, P., Girardi, L., et al. 2016, ApJ, 822, 73, doi: [10.3847/0004-637X/822/2/73](https://doi.org/10.3847/0004-637X/822/2/73)
- Schmidtobreick, L. 2017, ArXiv e-prints. <https://arxiv.org/abs/1705.09332>
- Shafter, A. W., & Szkody, P. 1984, ApJ, 276, 305, doi: [10.1086/161614](https://doi.org/10.1086/161614)
- Stassun, K. G., & Torres, G. 2018, ArXiv e-prints. <https://arxiv.org/abs/1805.03526>
- Steele, P. R., Burleigh, M. R., Farihi, J., et al. 2009, A&A, 500, 1207, doi: [10.1051/0004-6361/200911694](https://doi.org/10.1051/0004-6361/200911694)
- Subasavage, J. P., Henry, T. J., Bergeron, P., Dufour, P., & Hambley, N. C. 2008, AJ, 136, 899, doi: [10.1088/0004-6256/136/3/899](https://doi.org/10.1088/0004-6256/136/3/899)
- Subasavage, J. P., Henry, T. J., Bergeron, P., et al. 2007, AJ, 134, 252, doi: [10.1086/518739](https://doi.org/10.1086/518739)
- Subasavage, J. P., Jao, W.-C., Henry, T. J., et al. 2009, AJ, 137, 4547, doi: [10.1088/0004-6256/137/6/4547](https://doi.org/10.1088/0004-6256/137/6/4547)
- . 2017, AJ, 154, 32, doi: [10.3847/1538-3881/aa76e0](https://doi.org/10.3847/1538-3881/aa76e0)
- Toonen, S., Hollands, M., Gänsicke, B. T., & Boekholt, T. 2017, A&A, 602, A16, doi: [10.1051/0004-6361/201629978](https://doi.org/10.1051/0004-6361/201629978)
- Tremblay, P.-E., & Bergeron, P. 2009, ApJ, 696, 1755, doi: [10.1088/0004-637X/696/2/1755](https://doi.org/10.1088/0004-637X/696/2/1755)
- Tremblay, P.-E., Gianninas, A., Kilic, M., et al. 2015, ApJ, 809, 148, doi: [10.1088/0004-637X/809/2/148](https://doi.org/10.1088/0004-637X/809/2/148)
- Tremblay, P.-E., Ludwig, H.-G., Steffen, M., & Freytag, B. 2013, A&A, 559, A104, doi: [10.1051/0004-6361/201322318](https://doi.org/10.1051/0004-6361/201322318)
- Ulla, A., & Thejll, P. 1998, A&AS, 132, 1, doi: [10.1051/aas:1998439](https://doi.org/10.1051/aas:1998439)
- Ulla, A. M., & Solheim, J.-E. 1990, Ap&SS, 169, 189, doi: [10.1007/BF00640709](https://doi.org/10.1007/BF00640709)
- Vennes, S. 1990, ApJL, 361, L65, doi: [10.1086/185828](https://doi.org/10.1086/185828)
- Vennes, S., & Kawka, A. 2012, ApJL, 745, L12, doi: [10.1088/2041-8205/745/1/L12](https://doi.org/10.1088/2041-8205/745/1/L12)

- Wachter, S., Hoard, D. W., Hansen, K. H., et al.
2003, ApJ, 586, 1356, doi: [10.1086/367821](https://doi.org/10.1086/367821)
- Wesemael, F., Greenstein, J. L., Liebert, J., et al.
1993, PASP, 105, 761, doi: [10.1086/133228](https://doi.org/10.1086/133228)
- Xu, S., & Jura, M. 2012, ApJ, 745, 88,
doi: [10.1088/0004-637X/745/1/88](https://doi.org/10.1088/0004-637X/745/1/88)
- Zacharias, N., Urban, S. E., Zacharias, M. I., et al.
2004, The Astronomical Journal, 127, 3043
- Zuckerman, B., Koester, D., Melis, C., Hansen,
B. M., & Jura, M. 2007, ApJ, 671, 872,
doi: [10.1086/522223](https://doi.org/10.1086/522223)

APPENDIX

Table 19. GAIA Astrometry and Photometry

WD Number or Name	RA(2015) degrees	RA(2015) mas	Dec(2015) degrees	Dec(2015) mas	π mas	μ_{RA} mas yr $^{-1}$	μ_{Dec} mas yr $^{-1}$	Goodness of Fit	Excess Noise mas	<i>Gaia</i> G Significance	Excess Noise magnitudes
2359+636 ^a	0.6033724108 ± 0.057	63.9627280595 ± 0.061	38.080 ± 0.079	918.853 ± 0.126	108.269 ± 0.113	0.765395	0.089375	0.220290	17.0238 ± 0.0008		
0002+729 ^b	1.2812254420 ± 0.032	73.2197985339 ± 0.028	28.841 ± 0.033	188.090 ± 0.064	122.007 ± 0.053	10.121792	0.254077	12.341704	14.2866 ± 0.0004		
0003-103	1.4832881447 ± 0.173	-10.0369960449 ± 0.097	6.496 ± 0.213	83.637 ± 0.382	22.531 ± 0.199	1.867083	0.326108	0.990932	17.9770 ± 0.0039		
0003+176	1.5968322482 ± 0.091	18.0023371153 ± 0.082	17.259 ± 0.114	278.227 ± 0.210	-322.470 ± 0.136	-1.254582	0.000000	0.000000	16.9803 ± 0.0011		
0042-064	11.2768904848 ± 0.135	-6.1417281420 ± 0.104	33.336 ± 0.163	113.466 ± 0.315	-684.933 ± 0.197	-0.639422	0.000000	0.000000	17.9893 ± 0.0011		

Note—Table 19 is published in its entirety in the machine-readable format. A portion is shown here for guidance regarding its form and content.

a NOFS and *Gaia* parallax values differ by more than 2σ .

b The *Gaia* astrometric fit may be poor as indicated by a goodness of fit statistic > 3 or the significance of excess noise being > 2 (*Gaia* DR2 documentation).

Table 20. SDSS Photometry, AB magnitudes

WD/Name	<i>u</i>	<i>g</i>	<i>r</i>	<i>i</i>	<i>z</i>
0003–103	17.346 ± 0.014	17.701 ± 0.019	18.113 ± 0.019	18.480 ± 0.024	18.782 ± 0.055
0003+177	17.412 ± 0.029	17.113 ± 0.025	17.001 ± 0.021	17.055 ± 0.027	17.159 ± 0.025
0015+004	16.830 ± 0.012	16.935 ± 0.019	17.191 ± 0.009	17.430 ± 0.015	17.658 ± 0.022
0042–064	20.484 ± 0.061	18.673 ± 0.043	17.938 ± 0.020	17.630 ± 0.017	17.556 ± 0.019
0102+210A	19.600 ± 0.043	18.291 ± 0.016	17.683 ± 0.022	17.443 ± 0.018	17.367 ± 0.024

NOTE—Table 20 is published in its entirety in the machine-readable format. A portion is shown here for guidance regarding its form and content.

Table 21. 2MASS Photometry 2MASS System, Vega magnitudes

WD/Name	<i>J</i>	<i>H</i>	<i>K_s</i>
2359+636	15.799 ± 0.067	15.575 ± 0.136	15.513 ± 0.216
0002+729	14.615 ± 0.036	14.597 ± 0.055	14.758 ± 0.100
0003+177	16.208 ± 0.126	... ± ± ...
0042–064	16.691 ± 0.117	16.631 ± 0.225	15.682 ± 0.215
0102+210A	16.518 ± 0.097	16.504 ± 0.198	... ± ...

NOTE—Table 21 is published in its entirety in the machine-readable format. A portion is shown here for guidance regarding its form and content.

Table 22. UKIDSS Photometry MKO System, Vega magnitudes

WD/Name	Z	Y	J	H	K	Survey
0015+004	... ±	... 17.353 ± 0.015	17.346 ± 0.017	17.376 ± 0.066	17.554 ± 0.114	LAS10
0112+104	... ±	... 15.860 ± 0.007	15.945 ± 0.010	16.027 ± 0.018	16.059 ± 0.029	LAS10
0135–005	... ±	... 13.662 ± 0.002	12.985 ± 0.001	12.585 ± 0.002	12.360 ± 0.002	LAS10
0235+064	... ±	... 15.759 ± 0.007	... ± ...	15.794 ± 0.013	15.856 ± 0.023	LAS10
PG 0235+064B	... ±	... 12.209 ± 0.001	... ± ...	11.447 ± 0.001	10.997 ± 0.001	LAS10
0300–013	... ±	... 15.781 ± 0.006	15.821 ± 0.010	15.859 ± 0.011	15.789 ± 0.017	LAS10
0339+523	... ± ± ...	15.979 ± 0.005	15.997 ± 0.011	16.046 ± 0.025	GPS10
0343+247	17.374 ± 0.015	17.372 ± 0.016	17.601 ± 0.031	17.919 ± 0.062	18.982 ± 0.238	GCS10
0346–011	... ±	... 14.639 ± 0.003	14.794 ± 0.004	14.890 ± 0.007	15.046 ± 0.014	LAS10
0349+495	... ± ± ...	16.676 ± 0.011	16.533 ± 0.019	16.542 ± 0.045	GPS10
0357+513	... ± ± ...	15.939 ± 0.007	15.670 ± 0.010	15.585 ± 0.019	GPS10
0402+265	... ±	... 17.346 ± 0.014	17.091 ± 0.018	17.043 ± 0.051	16.956 ± 0.034	GCS10
0407+197	... ± ± ± ± ...	15.952 ± 0.034	GCS10
0409+237	... ± ± ± ± ...	18.024 ± 0.175	GCS10
0415+271	... ± ± ...	15.137 ± 0.006	... ± ...	15.143 ± 0.009	GCS10
0437+093	... ± ± ± ± ...	15.697 ± 0.019	GCS10
0452+103	... ± ± ± ± ...	15.970 ± 0.029	GCS10
0532+414	... ± ± ...	14.070 ± 0.002	13.920 ± 0.002	13.916 ± 0.004	GPS10
0541+260	... ± ± ...	15.737 ± 0.005	... ± ...	15.488 ± 0.015	GPS10
0546+234	... ± ± ...	16.655 ± 0.012	16.421 ± 0.016	16.351 ± 0.034	GPS10
0557+237	... ± ± ...	16.546 ± 0.009	16.444 ± 0.014	16.420 ± 0.033	GPS10
0559+158	... ± ± ...	16.113 ± 0.008	15.898 ± 0.010	15.881 ± 0.023	GPS10
0610+208	... ± ± ...	15.554 ± 0.005	15.496 ± 0.007	15.489 ± 0.017	GPS10
0625+100	... ± ± ...	16.337 ± 0.009	16.308 ± 0.016	16.336 ± 0.035	GPS10
0651–020	... ± ± ...	15.494 ± 0.004	15.585 ± 0.006	15.690 ± 0.019	GPS10
0654+027	... ± ± ...	16.014 ± 0.005	15.965 ± 0.009	15.969 ± 0.021	GPS10
0742+266	... ±	... 17.389 ± 0.014	17.112 ± 0.003	17.087 ± 0.051	17.184 ± 0.080	LAS10
0913+103	... ±	... 15.641 ± 0.006	15.609 ± 0.005	15.560 ± 0.010	15.561 ± 0.017	LAS10
0919+296	... ±	... 18.322 ± 0.039	18.301 ± 0.043	18.245 ± 0.135	... ± ...	LAS10
0922+053	... ±	... 15.293 ± 0.004	15.296 ± 0.005	15.264 ± 0.010	15.333 ± 0.014	LAS10
0922+005	... ±	... 18.036 ± 0.029	17.796 ± 0.026	17.790 ± 0.068	17.880 ± 0.136	LAS10
LHS 2140	... ±	... 12.542 ± 0.001	12.067 ± 0.001	11.719 ± 0.001	11.448 ± 0.001	LAS10
0939+071	... ±	... 14.147 ± 0.003	13.934 ± 0.002	13.664 ± 0.003	13.605 ± 0.004	LAS10
0956–017	... ±	... 18.434 ± 0.030	18.321 ± 0.050	18.180 ± 0.100	17.610 ± 0.080	LAS10
1012+083B	... ±	... 16.361 ± 0.010	16.065 ± 0.011	15.828 ± 0.013	15.672 ± 0.019	LAS10
1012+083A	... ±	... 15.323 ± 0.005	15.155 ± 0.005	14.943 ± 0.006	14.918 ± 0.010	LAS10

Table 22 continued on next page

Table 22 (*continued*)

WD/Name	Z	Y	J	H	K	Survey
1015+014	... ±	... 16.385 ± 0.009	16.333 ± 0.009	16.341 ± 0.017	16.315 ± 0.030	LAS10
1022+009	... ±	... 17.052 ± 0.013	... ± ...	16.479 ± 0.030	16.478 ± 0.041	LAS10
1035–003	... ±	... 16.917 ± 0.010	16.848 ± 0.014	16.864 ± 0.045	16.661 ± 0.052	LAS10
1042+593	... ± ± ...	17.737 ± 0.008	... ± ...	17.957 ± 0.021	DXS10
1046–017	... ± ± ± ...	16.102 ± 0.016	16.157 ± 0.030	LAS10
1111+020	... ±	... 17.422 ± 0.027	16.993 ± 0.030	16.811 ± 0.040	16.623 ± 0.053	LAS10
V* T Leo	... ±	... 14.601 ± 0.004	14.174 ± 0.003	14.235 ± 0.004	13.890 ± 0.005	LAS10
1153+135	... ±	... 16.307 ± 0.008	16.064 ± 0.008	15.776 ± 0.009	15.715 ± 0.017	LAS10
1208+076	... ±	... 15.625 ± 0.005	15.370 ± 0.005	15.093 ± 0.007	14.991 ± 0.011	LAS10
1219+130	... ±	... 18.612 ± 0.060	18.431 ± 0.072	18.392 ± 0.105	18.014 ± 0.151	LAS10
1239+302	... ±	... 17.651 ± 0.021	17.387 ± 0.024	17.077 ± 0.039	17.009 ± 0.060	LAS10
1241–010	... ±	... 14.414 ± 0.003	14.489 ± 0.006	14.886 ± 0.007	14.401 ± 0.007	LAS10
1300+263	... ±	... 17.145 ± 0.013	16.853 ± 0.014	16.715 ± 0.021	16.659 ± 0.039	LAS10
1309+296	... ±	... 17.464 ± 0.016	17.361 ± 0.022	17.223 ± 0.044	16.896 ± 0.056	LAS10
1310+027	... ±	... 16.650 ± 0.010	16.351 ± 0.012	16.174 ± 0.017	16.134 ± 0.031	LAS10
1328+307	... ±	... 15.533 ± 0.005	15.483 ± 0.007	15.395 ± 0.010	15.355 ± 0.015	LAS10
1335+002	... ±	... 19.926 ± 0.070	... ± ± ...	18.869 ± 0.357	LAS10
1338+023	... ±	... 16.829 ± 0.010	16.605 ± 0.015	16.322 ± 0.015	16.237 ± 0.030	LAS10
1645+325	... ±	... 14.009 ± 0.002	14.095 ± 0.002	14.194 ± 0.004	14.284 ± 0.007	LAS10
1827–106	... ± ± ...	15.482 ± 0.006	15.359 ± 0.013	... ± ...	GPS10
1845+019	... ± ± ...	12.453 ± 0.001	12.131 ± 0.001	11.828 ± 0.001	GPS10
1857+119	... ± ± ...	15.424 ± 0.004	15.403 ± 0.006	15.458 ± 0.012	GPS10
1910+047	... ± ± ...	17.324 ± 0.027	17.326 ± 0.052	17.297 ± 0.116	GPS10
1912+143	... ± ± ...	16.024 ± 0.007	15.850 ± 0.020	15.850 ± 0.030	GPS10
1950+250	... ± ± ...	15.231 ± 0.004	15.223 ± 0.006	15.236 ± 0.010	GPS10
2028+390	... ± ± ...	13.977 ± 0.010	14.085 ± 0.010	14.209 ± 0.020	GPS10
2148+539	... ± ± ...	16.867 ± 0.017	16.755 ± 0.025	16.800 ± 0.060	GPS10
2217–009	... ±	... 16.952 ± 0.013	16.724 ± 0.005	16.445 ± 0.025	16.271 ± 0.005	LAS10
2254+076	... ±	... 17.335 ± 0.015	17.295 ± 0.023	17.326 ± 0.040	17.166 ± 0.065	LAS10
2347+128	... ±	... 16.156 ± 0.007	16.132 ± 0.009	16.099 ± 0.019	16.166 ± 0.029	LAS10

NOTE—“apermag3” values are given as appropriate for point sources; DXS — Deep eXtragalactic Survey, GCS — Galactic Clusters Survey, GPS — Galactic Plane Survey, LAS — Large Area Survey.

Table 23. VISTA Photometry VISTA System, Vega magnitudes

WD/Name	<i>Z</i>	<i>Y</i>	<i>J</i>	<i>H</i>	<i>K</i>	Survey
0112–018	… ± …	16.401 ± 0.010	16.182 ± 0.010	15.940 ± 0.020	15.860 ± 0.020	VHS5
0114–049A	… ± …	… ± …	16.557 ± 0.009	16.340 ± 0.015	16.250 ± 0.030	VHS5
0115–049B	… ± …	… ± …	16.599 ± 0.010	16.406 ± 0.016	16.324 ± 0.032	VHS5
0202–055	… ± …	… ± …	16.531 ± 0.009	16.490 ± 0.010	16.480 ± 0.040	VHS5
0918–172	… ± …	… ± …	16.755 ± 0.017	… ± …	16.495 ± 0.052	VHS5
LP 787–25	… ± …	… ± …	12.748 ± 0.001	… ± …	11.919 ± 0.001	VHS5
1053–092	… ± …	17.024 ± 0.029	17.156 ± 0.050	17.281 ± 0.099	17.655 ± 0.274	VHS5
1212–022	16.984 ± 0.004	16.936 ± 0.007	16.857 ± 0.007	16.609 ± 0.013	16.462 ± 0.018	VIKING4
1314–153	… ± …	15.090 ± 0.004	15.170 ± 0.005	15.211 ± 0.008	15.214 ± 0.017	VHS5
1335+002	19.526 ± 0.027	19.845 ± 0.066	20.395 ± 0.090	… ± …	… ± …	VIKING4
1401–149	… ± …	17.373 ± 0.018	17.527 ± 0.028	17.768 ± 0.072	18.278 ± 0.219	VHS5
1408+029	15.718 ± 0.002	15.636 ± 0.004	15.439 ± 0.003	15.195 ± 0.005	15.077 ± 0.007	VIKING4
1439–195	… ± …	16.976 ± 0.012	16.789 ± 0.017	… ± …	16.549 ± 0.063	VHS5
1444–096	… ± …	15.252 ± 0.008	15.304 ± 0.006	15.386 ± 0.013	15.429 ± 0.022	VHS5
1717–014	… ± …	… ± …	16.664 ± 0.012	… ± …	16.406 ± 0.044	VHS5
2130–047	… ± …	14.809 ± 0.003	14.489 ± 0.002	15.029 ± 0.011	15.043 ± 0.013	VHS5
2151–015	… ± …	… ± …	12.519 ± 0.001	12.005 ± 0.001	11.552 ± 0.001	VHS5
2157–079	… ± …	18.471 ± 0.028	18.587 ± 0.046	… ± …	18.591 ± 0.242	VHS5
2217–009	… ± …	… ± …	16.690 ± 0.010	16.470 ± 0.010	16.290 ± 0.010	VHS5
2229–080	… ± …	17.300 ± 0.014	17.334 ± 0.023	… ± …	16.820 ± 0.060	VHS5
2253–062	… ± …	15.334 ± 0.005	15.436 ± 0.008	15.558 ± 0.013	15.603 ± 0.027	VHS5
2316–064	… ± …	16.642 ± 0.010	16.396 ± 0.011	16.169 ± 0.019	16.131 ± 0.039	VHS5
2349–031	… ± …	16.915 ± 0.014	16.951 ± 0.019	16.915 ± 0.041	16.963 ± 0.064	VHS5

NOTE—“apermag3” values are given as appropriate for point sources; VHS — VISTA Hemisphere Survey, VIKING — VISTA Kilo-degree Infrared Galaxy survey.

Table 24. UKIRT Hemisphere Survey MKO System, Vega magnitudes

WD/Name	<i>J</i>	WD/Name	<i>J</i>	WD/Name	<i>J</i>
0003+177	16.609 ± 0.018	0955+247	14.678 ± 0.004	1630+245	17.641 ± 0.045
0102+210A	16.528 ± 0.014	1002+430	16.636 ± 0.020	1632+177	13.016 ± 0.002
0102+210B	16.452 ± 0.013	1056+345	15.657 ± 0.008	1636+057	15.963 ± 0.010
GD 274	11.305 ± 0.001	1100+211	17.037 ± 0.022	1645+325	14.078 ± 0.003
0203+183	16.651 ± 0.019	1101+364	14.823 ± 0.005	1658+440	15.498 ± 0.007
0203+207	17.940 ± 0.038	1104+491	17.196 ± 0.027	1704+481B	14.112 ± 0.003
0228+269	15.797 ± 0.011	1108+207	15.947 ± 0.009	1704+481A	14.769 ± 0.005
0239+109	15.739 ± 0.011	1124+595	15.046 ± 0.006	1709+230	15.326 ± 0.007
0239+167	16.337 ± 0.014	1126+185	12.571 ± 0.001	1711+335	12.913 ± 0.002
0246+326	16.156 ± 0.014	1129+373	16.681 ± 0.021	1727+560	16.575 ± 0.017
0342+176	16.081 ± 0.010	LP 129-586	12.482 ± 0.001	1729+371	16.013 ± 0.011
0407+197	16.264 ± 0.014	1148+544	16.628 ± 0.015	1736+052	15.599 ± 0.009
0409+237	17.972 ± 0.056	1224+354	15.990 ± 0.010	1747+450	15.315 ± 0.007
0437+093	15.957 ± 0.011	1232+379	14.479 ± 0.004	1814+248	16.167 ± 0.012
0452+103	16.186 ± 0.011	1235+422	16.346 ± 0.015	V* AM Her	12.264 ± 0.001
0500+573	17.334 ± 0.038	1236+457	15.575 ± 0.009	1855+338	14.756 ± 0.005
0527+185	17.241 ± 0.026	1238+183	16.336 ± 0.014	1858+393	15.467 ± 0.007
0531+572	16.595 ± 0.020	1252+471	17.022 ± 0.026	1923+550	16.985 ± 0.021
0632+409	16.226 ± 0.012	1255+547	16.112 ± 0.010	1944+467B	15.870 ± 0.011
0637+335	16.969 ± 0.025	1302+597	15.026 ± 0.006	1944+467A	15.841 ± 0.010
0637+477	15.086 ± 0.006	1303+182	15.982 ± 0.010	2005+175	14.845 ± 0.005
0650+397	15.970 ± 0.010	1310+583	14.053 ± 0.003	2006+481	15.553 ± 0.007
0701+517	16.840 ± 0.019	1327+594	18.709 ± 0.094	2058+342	15.757 ± 0.009
0708+462	17.789 ± 0.045	1409+157	16.618 ± 0.016	2139+132B	16.939 ± 0.021
0714+458	15.120 ± 0.006	1434+437	15.819 ± 0.009	2139+132A	16.016 ± 0.011
0749+426	15.816 ± 0.009	1458+362	17.804 ± 0.040	2154+408	12.882 ± 0.002
0825+455	15.016 ± 0.006	1521+320	17.665 ± 0.039	2216+484	15.405 ± 0.007
0855+416	16.309 ± 0.014	1524+566	15.656 ± 0.009	2220+121	16.779 ± 0.020
0919+296	18.228 ± 0.074	1529+141	16.188 ± 0.011	LP 400-21	12.808 ± 0.002
0921+354	15.666 ± 0.010	1540+236	15.642 ± 0.008	2234+222	17.249 ± 0.023
G117-B15B	11.638 ± 0.001	1542+182	15.178 ± 0.007	2245+146	17.906 ± 0.046
0944+452B	19.559 ± 0.216	1552+177	17.061 ± 0.025	PG 2300+166	13.178 ± 0.002
0944+452A	17.571 ± 0.038	1602+011	16.069 ± 0.011	2303+242	15.445 ± 0.007
0954+342	18.393 ± 0.059	1611+176	17.429 ± 0.032	2328+510	15.383 ± 0.007

NOTE—“apermag3” values are given as appropriate for point sources.

Table 25. *WISE* and *Spitzer* Photometry, Vega magnitudes

WD/Name	W1	W2	W3	W4	$3.6\mu\text{m}$	$4.5\mu\text{m}$	$5.8\mu\text{m}$	$8.0\mu\text{m}$
2359+636	14.884 ± 0.030	15.192 ± 0.066	... ± ± ± ± ± ± ...
0002+729	14.743 ± 0.032	14.830 ± 0.054	... ± ± ± ...	14.743 ± 0.037	... ± ...	14.369 ± 0.015
0015+004	17.224 ± 0.155	... ± ± ± ...	17.418 ± 0.006	17.325 ± 0.007	... ± ± ...
0042-064	16.340 ± 0.072	... ± ± ± ± ± ± ± ...
0102+210A	15.962 ± 0.055	15.667 ± 0.123	... ± ± ...	16.102 ± 0.035	16.001 ± 0.039	15.829 ± 0.193	16.155 ± 0.588

NOTE—Table 25 is published in its entirety in the machine-readable format. A portion is shown here for guidance regarding its form and content.

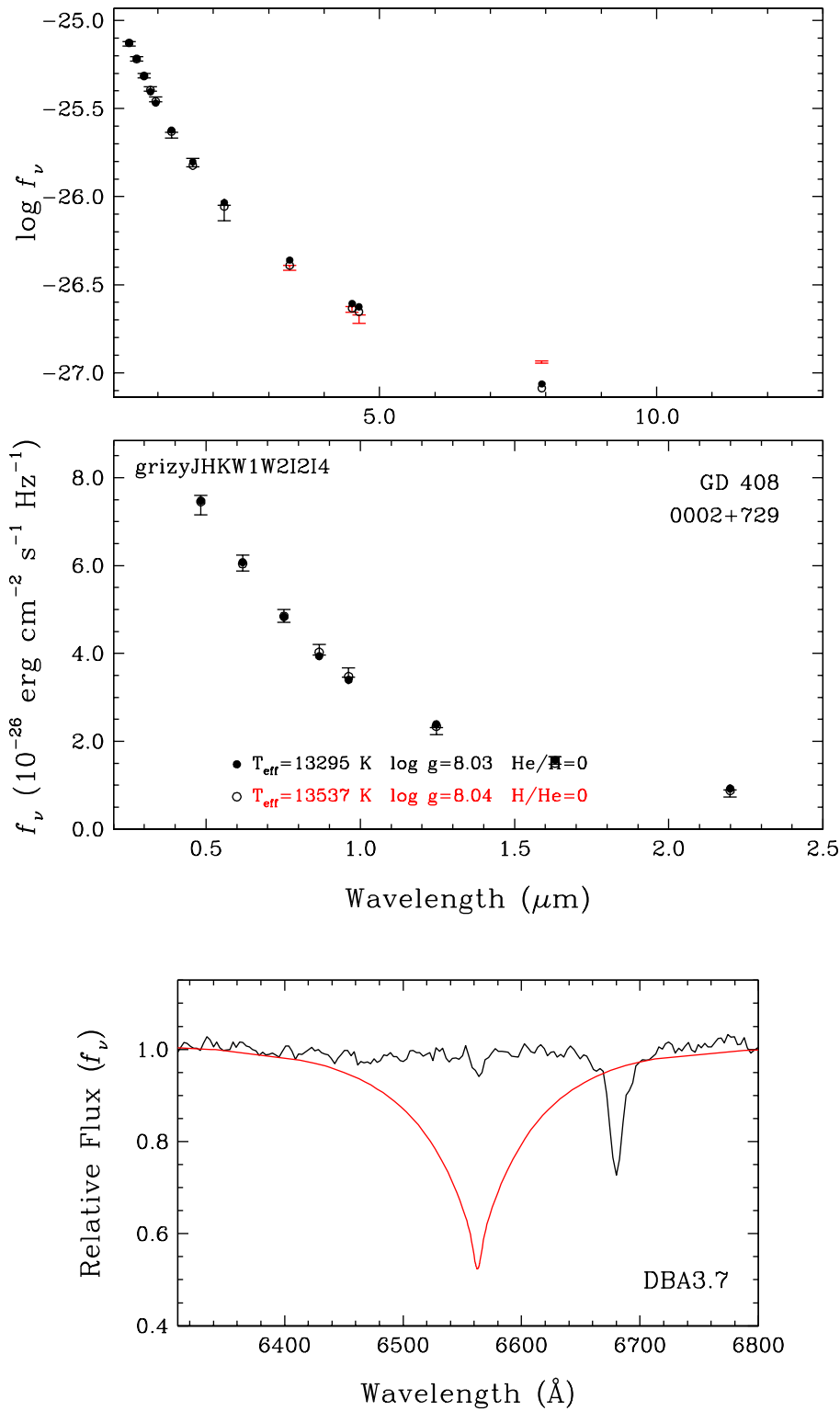


Figure 15. Example Figure of the model comparison to each WD. The Figure is published in its entirety in the on-line Journal.